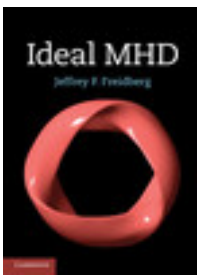

Ideal MHD

Jeffrey P. Freidberg

Book DOI: http://dx.doi.org/10.1017/CBO9780511795046

Online ISBN: 9780511795046

Hardback ISBN: 9781107006256

Chapter

6 - Equilibrium: two-dimensional configurations pp. 123-222

Chapter DOI: http://dx.doi.org/10.1017/CBO9780511795046.007

Cambridge University Press

6

Equilibrium: two-dimensional configurations

6.1 Introduction

In Chapter 5 it was shown that a one-dimensional, cylindrically symmetric magnetic geometry accurately describes radial pressure balance in many fusion configurations. The primary goal of Chapter 6 is to address the problem of toroidal force balance in a two-dimensional axisymmetric toroidal geometry. A secondary goal analyzes straight systems with two-dimensional helical symmetry.

The discussion starts with a derivation of the Grad–Shafranov equation, the basic equation describing axisymmetric toroidal equilibrium. For configurations possessing such symmetry, the solutions to this equation provide a complete description of ideal MHD equilibria: radial pressure balance, toroidal force balance, equilibrium β limits, rotational transform, and kink safety factor. A wide number of configurations are well described by the Grad–Shafranov equation. Included among them are all types of tokamaks, the reversed field pinch, the levitated dipole, the spheromak, and the field reversed configuration.

Two strategies are utilized to solve the Grad–Shafranov equation. The first makes use of asymptotic expansions, with the inverse aspect ratio $\varepsilon = a/R_0$ serving as the small expansion parameter. The asymptotic analysis mathematically separates the problems of radial pressure balance and toroidal force balance into two distinct parts. It thereby provides a method for obtaining analytic results as well as developing physical intuition. In a certain sense each different asymptotic expansion (i.e., corresponding to different orderings of β, q, B_p/B_t with respect to ε) serves to mathematically identify a specific MHD configuration. The small ε expansion works well for the ohmically heated tokamak and the reversed field pinch.

The second strategy focuses on configurations in which radial pressure balance and toroidal force balance cannot be separated. This clearly occurs for tight aspect ratio geometries where $\varepsilon \sim 1$, such as the spherical tokamak, spheromak, and field reversed configuration. Interestingly the non-separation of effects can also occur

for configurations where ε is small but β/ε is finite, such as the auxiliary heated tokamak. The analysis for this strategy makes use of special exact analytic solutions to the Grad–Shafranov equation where simple choices are made for the two free functions inherent in any MHD equilibrium.

The last section of the chapter focuses on two-dimensional helically (rather than toroidally), symmetric equilibria. The main configuration of interest here is the "straight" stellarator. A helically symmetric version of the Grad–Shafranov equation is derived and then analyzed for stellarators with a single helicity. Of interest are the evaluation of the rotational transform and the calculation of equilibria with zero net current. Bending a straight stellarator into a torus requires a full three-dimensional analysis and is discussed in Chapter 7. Even so, a straight helical system provides a good introduction to some of the basic MHD physics of the stellarator.

6.2 Derivation of the Grad–Shafranov equation

The Grad–Shafranov equation is a two-dimensional, non-linear, partial differential equation obtained from the reduction of the ideal MHD equations (Eq. (4.16)) for the case of toroidal axisymmetry (Grad and Rubin, 1958; Shafranov, 1960; Lust and Schluter, 1957). The geometry of interest is illustrated in Fig. 6.1.

Here, R, ϕ, Z correspond to the familiar right-handed cylindrical coordinate system. The assumption of toroidal axisymmetry implies that $\partial S/\partial\phi = 0$, where S is any scalar. The derivation proceeds by analyzing the equations in the order described in Chapter 4.

6.2.1 The $\nabla \cdot \mathbf{B} = 0$ equation

The axisymmetric assumption implies that $\nabla \cdot \mathbf{B} = 0$ can be written as

$$\frac{1}{R}\frac{\partial}{\partial R}(RB_R) + \frac{\partial B_Z}{\partial Z} = 0 \tag{6.1}$$

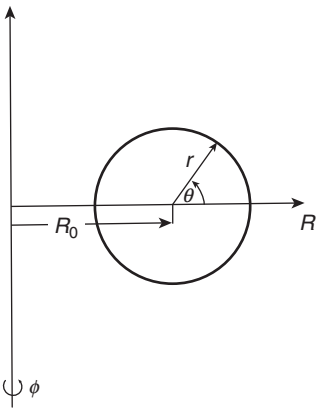

Figure 6.1 Geometry for axisymmetric toroidal equilibrium.

As with many two-dimensional systems it is useful to introduce a stream function ψ for the poloidal magnetic field:

$$B_R = -\frac{1}{R}\frac{\partial \psi}{\partial Z}$$
$$B_Z = \frac{1}{R}\frac{\partial \psi}{\partial R} \tag{6.2}$$

where $\psi = RA_\phi$ and A_ϕ is the toroidal component of vector potential. Note that B_ϕ is unaffected by Eq. (6.1). In more compact notation, one can write

$$\mathbf{B} = B_\phi \mathbf{e}_\phi + \mathbf{B}_p$$
$$\mathbf{B}_p = \frac{1}{R}\nabla\psi \times \mathbf{e}_\phi \tag{6.3}$$

The stream function ψ is closely related to the poloidal flux in the plasma ψ_p, which is given by

$$\psi_p = \int \mathbf{B}_p \cdot d\mathbf{A} \tag{6.4}$$

The area of interest in the integral is a washer-shaped surface lying in the $Z = 0$ plane as shown in Fig. 6.2. The inner radius of the washer is located at $R = R_a$ corresponding to the magnetic axis. The outer radius extends to an arbitrary ψ contour defined by $\psi = \psi(R, 0)$. It then follows that

$$\psi_p = \int_0^{2\pi} d\phi \int_{R_a}^{R} R' B_Z(R', 0)\, dR' = 2\pi\psi \tag{6.5}$$

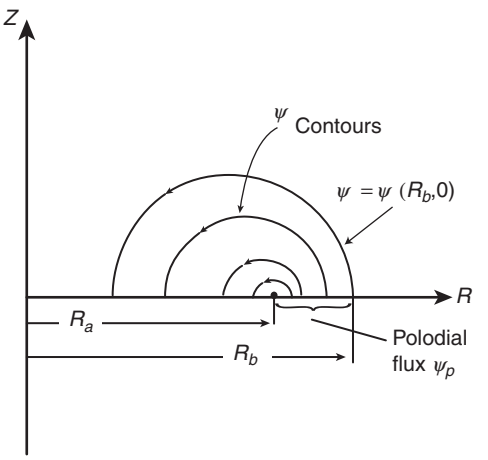

Figure 6.2 Washer-shaped surface through which the poloidal flux ψ_p passes.

Here, the arbitrary integration constant associated with ψ has been chosen so that the poloidal magnetic flux on the axis is zero: $\psi(R_a, 0) = 0$.

As previously stated, it is convenient to label the flux surfaces with the values of ψ rather than p.

6.2.2 Ampere's law

The next step is to substitute the expression for the magnetic field into Ampere's law to obtain an expression for the current density. A straightforward calculation leads to

$$\begin{aligned} \mu_0 \mathbf{J} &= \mu_0 J_\phi \mathbf{e}_\phi + \frac{1}{R}\nabla(RB_\phi) \times \mathbf{e}_\phi \\ \mu_0 J_\phi &= -\frac{1}{R}\Delta^* \psi \end{aligned} \tag{6.6}$$

where the operator Δ^* is defined by

$$\Delta^* \psi \equiv R^2 \nabla \cdot \left(\frac{\nabla \psi}{R^2}\right) = R\frac{\partial}{\partial R}\left(\frac{1}{R}\frac{\partial \psi}{\partial R}\right) + \frac{\partial^2 \psi}{\partial Z^2} \tag{6.7}$$

6.2.3 Momentum equation

The final step in the derivation is to substitute the expressions for **B** and **J** (Eqs. (6.3) and (6.6)) into the momentum equation (Eq. (4.1)). An efficient way to carry out this step is to decompose the momentum equation into three components along **B**, **J**, and $\nabla\psi$. The **B** component yields $\mathbf{B} \cdot \nabla p = 0$, which can be rewritten as

$$\mathbf{e}_\phi \cdot \nabla\psi \times \nabla p = 0 \tag{6.8}$$

The general solution to this equation is

$$p = p(\psi) \tag{6.9}$$

As expected, the pressure is a surface quantity. It is a free function; that is, one can specify $p(\psi)$ arbitrarily. The MHD model does not contain sufficient physics to determine the functional dependence of the pressure on the flux. Transport theory, experimental data, or physical intuition are needed to properly specify $p(\psi)$ as well as $F(\psi)$ introduced below. Also, note that the pressure is a function of a single variable ψ even though the geometry is two dimensional.

Consider next the **J** component of the momentum equation which reduces to $\mathbf{J} \cdot \nabla p = 0$. Substituting for **J** leads to

$$\mathbf{e}_\phi \cdot \nabla\psi \times \nabla(RB_\phi) = 0 \tag{6.10}$$

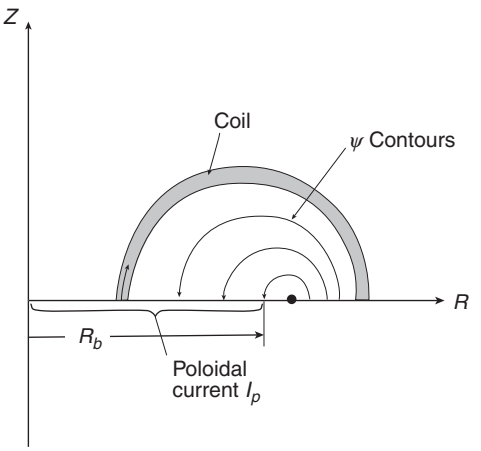

Figure 6.3 Disk-shaped surface through which the total (plasma plus coil) poloidal current I_p flows.

Hence, RB_ϕ is also a free surface function,

$$RB_\phi = F(\psi) \tag{6.11}$$

The quantity $F(\psi)$ is related to the combined poloidal current flowing in the plasma plus toroidal field coils. To see this examine Fig. 6.3 and focus on the poloidal current flowing through a disk-shaped surface lying in the $Z = 0$ plane. The disk extends from the center line $R = 0$ out to an arbitrary flux surface defined by $\psi = \psi(R, 0)$. The value of the total enclosed poloidal current is given by

$$I_p = \int \mathbf{J}_p \cdot d\mathbf{A} = \int_0^{2\pi} d\phi \int_0^R R' J_Z(R', 0) dR' \tag{6.12}$$

which reduces to

$$I_p(\psi) = 2\pi F(\psi) \tag{6.13}$$

Lastly, substituting into the $\nabla\psi$ component of the momentum equation yields the Grad–Shafranov equation. The individual terms appearing simplify as follows:

$$\begin{aligned}
\nabla\psi \cdot \nabla p &= (\nabla\psi)^2 \frac{dp}{d\psi} \\
\nabla\psi \cdot \mathbf{J}_p \times (B_\phi\, \mathbf{e}_\phi) &= -(\nabla\psi)^2 \frac{F}{\mu_0 R^2} \frac{dF}{d\psi} \\
\nabla\psi \cdot \left(J_\phi\, \mathbf{e}_\phi\right) \times \mathbf{B}_p &= -(\nabla\psi)^2 \frac{\Delta^* \psi}{\mu_0 R^2} \\
\nabla\psi \cdot \mathbf{J}_p \times \mathbf{B}_p &= 0 \\
\nabla\psi \cdot \left(J_\phi\, \mathbf{e}_\phi\right) \times (B_\phi\, \mathbf{e}_\phi) &= 0
\end{aligned} \tag{6.14}$$

The final step is to combine these terms. The result, including a summary of the field relations, can be written as

$$\Delta^* \psi = -\mu_0 R^2 \frac{dp}{d\psi} - \frac{1}{2}\frac{dF^2}{d\psi} \tag{6.15}$$

with

$$\begin{aligned} \mathbf{B} &= \frac{1}{R}\nabla\psi \times \mathbf{e}_\phi + \frac{F}{R}\mathbf{e}_\phi \\ \mu_0 \mathbf{J} &= \frac{1}{R}\frac{dF}{d\psi}\nabla\psi \times \mathbf{e}_\phi - \frac{1}{R}\Delta^*\psi\, \mathbf{e}_\phi \end{aligned} \tag{6.16}$$

Equation (6.15) is the Grad–Shafranov equation (Grad and Rubin, 1958; Shafranov, 1960, 1966), a second-order, non-linear partial differential equation describing general axisymmetric toroidal equilibria. The nature of the equilibria (e.g., tokamak, reversed field pinch, etc.) is to a large extent determined by the choice of the free functions $p(\psi)$ and $F(\psi)$ and, of course, the boundary conditions. The properties of the reversed field pinch and straight tokamak are discussed individually in the sections that follow once relations are obtained for the basic plasma parameters and figures of merit.

6.3 Plasma parameters and figures of merit

Consider now the evaluation of the basic plasma parameters and figures of merit. By exploiting the axisymmetry it is possible to obtain general expressions for the quantities of interest in terms of the flux function ψ. In the analysis that follows it is assumed that $p(\psi)$ and $F(\psi)$ have been specified and that a solution has been found that gives ψ and the corresponding magnetic fields and current densities as functions of (R, Z). The calculations below are relatively straightforward. It is, however, convenient for purposes of intuition to first introduce a set of simple "flux coordinates." These coordinates are analogous to polar coordinates which are easier to visualize for circular-like cross sections than the (R, Z) coordinates. The (R, Z) coordinates are more rectangular in nature with respect to the plasma cross section. Once the coordinates are defined it is then an easy task to derive expressions for the plasma parameters and figures of merit.

6.3.1 Simple flux coordinates

The motivation to introduce flux coordinates arises because the evaluation of many of the figures of merit involves averages over the plasma volume or cross section. For example, when calculating the toroidal plasma current one needs to integrate

the current density over the cross sectional area $d\mathbf{A} = dR\, dZ\, \mathbf{e}_\phi$. While this is a formally correct expression it is cumbersome to use and visualize because the plasma boundary is a complicated function of (R, Z). If the plasma cross section is circular then cylindrical-like coordinates (r, θ) as shown in Fig. 6.1 would be easier to use. For an arbitrary cross section one would like to introduce generalized radial-like and angular-like coordinates for which the plasma surface and interior flux surfaces have a simple representation.

The choice of flux coordinates made here is as follows. For the radial-like coordinate a good choice is the flux ψ itself. Any flux surface, including the plasma surface, is defined by $\psi =$ constant. For the angular-like coordinate a simple and convenient choice is poloidal arc length l. Other choices are possible and often used when one considers stability, but for present purposes arc length is perhaps the easiest coordinate to visualize.

In the analysis that follows one should view the quantities (ψ, l) as a two-dimensional coordinate transformation replacing the (R, Z) coordinates: $\psi = \psi(R, Z)$, $l = l(R, Z)$ and the inverse transformation $R = R(\psi, l)$, $Z = Z(\psi, l)$. The definition of the flux $\psi(R, Z)$ is given by the solution to the Grad–Shafranov equation and, as stated, is assumed to be known. What remains is to define the arc length coordinate and in particular to evaluate the Jacobian of the transformation J: $dRdZ = Jd\psi dl$.

Now, for any general 2-D coordinate transformation (not necessarily corresponding to arc length) it follows that

$$\frac{1}{J} = \begin{vmatrix} \psi_R & \psi_Z \\ l_R & l_Z \end{vmatrix} = \psi_R l_Z - \psi_Z l_R = R\, \mathbf{B}_p \cdot \nabla l \tag{6.17}$$

The definition of l equivalent to the special choice of poloidal arc length requires two additional properties: (1) the direction of the arc length vector should be parallel to the poloidal magnetic field and (2) the magnitude of its poloidal gradient should be unity; in other words $\nabla l = \mathbf{B}_p/B_p$. This definition implies that as expected $\mathbf{B}_p \cdot \nabla l = B_p$ and

$$J = 1/RB_p \tag{6.18}$$

Lastly, it is worth noting that if $\psi(R, Z)$ is known then one practical way to calculate $l(R, Z)$ is by taking the divergence of $\nabla l = \mathbf{B}_p/B_p$ and then solving

$$\nabla^2 l = -\frac{1}{B_p^2}\mathbf{B}_p \cdot \nabla B_p \tag{6.19}$$

With the coordinate transformation in hand, it now becomes a simple task to calculate the various differential volume and area elements needed to evaluate the plasma parameters and figures of merit. These elements are given by

$$\begin{aligned} &\text{Volume:} && d\mathbf{r} = R\,dR\,dZ\,d\phi = 2\pi\frac{d\psi\,dl}{B_p} \\ &\text{Poloidal surface area:} && d\mathbf{S} = dR\,dZ\,\mathbf{e}_\phi = \frac{d\psi\,dl}{RB_p}\mathbf{e}_\phi \\ &\text{Plasma surface area:} && d\mathbf{A} = R\,dl\,d\phi\,\frac{\nabla\psi}{|\nabla\psi|} = 2\pi R\,dl\,\mathbf{n} \end{aligned} \tag{6.20}$$

Here, $\mathbf{n} = \nabla\psi/|\nabla\psi|$ is the outward normal vector on the plasma surface.

6.3.2 The volume of a flux surface

The volume contained within any specified flux surface ψ is given by

$$V(\psi) = \int d\mathbf{r} = 2\pi\int_0^{\psi} d\psi \oint \frac{dl}{B_p} \tag{6.21}$$

Here, the poloidal flux on the magnetic axis has been set to zero. Note also that

$$\frac{dV(\psi)}{d\psi} = 2\pi\oint\frac{dl}{B_p} \tag{6.22}$$

The volume of the entire plasma V_p is obtained by setting $\psi = \psi_a$, the value of flux on the plasma surface,

$$V_p = V(\psi_a) = 2\pi\int_0^{\psi_a} d\psi \oint \frac{dl}{B_p} \tag{6.23}$$

6.3.3 The plasma beta

The plasma beta is determined from the definitions in Eqs. (4.19) and (4.20). Consider first the toroidal beta:

$$\beta_t = \frac{2\mu_0\langle p\rangle}{B_0^2} \tag{6.24}$$

Once the solution to the Grad–Shafranov equation is known one can evaluate $\langle p\rangle$ as follows:

$$\langle p\rangle = \frac{1}{V_p}\int p\,d\,\mathbf{r} = \frac{1}{V_p}\int_0^{\psi_a} p(\psi)\frac{dV}{d\psi}\,d\psi = \frac{1}{V_p}\int_0^{V_p} p(V)dV \tag{6.25}$$

Similarly, to evaluate the poloidal beta,

$$\beta_p = \frac{4\pi^2a^2(1+\kappa^2)\langle p\rangle}{\mu_0 I^2} \tag{6.26}$$

one needs an expression for the toroidal current I, which can be written as

$$\mu_0 I = \oint \mathbf{B}_p \cdot d\,\mathbf{l} = \oint B_p dl \tag{6.27}$$

where the line integral is carried out on the plasma surface $\psi = \psi_a$. The total beta is given by

$$\beta = \frac{\beta_t \beta_p}{\beta_t + \beta_p} \tag{6.28}$$

6.3.4 The kink safety factor

The kink safety factor is defined as

$$q_* = \frac{2\pi a^2 B_0}{\mu_0 R_0 I}\left(\frac{1+\kappa^2}{2}\right) \tag{6.29}$$

It is only the current I that needs to be evaluated from the solution to the Grad–Shafranov equation and this task has already been described in Eq. (6.27).

6.3.5 Rotational transform and the MHD safety factor

The concepts of rotational transform and MHD safety factor have been discussed in Section 4.6.4. Recall that the normalized transform $\iota/2\pi$ is defined as the average change in poloidal angle $\Delta\theta$ of a magnetic field line per single transit in the toroidal direction, $\Delta\phi = 2\pi$; that is, $\iota/2\pi \equiv \langle\Delta\theta\rangle/2\pi$. The average is taken over many toroidal transits. (Here, in terms of the present notation the relation between the (R, ϕ, Z) coordinates and the cylindrical-like (r, θ, z) coordinates is given by $R = R_0 + r\cos\theta$, $Z = r\sin\theta$, and $\phi = -z/R_0$.)

Because of axisymmetry the general expression for the safety factor $q(\psi) = 2\pi/\iota$ given by Eq. (4.28) can be simplified as follows. To begin Eq. (4.28) is repeated here for convenience:

$$q(\psi) = \frac{\lim\limits_{L\to\infty}\int_0^L \frac{B_\phi}{RB}\,dl_{\text{tot}}}{\lim\limits_{L\to\infty}\int_0^L \frac{B_\theta}{rB}\,dl_{\text{tot}}} \tag{6.30}$$

where l_{tot} is arc length along the total field. The integrands are converted from line integrals parallel to the total magnetic field to line integrals parallel to the poloidal magnetic field by the geometric relation

$$\frac{dl_{\text{tot}}}{B} = \frac{dl}{B_p} \tag{6.31}$$

The integrals over the infinite length L are now replaced by an infinite sum of integrals, each one over one poloidal period L_p.

$$q(\psi) = \frac{\lim_{m\to\infty} \int_0^{mL_p} \frac{B_\phi}{RB_p}\, dl}{\lim_{m\to\infty} \int_0^{mL_p} \frac{B_\theta}{rB_p}\, dl} = \frac{\sum_{m=0}^{\infty} \int_{mL_p}^{(m+1)L_p} \frac{B_\phi}{RB_p}\, dl}{\sum_{m=0}^{\infty} \int_{mL_p}^{(m+1)L_p} \frac{B_\theta}{rB_p}\, dl} \tag{6.32}$$

The critical point is that as a consequence of toroidal axisymmetry each term in the numerator sum is identical. After one complete poloidal transit, the magnetic line trajectory repeats itself because of the toroidal symmetry. A similar conclusion applies to the denominator. Thus, the average over many poloidal periods is the same as the average over one poloidal period:

$$q(\psi) = \frac{\oint \frac{B_\phi}{RB_p}\, dl}{\oint \frac{B_\theta}{rB_p}\, dl} \tag{6.33}$$

Finally, the numerator is simplified by recalling that $F(\psi) = RB_\phi$ with $F(\psi)$ a constant on a flux surface. The denominator is simplified by noting that $dl/B_p = rd\theta/B_\theta$ implying that

$$\oint \frac{B_\theta}{rB_p}\, dl = \int_0^{2\pi} d\theta = 2\pi \tag{6.34}$$

Combining these results leads to the desired expression for the safety factor in an axisymmetric torus:

$$q(\psi) = \frac{F(\psi)}{2\pi} \oint \frac{dl}{R^2 B_p} \tag{6.35}$$

6.3.6 The MHD safety factor on axis

Equation (6.35) is a general expression for the safety factor. In most practical cases it is evaluated numerically. However, the value on axis can be difficult to evaluate because the circumference of the flux surface and the value of B_p simultaneously approach zero, leading to an undefined limit. The limit is finite and in this subsection an explicit practical expression for the safety factor on axis is derived.

The analysis proceeds as follows. On the magnetic axis $R = R_a$, $Z = Z_a$, the value of ψ can be set to zero without loss in generality. Also, by definition, the first

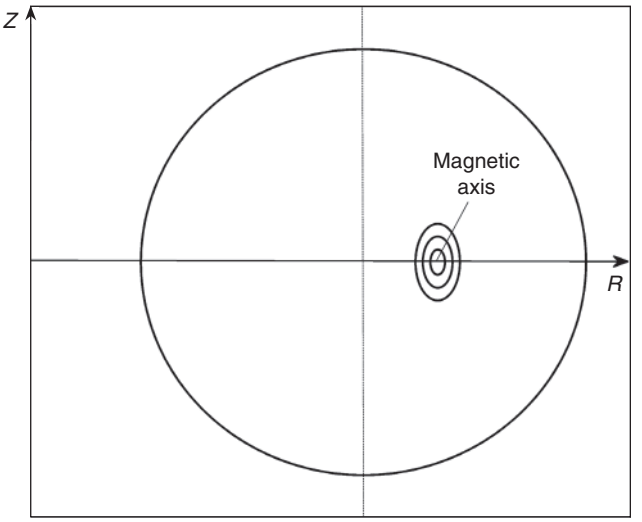

Figure 6.4 Elliptical flux surfaces near the magnetic axis.

derivatives of ψ vanish on the axis: $\psi_R(R_a, Z_a) = \psi_Z(R_a, Z_a) = 0$. Therefore, the Taylor expansion of ψ in the vicinity of the magnetic axis can be written as

$$\psi \approx \frac{\psi_{RR}}{2}(R - R_a)^2 + \frac{\psi_{ZZ}}{2}(Z - Z_a)^2 + \cdots \tag{6.36}$$

Here, the second derivatives are constants evaluated on the magnetic axis: $\psi_{RR} = \psi_{RR}(R_a, Z_a)$ and $\psi_{ZZ} = \psi_{ZZ}(R_a, Z_a)$. As shown in Fig. 6.4 the flux surfaces near the axis are ellipses.

Since the shape of the flux surfaces is known the general expression for the safety factor can now be easily integrated. One introduces new coordinates (ρ, α) defined by

$$\begin{aligned} R - R_a &= \left(\frac{2}{\psi_{RR}}\right)^{1/2} \rho \cos\alpha \\ Z - Z_a &= \left(\frac{2}{\psi_{ZZ}}\right)^{1/2} \rho \sin\alpha \end{aligned} \tag{6.37}$$

In these coordinates the equation for the flux surfaces become $\psi = \rho^2$.

To evaluate the integral, note that on a $\rho =$ constant flux surface,

$$dl = \left[(dR)^2 + (dZ)^2\right]^{1/2} = \left(\frac{2}{\psi_{RR}\psi_{ZZ}}\right)^{1/2} \left(\psi_{ZZ} \sin^2\alpha + \psi_{RR} \cos^2\alpha\right)^{1/2} \rho \, d\alpha \tag{6.38}$$

Similarly, the components of the poloidal magnetic field can be written as

$$B_R = -\frac{1}{R}\frac{\partial \psi}{\partial Z} = -\frac{1}{R_a}\psi_{ZZ}\,(Z - Z_a) = -\frac{1}{R_a}(2\psi_{ZZ})^{1/2}\rho\,\sin\alpha$$
$$B_Z = \frac{1}{R}\frac{\partial \psi}{\partial R} = \frac{1}{R_a}\psi_{RR}\,(R - R_a) = \frac{1}{R_a}(2\psi_{RR})^{1/2}\rho\,\cos\alpha \tag{6.39}$$

implying that

$$B_p = \left(B_R^2 + B_Z^2\right)^{1/2} = \frac{2^{1/2}}{R_a}\left(\psi_{ZZ}\,\sin^2\alpha + \psi_{RR}\,\cos^2\alpha\right)^{1/2}\rho \tag{6.40}$$

Observe that in the ratio dl/B_p the ρ factors exactly cancel thereby showing that as one approaches the magnetic axis, $\psi = \rho^2 \to 0$, the integrand remains finite.

Combining these results leads to the following simple integral for the safety factor on axis

$$q_0 \equiv q(0) = \frac{F(0)}{2\pi R_a}\frac{1}{(\psi_{RR}\psi_{ZZ})^{1/2}}\int_0^{2\pi} d\alpha \tag{6.41}$$

which reduces to the desired expression

$$q_0 = \frac{B_\phi}{(\psi_{RR}\psi_{ZZ})^{1/2}} = \left(\frac{B_\phi}{\mu_0 R_a J_\phi}\right)\left(\frac{1+\kappa_0^2}{\kappa_0}\right) \tag{6.42}$$

where $B_\phi = B_\phi(R_a, Z_a)$, $J_\phi = J_\phi(R_a, Z_a)$, and the elongation κ_0 are the on axis values.[1] The second form of q_0 is obtained from the facts that on the axis $\psi_{RR}/\psi_{ZZ} = \kappa_0^2$ and $\psi_{RR} + \psi_{ZZ} = -\mu_0 R_a J_\phi(R_a, Z_a)$.

6.3.7 *Alternate choices for* $\mathbf{F(\psi)}$

To solve the Grad–Shafranov equation it is necessary to specify the two free functions $p(\psi)$ and $F(\psi)$. Usually one has reasonable intuition based on experimental data or transport modeling to specify the pressure profile $p(\psi)$. The situation is not as straightforward with respect to the toroidal field profile $F(\psi)$. The reason is that $F(\psi)$ is often nearly a constant. Thus, the evaluation of $dF/d\psi$, the function actually needed in the Grad–Shafranov equation, is entirely dependent on the small deviation of $F(\psi)$ away from constancy. In practice, this small deviation is not easily known from intuition.

[1] Unfortunately the symbol κ is widely used in the fusion community for two descriptive purposes, the curvature and the plasma elongation. No attempt is made to counter this long standing tradition but it will be clear in the text which application is under consideration.

To resolve this problem it is sometimes useful to replace $F(\psi)$ with an alternate free function that is easier to specify intuitively. Two common replacements are the safety factor profile $q(\psi)$ and the average toroidal current density profile (which is defined below). For each case one needs to determine the relation between the alternate function and $dF^2/d\psi$ in order to make the proper replacement in the Grad–Shafranov equation.

Consider first the safety factor given by Eq. (6.35). The relation is straightforward in principle but complicated in practice:

$$F(\psi) = q(\psi)\left(\frac{1}{2\pi}\oint \frac{dl}{R^2 B_p}\right)^{-1} \tag{6.43}$$

Thus, if $q(\psi)$ is specified as a free function, one sees that the Grad–Shafranov equation becomes

$$\Delta^* \psi = -\mu_0 R^2 \frac{dp}{d\psi} - \frac{1}{2}\frac{d}{d\psi}\left[q^2(\psi)\left(\frac{1}{2\pi}\oint \frac{dl}{R^2 B_p}\right)^{-2}\right] \tag{6.44}$$

Note that the integrand must be viewed as a function of ψ and l. Specifically, $R^2 B_p = f(R,Z) = f[R(\psi,l), Z(\psi,l)] = \hat{f}(\psi,l)$.

Observe that the equation is now more complicated than the original one where $F(\psi)$ is specified. The right-hand side now contains not only functions of ψ, but poloidal arc length integrals over functions of ψ. The Grad–Shafranov equation has become an integro-differential equation whose properties are more difficult to understand analytically. However, in numerical schemes involving an iteration procedure, the more complicated right-hand side has little impact on obtaining a converged solution.

The second choice for an alternate free function is $\langle J_\phi \rangle$, the average toroidal current density. It is defined as follows. With the help of Eq. (6.20) one sees that the total toroidal current flowing within any given flux surface can be written as

$$I_\phi(\psi) = \int J_\phi \, \mathbf{e}_\phi \cdot d\mathbf{S} = \int_0^\psi d\psi \left(\oint J_\phi \frac{dl}{RB_p}\right) \tag{6.45}$$

The quantity $\langle J_\phi \rangle$ is the average current density, defined so that when integrated over the cross sectional area it yields the same value for $I_\phi(\psi)$:

$$I_\phi(\psi) \equiv \int \langle J_\phi \rangle \, \mathbf{e}_\phi \cdot d\mathbf{S} = \int_0^\psi d\psi \left(\langle J_\phi \rangle \oint \frac{dl}{RB_p}\right) \tag{6.46}$$

Since both expressions for $I_\phi(\psi)$ must be equal for any value of ψ it follows that $\langle J_\phi \rangle$, which is a function only of ψ, is given by

$$\langle J_\phi \rangle = \frac{\oint J_\phi \dfrac{dl}{RB_p}}{\oint \dfrac{dl}{RB_p}} \tag{6.47}$$

The relation between $\langle J_\phi \rangle$ and $dF^2/d\psi$ is obtained by recalling from Eqs. (6.15) and (6.16) that $\mu_0 R J_\phi$ is the negative of the right-hand side of the Grad–Shafranov equation. Substituting this information into the integral in the numerator of Eq. (6.47) leads to a relation between $\langle J_\phi \rangle$, $dp/d\psi$, and $dF^2/d\psi$. Assuming that $p(\psi)$ and $\langle J_\phi \rangle$ are the two free functions, one then finds from a short calculation that the Grad–Shafranov equation has the form

$$\Delta^* \psi = -\mu_0 R^2 \frac{dp}{d\psi} + \left(\mu_0 \frac{dp}{d\psi} \oint \frac{dl}{B_p} - \mu_0 \langle J_\phi \rangle \oint \frac{dl}{RB_p} \right) \left(\oint \frac{dl}{R^2 B_p} \right)^{-1} \tag{6.48}$$

The equation has again been transformed into an integro-differential equation.

Other choices for an alternate free function to replace $dF^2/d\psi$ can be made depending upon the application of interest. By and large these choices also lead to integro-differential equations.

6.4 Analytic solution in the limit $\varepsilon \ll 1$ and $\beta_p \sim 1$

The Grad–Shafranov equation has been derived and the figures of merit defined. The next step is to analyze the equation with the goals of obtaining some insight plus quantitative information as to how toroidal effects modify a purely cylindrical MHD equilibrium. The approach used in this section makes use of an asymptotic expansion in which the inverse aspect ratio is assumed to be small: $\varepsilon \ll 1$. Also, the poloidal beta is assumed to be of order unity: $\beta_p \sim 1$. It is shown that these assumptions lead to a sharp separation between the effects of radial pressure balance and toroidal force balance. Specifically, toroidal force balance enters the analysis as an order ε correction to radial pressure balance.

The separation of the two effects provides good insight into plasma behavior as the geometry is bent from a cylinder into a torus. Qualitatively, one consequence of toroidicity is to shift the inner flux surfaces outward (along R) with respect to the location of the plasma surface. A second consequence is that the plasma surface itself can be shifted outward with respect to the geometric center of the confining vacuum vessel. In fact the main goal of much of the analysis is to obtain quantitative, analytic expressions for these shifts.

With respect to the plasma parameters and figures of merit, one might expect that toroidicity simply adds small, relatively unimportant ε corrections to the cylindrical values. This is a correct intuition in the large aspect ratio, $\beta_p \sim 1$ regime.

The analysis is carried out by converting from the general R, ϕ, Z coordinates to a set of cylindrical-like coordinates r, θ, z centered in the plasma chamber. It then becomes a relatively straightforward procedure to solve the equations order by order in ε with the leading order corresponding to radial pressure balance and the first-order correction corresponding to toroidal force balance. Interestingly, the solution for the first-order correction can be obtained essentially analytically for an arbitrary zeroth-order circular cross section equilibrium.

Once derived the asymptotic analysis is then applied to the two cylindrical configurations already discussed in Chapter 5: the reversed field pinch and the low β, circular cross section, ohmically heated tokamak.

6.4.1 The coordinate transformation

To exploit the small ε expansion it is useful to transform the coordinates used in the Grad–Shafranov equation from R, ϕ, Z to a set of cylindrical-like coordinates r, θ, z. This transformation has been previously introduced (see Fig. 6.1) and is repeated here for convenience:

$$\begin{aligned} R &= R_0 + r\ \cos\ \theta \\ Z &= r\ \sin\ \theta \\ \phi &= -z/R_0 \end{aligned} \tag{6.49}$$

Note that both R, ϕ, Z and r, θ, z are right-handed coordinate systems. After a straightforward calculation one finds that the basic vector operations are given by

$$\begin{aligned} \nabla\psi &= \nabla_c\psi \\ \nabla\cdot\mathbf{B} &= \nabla_c\cdot\mathbf{B} + \frac{\mathbf{e}_R\cdot\mathbf{B}}{R} = \frac{1}{rR}\frac{\partial}{\partial r}(rRB_r) + \frac{1}{rR}\frac{\partial}{\partial\theta}(RB_\theta) + \frac{R_0}{R}\frac{\partial B_z}{\partial z} \\ \nabla\times\mathbf{B} &= \nabla_c\times\mathbf{B} - \frac{B_z}{R}\mathbf{e}_Z = \left[\frac{1}{rR}\frac{\partial}{\partial\theta}(RB_z) - \frac{R_0}{R}\frac{\partial B_\theta}{\partial z}\right]\mathbf{e}_r \\ &\quad + \left[\frac{R_0}{R}\frac{\partial B_r}{\partial z} - \frac{1}{R}\frac{\partial}{\partial r}(RB_z)\right]\mathbf{e}_\theta + \left[\frac{1}{r}\frac{\partial}{\partial r}(rB_\theta) - \frac{1}{r}\frac{\partial B_r}{\partial\theta}\right]\mathbf{e}_z \\ \mathbf{e}_R &= \cos\ \theta\,\mathbf{e}_r - \sin\ \theta\,\mathbf{e}_\theta \\ \mathbf{e}_Z &= \sin\ \theta\,\mathbf{e}_r + \cos\ \theta\,\mathbf{e}_\theta \\ \mathbf{e}_\phi &= -\mathbf{e}_z \end{aligned} \tag{6.50}$$

Here, ∇_c is the standard gradient operator in a linear r, θ, z cylindrical coordinate system with $\partial/\partial z$ replaced by $(R_0/R)\partial/\partial z$.

$$\nabla_c = \mathbf{e}_r\,\frac{\partial}{\partial r} + \mathbf{e}_\theta\,\frac{1}{r}\frac{\partial}{\partial\theta} + \mathbf{e}_z\,\frac{R_0}{R}\frac{\partial}{\partial z} \tag{6.51}$$

A short calculation that makes use of these results shows that the two-dimensional Δ^* operator appearing in the Grad–Shafranov equation can be expressed as

$$\Delta^* \psi = \frac{1}{r}\frac{\partial}{\partial r}\left(r\frac{\partial \psi}{\partial r}\right) + \frac{1}{r^2}\frac{\partial^2 \psi}{\partial \theta^2} - \frac{1}{R}\left(\cos\,\theta \frac{\partial \psi}{\partial r} - \frac{\sin\,\theta}{r}\frac{\partial \psi}{\partial \theta}\right) \tag{6.52}$$

Consequently, in terms of the cylindrical-like coordinates the Grad–Shafranov equation becomes

$$\nabla_c^2 \psi = -\mu_0 R^2 \frac{dp}{d\psi} - \frac{1}{2}\frac{dF^2}{d\psi} + \frac{1}{R}\left(\cos\,\theta \frac{\partial \psi}{\partial r} - \frac{\sin\,\theta}{r}\frac{\partial \psi}{\partial \theta}\right) \tag{6.53}$$

where $R = R_0 + r\cos\,\theta$.

6.4.2 The asymptotic expansion

An asymptotic solution to the Grad–Shafranov equation can be obtained by focusing attention on a large aspect ratio, circular cross section plasma whose pressure corresponds to $\beta_p \sim 1$. In order to carry out the analysis a small parameter must be identified and all quantities ordered with respect to this parameter. For the situation of interest the small parameter is the inverse aspect ratio

$$\varepsilon \equiv a/R_0 \ll 1 \tag{6.54}$$

where R_0 and a are the major and minor radii of the plasma respectively. Conceptually, the plasma geometry is more akin to a bicycle tire than a donut.

To define the expansion it is convenient to normalize all quantities with respect to the poloidal magnetic field in the plasma. The assumption $\beta_p \sim 1$ thus requires that the pressure be ordered as

$$\frac{2\mu_0 p}{B_p^2} \sim 1 \tag{6.55}$$

Similarly, the definition of the flux function requires that

$$\frac{\psi}{aR_0B_p} \sim 1 \tag{6.56}$$

The situation with the free function $F(\psi)$ is slightly more complicated. The reason is that, in general, F^2 can be written as $F^2(\psi) = R_0^2B_0^2 + G(\psi)$, where $B_0 =$ constant is the applied vacuum toroidal field. The quantity R_0B_0 can be zero, small, medium, or large. Its value does not affect the Grad–Shafranov equation since only the derivative $dF^2/d\psi$ is required. The value of $dF^2/d\psi$ thus depends only on the new free function $G(\psi)$, which represents the diamagnetism

or paramagnetism of the toroidal field. The magnitude of $G(\psi)$ cannot be too large. For large positive G (i.e., too much paramagnetism) radial pressure balance is possible only if $\beta_p \ll 1$. For large negative G (i.e., too much diamagnetism) radial pressure balance is possible but only if $\beta_p \gg 1$. Both of these extremes thereby violate the basic ordering assumption $\beta_p \sim 1$. The net result is that the quantity $dF^2/d\psi = dG/d\psi$ can be positive or negative but must be ordered such that it is competitive in size with the pressure gradient term. This requires that

$$\frac{\varepsilon}{B_p}\frac{dF^2}{d\psi} \sim 1 \tag{6.57}$$

Equations (6.55)–(6.57) define the ordering scheme necessary to solve the Grad–Shafranov equation. The asymptotic analysis now proceeds as follows. First, the flux function is expanded as a series in ε:

$$\begin{aligned} \psi(r,\theta) &= \psi_0(r) + \psi_1(r,\theta) + \cdots \\ \psi_0/aR_0B_p &\sim 1 \\ \psi_1/aR_0B_p &\sim \varepsilon \end{aligned} \tag{6.58}$$

Here, $\psi_0(r)$ represents the leading order cylindrically symmetric contribution to ψ while $\psi_1(r, \theta)$ represents the small correction due to toroidal effects. Similarly, the free functions are Taylor expanded as

$$\begin{aligned} \frac{dp(\psi)}{d\psi} &= \frac{dp}{d\psi_0} + \frac{d^2p}{d\psi_0^2}\psi_1 + \cdots \\ \frac{dF^2(\psi)}{d\psi} &= \frac{dF^2}{d\psi_0} + \frac{d^2F^2}{d\psi_0^2}\psi_1 + \cdots \end{aligned} \tag{6.59}$$

One substitutes these expansions into the Grad–Shafranov equation (i.e., Eq. (6.53)), and sets the coefficient of each power of ε to zero. This leads to a sequence of equations, one for each power of ε. For the present analysis only the ε^0 and ε^1 equations are needed and these are discussed below.

6.4.3 The ε^0 equation: radial pressure balance

The zeroth-order contribution to the Grad–Shafranov equation is given by

$$\frac{1}{r}\frac{d}{dr}\left(r\frac{d\psi_0}{dr}\right) = -\mu_0 R_0^2\frac{dp}{d\psi_0} - \frac{1}{2}\frac{dF^2}{d\psi_0} \tag{6.60}$$

This equation can be put in a more familiar form by noting that the zeroth-order fields can be written as

$$\begin{aligned} B_{r0}(r) &= 0 \\ B_{\theta 0}(r) &= \frac{1}{R_0}\frac{d\psi_0}{dr} \\ B_{z0}(r) &= -\frac{F(\psi_0)}{R_0} \\ p_0(r) &= p(\psi_0) \end{aligned} \tag{6.61}$$

Then, after making the replacement $(d/d\psi_0) = (1/R_0 B_{\theta 0})(d/dr)$, one obtains

$$\frac{d}{dr}\left(p_0 + \frac{B_{z0}^2}{2\mu_0}\right) + \frac{B_{\theta 0}}{\mu_0 r}\frac{d}{dr}(rB_{\theta 0}) = 0 \tag{6.62}$$

As expected, this is just the radial pressure balance for the general screw pinch.

An important step that further simplifies the analysis is the following. To solve the Grad–Shafranov equation it is necessary to specify two free "one-dimensional" functions, $p(\psi)$ and $F(\psi)$. They are "one dimensional" in the sense that even though the geometry is two dimensional, each free function depends only on a single variable, ψ. Therefore, it is entirely equivalent to specify two alternate "one-dimensional" functions. For the present analysis a convenient choice is $p_0(r)$ and $B_{\theta 0}(r)$. Radial pressure balance then gives $B_{z0}(r)$ and the flux is obtained from $\psi_0(r) = R_0 \int B_{\theta 0} dr$. Finally, the original free functions can be evaluated by inverting the flux relation, giving $r = r(\psi_0)$ and then substituting into $p(\psi_0) = p_0[r(\psi_0)]$ and $F(\psi_0) = -R_0 B_{z0}[r(\psi_0)]$.

Hereafter it is assumed that a zeroth-order cylindrical equilibrium solution has been specified that satisfies Eq. (6.62) with $p_0(r)$ and $B_{\theta 0}(r)$ serving as the two free functions.

6.4.4 The ε^1 equation: toroidal force balance

Consider now the first-order toroidal corrections to the Grad–Shafranov equation. A straightforward calculation leads to a complicated looking equation for determining the perturbed flux $\psi_1(r, \theta)$:

$$\nabla^2 \psi_1 + \left[\frac{d^2}{d\psi_0^2}\left(\mu_0 R_0^2 p + \frac{F^2}{2}\right)\right]\psi_1 = -\left(2\mu_0 R_0 r \frac{dp}{d\psi_0} - \frac{1}{R_0}\frac{d\psi_0}{dr}\right)\cos\theta \tag{6.63}$$

Here, $\nabla^2 = \nabla_c^2$ is the usual two-dimensional cylindrical Laplacian (with the subscript c suppressed from ∇_c^2 for simplicity) and p, F are free functions of ψ_0 whose dependence is determined by the procedure described in the previous subsection.

Equation (6.63) can actually be solved analytically. To begin, observe that the inhomogeneous forcing terms all have the same dependence on poloidal angle,

proportional to cos θ. This fact, coupled with the assumption that the plasma boundary is circular, implies that $\psi_1(r, \theta)$ can be written as

$$\psi_1(r, \theta) = \overline{\psi}_1(r) \cos \theta \tag{6.64}$$

After some algebra, where multiple use is again made of the replacement $(d/d\psi_0) = (1/R_0 B_{\theta 0})(d/dr)$ and then combined with the zeroth-order radial pressure balance relation, one obtains the following simplified equation for $\overline{\psi}_1(r)$:

$$\frac{d}{dr}\left[rB_\theta^2 \frac{d}{dr}\left(\frac{\overline{\psi}_1}{B_\theta}\right)\right] = rB_\theta^2 - 2\mu_0 r^2 \frac{dp}{dr} \tag{6.65}$$

Here the subscript 0 has been dropped from the zeroth-order quantities to simplify the notation.

This equation can be easily integrated once boundary conditions are specified. For the moment, however, the boundary conditions are left open and the general solution is written in terms of two arbitrary integrations constants. The choices for these constants depend upon the configuration of interest. Specific choices are described in the next two subsections where the theory is applied to the reversed field pinch and the low β tokamak.

To solve for $\overline{\psi}_1(r)$ observe that the first integral of Eq. (6.65) is given by

$$\frac{d}{dr}\left(\frac{\overline{\psi}_1}{B_\theta}\right) = \frac{1}{rB_\theta^2(r)} \int_{r_1}^{r} \left[yB_\theta^2(y) - 2\mu_0 y^2 \frac{dp(y)}{dy}\right] dy \tag{6.66}$$

Here, r_1 is the first free integration constant. Equation (6.66) can be integrated a second time yielding an expression for $\overline{\psi}_1(r)$:

$$\overline{\psi}_1(r) = B_\theta(r) \int_{r_2}^{r} \frac{dx}{xB_\theta^2(x)} \int_{r_1}^{x} \left[yB_\theta^2(y) - 2\mu_0 y^2 \frac{dp(y)}{dy}\right] dy \tag{6.67}$$

with r_2 being the second integration constant.

This is the desired solution for the toroidal correction to the Grad–Shafranov equation. Once the cylindrical profiles $p(r)$, $B_\theta(r)$ plus two boundary conditions are specified, it is then a straightforward task, at least in principle, to evaluate the integrals to determine $\overline{\psi}_1(r)$.

Lastly, observe that qualitatively the toroidal solution shows that bending a cylindrical screw pinch into a torus results in a set of nested circular flux surfaces whose centers are no longer concentric but are now shifted radially outward along R with respect to one another. This can be seen by noting that the equation for a shifted circle of radius r_0 is given by

$$(x - \Delta)^2 + y^2 = r_0^2 \tag{6.68}$$

where Δ is the shift along R and the coordinate system is centered about the major radius $R = R_0$. If one sets $x = r\cos\theta$, $y = r\sin\theta$, and assumes that the shift is small, $\Delta/r_0 \sim r_0/R_0 \ll 1$, it then follows that in (r, θ) coordinates the equation for a shifted circle can be approximated by

$$r \approx r_0 + \Delta\cos\ \theta \tag{6.69}$$

Now, the equation for the flux surfaces is given by

$$\psi(r,\theta) \approx \psi_0(r) + \overline{\psi}_1(r)\cos\ \theta = \text{constant} \tag{6.70}$$

For the surface whose minor radius is r_0 this equation can be inverted to give $r = r(r_0, \theta)$ by writing $r \approx r_0 + r_1(r_0, \theta)$ assuming that $r_1 \ll r_0$. The result is

$$r \approx r_0 + r_1(r_0,\theta) \approx r_0 - \frac{\overline{\psi}_1(r_0)}{\psi_0'(r_0)}\cos\ \theta \tag{6.71}$$

A comparison of Eqs. (6.71) and (6.69) shows that the flux surfaces are indeed shifted circles with the shift given by

$$\Delta(r_0) = -\frac{\overline{\psi}_1(r_0)}{R_0\, B_\theta(r_0)} \tag{6.72}$$

The shift is outward since $\overline{\psi}_1 < 0$ for realistic boundary conditions. In the applications that follow attention is focused on the evaluation of the flux surface shift.

6.4.5 Application to early reversed field pinches (RFP)

The first application of the toroidal correction to the Grad–Shafranov equation is to early RFP experiments. Such experiments were relatively short lived, usually due to power supply limitations. Importantly, the plasma was surrounded by a thick conducting wall. Relative to the short plasma lifetime the skin diffusion time of the conducting wall was long, implying that for practical purposes the wall behaved like a perfect conductor. The wall thus defined the edge of the plasma: $p(a) = 0$.

The question of interest that then arises is to determine the shift of the magnetic axis with respect to the center of the conducting wall. The geometry is illustrated in Fig. 6.5. To address this question two boundary conditions are needed to determine $\overline{\psi}_1$ and the corresponding shift of the axis. Since the conducting wall defines the edge of the plasma the first boundary condition requires that $\psi(a, \theta) =$ constant or equivalently $\overline{\psi}_1(a) = 0$. From Eq. (6.67) it then follows that the integration constant $r_2 = a$.

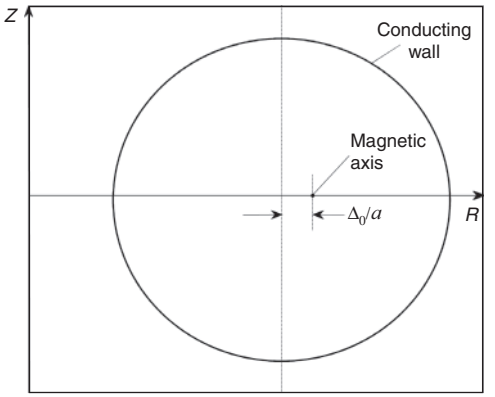

Figure 6.5 Magnetic axis shift with respect to the center of the conducting wall.

The other integration constant is determined from the condition that the solution for $\overline{\psi}_1$ be regular everywhere in the plasma, including $r = 0$. Equation (6.66) shows that regularity requires $r_1 = 0$. The solution for the perturbed flux function reduces to

$$\overline{\psi}_1(r) = -B_\theta(r)\int_r^a \frac{dx}{xB_\theta^2(x)}\int_0^x \left[yB_\theta^2(y) - 2\mu_0 y^2\frac{dp(y)}{dy}\right]dy \tag{6.73}$$

The quantity $\overline{\psi}_1(r)$ is determined by using the profiles discussed in Section 5.5.2, repeated here for convenience:

$$\begin{aligned}
\frac{2\mu_0 p(\rho)}{B_{z0}^2} &= \frac{140}{81}\alpha_p(1-\rho^6)^3 \\
\frac{B_\theta^2(\rho)}{B_{z0}^2} &= \frac{\alpha_p}{9}(35\rho^6 - 40\rho^{12} + 14\rho^{18}) + \frac{\alpha_z}{15}[30\rho^2 - 20(2\alpha_z+1)\rho^4 + 45\alpha_z\rho^6 - 12\alpha_z\rho^8] \\
\alpha_z &= 1 - \frac{B_{za}}{B_{z0}} \\
\alpha_p &= \frac{\alpha_z(10-7\alpha_z)}{15}\frac{\beta_p}{1-\beta_p} \\
\rho &= \frac{r}{a}
\end{aligned} \tag{6.74}$$

These are substituted into Eq. (6.73). The y integration can be carried out analytically. The resulting expression for $\overline{\psi}_1(r)$ is then used to calculate the shift of the

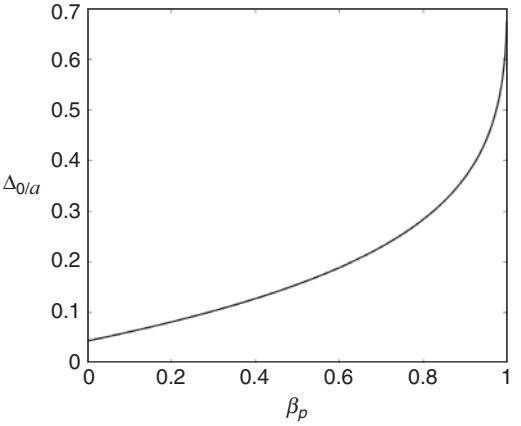

Figure 6.6 Curve of Δ_0/a vs. β_p for the case of $R_0/a = 5$ and $\alpha_z = 1.1$.

axis, defined by Eq. (6.72): $\Delta_0 = -\psi_1(r \to 0)/R_0 B_\theta(r \to 0)$. The limit as $r \to 0$ is finite and a short calculation yields

$$\frac{\Delta_0}{a} = \frac{a}{R_0}\int_0^1 dx \frac{x^3}{B_\theta^2/B_{z0}^2}\, g(x, \alpha_p, \alpha_z)$$
$$g = \frac{\alpha_p}{3}(109x^4 - 200x^{10} + 98x^{16}) + \frac{\alpha_z}{2}\left[1 - \frac{4}{9}(2\alpha_z + 1)x^2 + \frac{3}{4}\alpha_z\, x^4 - \frac{4}{25}\alpha_z\, x^6\right] \tag{6.75}$$

A numerically obtained curve of Δ_0/a vs. β_p is illustrated in Fig. 6.6 for the case of $R_0/a = 5$ and $\alpha_z = 1.1$ corresponding to a 10% reversal. Observe that as expected the shift of the axis increases with β_p primarily because of the larger tire tube force. The shift increases substantially as β_p increases. Even so the absolute shift remains relatively small for moderate β_p in an RFP because of the small inverse aspect ratio, $a/R_0 \sim 0.2$.

6.4.6 Application to early ohmic tokamaks and modern reversed field pinches

The last application of interest involves early ohmically heated tokamaks and modern RFPs. These devices are characterized by circular cross section plasmas with values of poloidal beta satisfying $\beta_p \lesssim 1$. The plasmas are often surrounded by a thin circular conducting wall of moderate resistivity (e.g. stainless steel), which serves as the vacuum chamber. Such devices therefore satisfy the assumptions made in the derivation of the perturbed flux function.

The key point to recognize is that typical experimental pulse lengths are long compared to the skin diffusion time of the wall. The implication is that during an experimental pulse the fields have time to diffuse through the wall which then loses its ability to provide a toroidal restoring force. A vertical field is thus required to hold the plasma in toroidal force balance.

The fact that the wall is thin has both pros and cons. On the positive side a thin wall is good in order to (1) allow rapid vertical field penetration, resulting in a sufficiently fast response time for the horizontal positioning feedback system, and (2) keep the transient currents in the vacuum chamber to a tolerable level because of the higher wall resistivity. On the negative side the faster wall diffusion time through a thin wall implies a quicker loss of plasma equilibrium. Solving this problem requires a faster response time in the feedback system, which adds to the technological difficulty. In practice, careful engineering tradeoffs are balanced to arrive at an optimum design.

In this subsection the basic MHD question addressed (originally by Shafranov, 1960) is to determine the magnitude and direction of the vertical field required to keep the plasma centered in the vacuum chamber.

Now, from a practical point of view, any metallic wall in contact with the plasma would force the edge temperature of the plasma to become low and the wall temperature to become high. In particular, as particles and energy are transported across the field, they would have to be absorbed by the thin wall which, because of its fragile structure, would rapidly become damaged, perhaps developing burn spots and leaks. Clearly this is unacceptable.

Two methods have been proposed to alleviate this problem: limiters and divertors. The limiter idea is most applicable to early tokamaks and modern RFPs. As such, a temporary digression is made from the toroidal equilibrium calculation to describe the operation of a limiter. This discussion will help formulate the proper boundary conditions required to calculate $\overline{\psi}_1$. The divertor is discussed in Section 6.6.5.

Operation of a limiter

A limiter is a robust piece of material often made of tungsten, molybdenum, or graphite, placed just inside the vacuum chamber. It protects the vacuum chamber from plasma bombardment and serves to define the edge of the plasma. Limiters come in various shapes. Three common examples are the poloidal ring limiter, the toroidal hoop limiter, and the rail limiter, shown in Fig. 6.7.

The basic idea of limiter operation is as follows. To a lowest approximation, within the plasma, particles spiral along the magnetic field with a typical velocity comparable to their thermal speed: $v_{\|} \sim V_T$. Both electrons and ions slowly diffuse across the magnetic field at the same collisional transport rate (i.e., due to

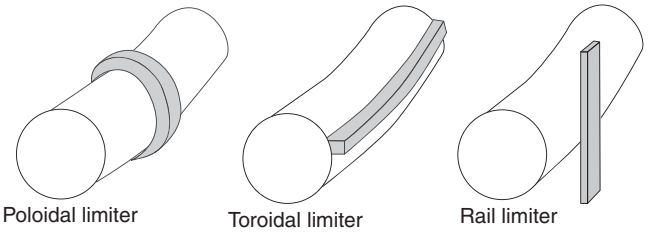

Figure 6.7 Schematic diagram of a poloidal ring limiter, toroidal hoop limiter, and toroidal rail limiter.

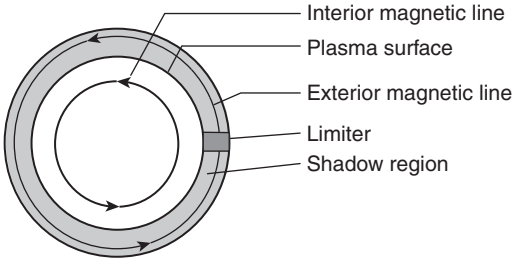

Figure 6.8 Shadow region of a limiter. Observe that magnetic lines in the shadow region make direct contact with the limiter.

ambipolar diffusion) and enter the shadow region of the limiter as shown in Fig. 6.8. In the shadow region the particles, because of their high parallel velocities, strike the limiter surface in a short time, well before they have a chance to diffuse radially and strike the vacuum chamber wall: $L_\parallel/C_\parallel \ll L_\perp^2/D_\perp$. Here, $L_\parallel$ is the parallel distance traveled by a particle, $C_\parallel = (T_e + T_i)^{1/2}/m_i^{1/2}$ is the parallel sound speed, $L_\perp$ is the perpendicular width of the scrape-off layer, and $D_\perp$ is the cross field diffusion rate, usually anomalous. Note that parallel to the field, electrons and ions must be lost at the same rate (again because of ambipolarity) in a characteristic time $\tau \sim L_\parallel/C_\parallel$. By this operation the limiter protects the vacuum chamber and defines the edge of the plasma.

Ideally one wants a limiter of sturdy and durable construction that can absorb a large flux of particles and energy while maintaining its structural integrity and not producing any adverse effects on the plasma. In practice plasma bombardment slowly causes damage but limiters are designed for much easier replacement than the vacuum chamber itself. Even so there remains an important problem. The plasma–limiter interaction causes particles to escape from the limiter surface, usually by sputtering. Especially troublesome are limiter neutrals that can penetrate some distance into the plasma before becoming ionized. These high-Z impurities can lead to significant energy loss through radiation. It is clearly important to minimize these losses. This may not be possible in very long pulse experiments, or

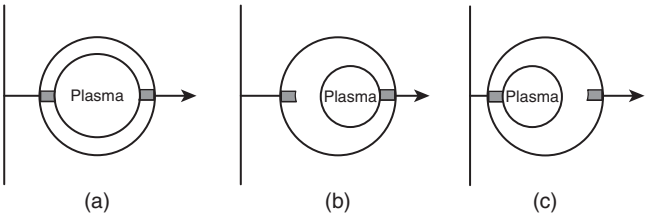

Figure 6.9 Plasma position between the limiters with (a) a correct choice of vertical field, (b) too small a vertical field, and (c) too large a vertical field.

in fusion reactors. The need for impurity shielding in addition to wall protection has led to the development of a second idea, the plasma divertor discussed in Section 6.6.5.

From the ideal MHD point of view the boundary conditions appropriate to a system with axisymmetric toroidal limiters correspond to those of a plasma whose last closed flux surface coincides with the inner surface of each limiter. For a plasma with a minor radius $r = a$ the limiters are located at $R = R_0 \pm a$. The wall radius is denoted by $r = b > a$. Between a and b is a cold, low-density plasma with a small pressure and very little, if any, current. For all practical purposes the magnetic field in the region $a < r < b$ is a vacuum field. The purpose of the vertical field is thus to position the last closed plasma flux surface exactly between the limiters as shown in Fig. 6.9. Also shown are the consequences of too little or too much applied vertical field.

Mathematically, the goal of the MHD analysis is to calculate the shift of the last closed flux surface with respect to the center of the vacuum chamber and then choose the vertical field so that this shift is zero: $\Delta(a) \equiv \Delta_a = 0$. One could also easily calculate the shift of the magnetic axis but this is of less interest.

Calculation of the vertical field

The discussion of the limiter enables one to specify the boundary conditions necessary to complete the solution for $\overline{\psi}_1$ given by Eq. (6.67); that is, to give values for the integration constants r_1 and r_2.

Regularity of the solution in the interior of the plasma again requires that $r_1 = 0$. The constant r_2 is evaluated by the following argument. The end goal is to determine the vertical field necessary to keep the plasma surface, $r = a$, centered in the vacuum chamber which, as stated above, is equivalent to setting $\Delta_a = 0$. Now, recall from Eq. (6.72) that the shift of the last closed flux surface is given by

$$\Delta_a = -\frac{\overline{\psi}_1(a)}{R_0 B_\theta(a)} \tag{6.76}$$

The $\Delta_a = 0$ requirement, therefore, corresponds to the boundary condition $\overline{\psi}_1(a) = 0$ which implies that $r_2 = a$. The perturbed flux function reduces to

$$\overline{\psi}_1(r) = B_\theta(r) \int_a^r \frac{dx}{xB_\theta^2(x)} \int_0^x \left[yB_\theta^2(y) - 2\mu_0 y^2 \frac{dp(y)}{dy} \right] dy \tag{6.77}$$

The vertical field is determined by extending the solution for $\overline{\psi}_1(r)$ to the region far outside the plasma surface, $a \ll r \ll R_0$, and then matching the solution to the known fields in this region. Specifically, in this region the magnetic field consists of two contributions: the vacuum field due to a "plasma wire" carrying a current I centered at $R = R_0 + \Delta_a \approx R_0$, and an externally applied vacuum vertical field $\mathbf{B}_V = B_V \mathbf{e}_Z$, which is treated as a small, first-order quantity. All plasma diamagnetic effects are small and can be neglected far from the plasma corresponding to $a \ll r \ll R_0$.

The magnetic flux due to the plasma wire is easily evaluated from the standard theory of magnetostatics. For a thin circular wire of major radius R_0 carrying a current I the flux can be expressed as (Stratton, 1941)

$$\begin{aligned} \psi_I &= -\frac{\mu_0 I}{\pi} \frac{(RR_0)^{1/2}}{2k} \left[\left(2 - k^2\right) K - 2E \right] + C_0 \\ k^2 &= \frac{4RR_0}{(R + R_0)^2 + Z^2} \end{aligned} \tag{6.78}$$

where $K(k)$ and $E(k)$ are the complete elliptic integrals and C_0 is an arbitrary, additive constant. In the relevant regime where $a \ll r \ll R_0$ the elliptic functions can be expanded as follows:

$$\begin{aligned} k &\approx 1 \\ k' &= \left(1 - k^2\right)^{1/2} \approx \frac{r}{2R_0} \left(1 - \frac{r}{2R_0} \cos\ \theta \right) \\ E &\approx 1 \\ K &\approx \ln \frac{4}{k'} = \ln \frac{8R_0}{r} + \frac{r}{2R_0} \cos\ \theta \end{aligned} \tag{6.79}$$

Substituting these relations into Eq. (6.78) leads to a simplified form of the wire contribution to the flux far from the plasma:

$$\psi_I(r, \theta) \to -\frac{\mu_0 I R_0}{2\pi} \left[\ln \frac{8R_0}{r} - 2 + C_0' + \left(\ln \frac{8R_0}{r} - 1 \right) \frac{r}{2R_0} \cos\ \theta \right] \tag{6.80}$$

Here, C_0' is a new arbitrary constant replacing C_0. Its value is not important for calculating the flux surface shift; that is, the zeroth-order magnetic field, whose value is necessary to calculate the shift, is given by $R_0 B_\theta = d\psi_0/dr$, which is independent of the additive constant.

Next, note that the flux function for a vacuum vertical field of magnitude B_V is given by $\psi_V = R_0 B_V r \cos\theta$. Thus, combining this relation with Eq. (6.80) shows that the total flux function $\psi = \psi_I + \psi_V$ for $r \gg a$ must approach

$$\psi(r,\theta) \to -\frac{\mu_0 R_0 I}{2\pi}\left[\ln\frac{8R_0}{r} - 2 + C_0' + \left(\ln\frac{8R_0}{r} - 1\right)\frac{r}{2R_0}\cos\theta\right] + R_0 B_V r\cos\theta \tag{6.81}$$

The condition on the zeroth-order contribution to ψ is satisfied automatically; that is, for $r \gg a$ one finds from Eq. (6.81) that $B_\theta(r) = (1/R_0)d\psi_0/dr = \mu_0 I / 2\pi r$, which is the correct result. The first-order contribution requires matching the $\cos\theta$ in Eq. (6.81) with $\overline{\psi}_1(r)\cos\theta$ evaluated at $r \gg a$,

$$\overline{\psi}_1(r) \to -\frac{\mu_0 I}{4\pi}\left(\ln\frac{8R_0}{r} - 1\right)r + R_0 B_V r \tag{6.82}$$

The task now is to evaluate the $\overline{\psi}_1$, given by Eq. (6.77), for large r. Matching in accordance with Eq. (6.82) then yields the desired value of B_V.

Consider first the terms in the square bracket in Eq. (6.77), keeping in mind that the regime of interest corresponds to $x > a$. In this regime the pressure is zero, implying that

$$\begin{aligned} -\int_0^x 2\mu_0 y^2 \frac{dp(y)}{dy}\,dy &= -\int_0^a 2\mu_0 y^2 \frac{dp(y)}{dy}\,dy \\ &= 4\mu_0 \int_0^a p(y) y\,dy \\ &= a^2 B_{\theta a}^2 \beta_p \end{aligned} \tag{6.83}$$

where $B_{\theta a} = \mu_0 I / 2\pi a$.

Next, in the region $x > a$ there is zero toroidal current, implying that B_θ is a vacuum field: $B_\theta = B_{\theta a}(a/r)$. Therefore, the magnetic energy term can be split into two contributions, one from $0 < y < a$ and the other from $a < y < x$:

$$\begin{aligned} \int_0^x y B_\theta^2(y)dy &= \int_0^a y B_\theta^2(y)dy + \int_a^x y B_\theta^2(y)dy \\ &= a^2 B_{\theta a}^2\left(\frac{l_i}{2} + \ln\frac{x}{a}\right) \end{aligned} \tag{6.84}$$

Here, l_i is the normalized internal plasma inductance per unit length defined by

$$\begin{aligned} l_i &\equiv \frac{L_i/2\pi R_0}{\mu_0/4\pi} \\ \frac{1}{2}L_i I^2 &= \int_P \frac{B_\theta^2}{2\mu_0}\,d\mathbf{r} \end{aligned} \tag{6.85}$$

which leads to

$$l_i = \frac{2}{a^2 B_{\theta a}^2} \int_0^a B_\theta^2 \, y dy \tag{6.86}$$

For the model ohmic tokamak profiles discussed in Section 5.5.2, where $\rho = y/a$ and $B_\theta = B_{\theta a} J_1(k\rho)/J_1(k)$, the value of the normalized internal inductance is $l_i = 1$.

Combining these results leads to the following expression for the square bracket in Eq. (6.77):

$$\int_0^x \left[y B_\theta^2(y) - 2\mu_0 y^2 \frac{dp(y)}{dy} \right] dy = a^2 B_{\theta a}^2 \left(\beta_p + \frac{l_i}{2} + \ln \frac{x}{a} \right) \tag{6.87}$$

The remaining integral over x can be easily evaluated by again recalling that for $x > a$, the magnetic field $B_\theta = B_{\theta a}(a/x)$. This yields

$$\overline{\psi}_1(r) = \frac{\mu_0 I}{4\pi r} \left[\left(\beta_p + \frac{l_i}{2} - \frac{1}{2} \right) (r^2 - a^2) + r^2 \ln \frac{r}{a} \right] \tag{6.88}$$

The limit of this expression for $r \gg a$ is

$$\overline{\psi}_1(r) \to \frac{\mu_0 I}{4\pi} \left(\beta_p + \frac{l_i}{2} - \frac{1}{2} + \ln \frac{r}{a} \right) r \tag{6.89}$$

The final step is to equate Eq. (6.89) to Eq. (6.82) and solve for B_V:

$$B_V = \frac{\mu_0 I}{4\pi R_0} \left(\beta_p + \frac{l_i - 3}{2} + \ln \frac{8R_0}{a} \right) \tag{6.90}$$

This well-known and often used result was first derived by Shafranov (1966). It provides valuable information about the design requirements for the vertical field circuit, in particular how large is the required vertical field to center the plasma as a function of toroidal current and geometry. The formula also shows that B_V is positive which, with the present sign convention, implies that the vertical field increases the overall B_p on the outside of the torus and decreases it on the inside. As expected the magnetic tension on the outside increases in order to support higher values of pressure in toroidal force balance.

While Eq. (6.90) is simple in appearance, it is somewhat unintuitive in that the individual contributions are not easily recognizable in terms of the forces holding the plasma in toroidal equilibrium. A more intuitive form, valid for an ohmic tokamak, is obtained by multiplying by $2\pi R_0 I$ and then performing some standard manipulations. This enables Eq. (6.90) to be rewritten as

$$2\pi R_0 I B_V = \frac{I^2}{2} \frac{\partial}{\partial R_0} (L_e + L_i) + 4\pi^2 \int_0^a \left(p - \frac{B_0 \delta B_z}{\mu_0} \right) r dr \tag{6.91}$$

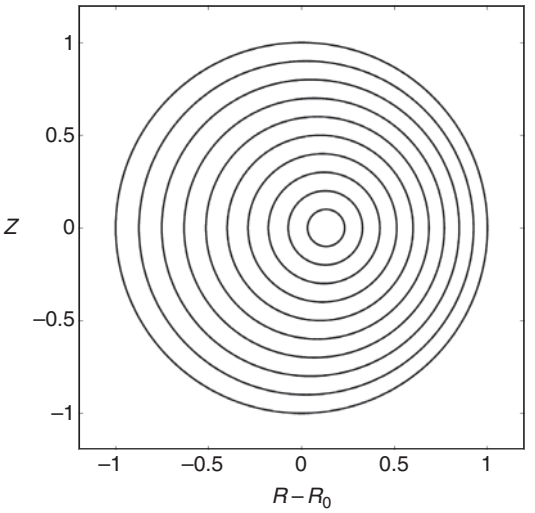

Figure 6.10 Numerically computed equilibrium for the Alcator C tokamak at MIT. Shown are flux surface plots for a typical low β ohmically heated plasma.

where $\delta B_z(r) = B_z(r) - B_0 \ll B_0$. The left-hand side represents the vertical field force. The first term on the right-hand side represents the hoop force[2] and includes the total internal plus external poloidal flux. To obtain this term requires use of the facts that $L_i(R_0) = \mu_0 R_0 l_i/2 \propto R_0$ and for a thin wire $L_e(R_0) = \mu_0 R_0[\ln(8R_0/a) - 2]$. The pressure term represents the tire tube force while the last term represents the $1/R$ force due to the toroidal field.

The basic MHD features of an ohmically heated tokamak as described by the large aspect ratio expansion are verified by a full non-linear numerical solution of the Grad–Shafranov equation for the Alcator C tokamak as illustrated in Fig. 6.10. The analytic, shifted circle equilibrium does indeed appear to be a good approximation to the exact numerical results.

6.4.7 Summary

The Grad–Shafranov equation has been solved by means of an asymptotic expansion in the inverse aspect ratio: $\varepsilon \ll 1$ and $\beta_p \sim 1$. The ε^0 contribution describes cylindrical radial pressure balance. The ε^1 contribution is a small correction that describes toroidal force balance. The main consequence of toroidicity is to shift the central flux surfaces outward along R with respect to the plasma surface.

[2] Conceptually, the hoop force can be calculated as the gradient of the "potential energy" subject to the perfect conductivity constraint of fixed flux within the plasma: $F_{\text{hoop}} = -\mathbf{e}_R \cdot \nabla\,(LI^2/2)$ subject to $LI =$ constant.

An analytic formula is derived that gives the value of the flux surface shift. This formula is applied to two configurations of interest: (1) the early RFP in which the shift of the magnetic axis with respect to the plasma surface is calculated, and (2) the ohmic tokamak and modern RFP in which the vertical field necessary to center the plasma within the limiter is calculated.

Because of the assumption of small ε the plasma parameters and figures of merit are nearly identical to their simple cylindrical values.

6.5 Analytic solution in the limit $\varepsilon \ll 1$ and $\beta_p \sim 1/\varepsilon$ (the high β tokamak)

The discussion in the previous section has demonstrated several desirable MHD features of the ohmically heated tokamak: good toroidal equilibrium (i.e., small shift), good stability (i.e., $q \sim 1$). Experimentally, ohmically heated tokamaks also exhibit good confinement, and good ohmic heating. Nevertheless, the fact that β is inherently small is an important disadvantage with respect to the efficient production of energy in a fusion reactor. It is thus of interest to investigate modifications to the basic ohmic tokamak which attempt to alleviate this problem. This is the motivation behind the high β tokamak.

Qualitatively, there are two modifications to the ohmic tokamak that lead to higher values of β. The first is the application of external heating sources such as neutral beams or RF power. In addition to raising β, external heating sources are required because ohmic heating by itself, while good, is still not sufficient to raise the temperature of a plasma to the level needed for ignition. To reach ignition the externally applied power in a modern tokamak must be several to many times larger than the ohmic power.

The second modification changes the cross section of the plasma from circular to non-circular. Typical modern tokamaks have vertically elongated cross sections with an outward pointing "D" shape. Cross sectional optimization represents a new degree of freedom in machine design and is shown to lead to higher values of β for the same q_*. This section presents a description of both the circular and elliptical high β tokamak configurations to demonstrate the benefits of external heating and cross sectional optimization.

The basic physics of the high β tokamak is as follows. Application of an independent source of external heating at fixed toroidal current, toroidal field, and number density causes an increase in plasma temperature and hence pressure. The higher β that results is confined by newly generated poloidal diamagnetic currents induced in the plasma. When the external heating becomes sufficiently large, radial pressure balance is provided almost entirely by the toroidal field rather than the poloidal field as in an ohmic tokamak. This is the regime of the high β tokamak: the plasma pressure is decoupled from the ohmic heating current and

confinement is more closely related to that of a θ-pinch than a Z-pinch. The critical physics limitation of the high β tokamak is that β can only be externally raised to a certain maximum value that is consistent with toroidal force balance and subject to the constraint that $q_* \gtrsim 1$ for good stability.

6.5.1 The high β tokamak expansion

Taking these requirements into account leads to the following inverse aspect ratio expansion for the high β tokamak:

$$\begin{aligned} \frac{B_p}{B_\phi} &\sim \varepsilon \\ \beta_t &\sim \frac{2\mu_0 p}{B_\phi^2} \sim \varepsilon \\ \beta_p &\sim \frac{2\mu_0 p}{B_p^2} \sim \frac{1}{\varepsilon} \\ q &\sim \frac{rB_\phi}{RB_p} \sim 1 \end{aligned} \tag{6.92}$$

Note that $\beta_t \sim \varepsilon$ is one order larger in ε than in an ohmic tokamak. Also, the ordering $\beta_p \sim 1/\varepsilon$ indicates that the poloidal field plays only a minor role in radial pressure balance. Indeed, it is shown that radial pressure balance is provided by a small diamagnetic depression in the toroidal field. Even though the depression is small, of order ε, it still confines $1/\varepsilon$ more plasma than the small poloidal pressure $B_p^2 \sim \varepsilon^2 B_\phi^2$. The conclusion is that in a high β tokamak the toroidal field provides both radial pressure balance and stability while the poloidal field is required primarily for toroidal force balance with a small contribution to the heating.

Because of the higher values of β the toroidal shift of the flux surfaces is no longer small but is of order unity: $\Delta/a \sim 1$. Similarly, even with a circular plasma surface, the interior flux surfaces are no longer shifted circles, but develop a finite non-circularity. The mathematical consequence is that while the inverse aspect ratio expansion does somewhat simplify the Grad–Shafranov equation, the leading-order (in ε) contribution remains inherently two dimensional; that is, radial pressure balance and toroidal force balance enter simultaneously.

As a result of this behavior only the 2-D leading order contribution to the Grad–Shafranov equation is required to understand the high β tokamak. The appropriate formal expansion for the high β tokamak analysis is thus given by

$$\begin{aligned} \psi(r,\theta) &= \psi_0(r,\theta) + \cdots \\ p(\psi) &= p(\psi_0) + \cdots \end{aligned} \tag{6.93}$$

where

$$\frac{\psi_0}{rRB_\phi} \sim \varepsilon$$
$$\frac{2\mu_0 p(\psi_0)}{B_\phi^2} \sim \varepsilon \tag{6.94}$$

The expansion for $F(\psi)$ is slightly subtle because the Grad–Shafranov equation basically determines the poloidal field whereas radial pressure balance is dominated by the toroidal field. The expansion for $F(\psi)$ must automatically take this into account. The procedure is to introduce a new function $\tilde{B}(\psi)$ in place of $F(\psi)$ as follows:

$$F^2(\psi) = R_0^2 B_0^2 \left[1 - \frac{2\mu_0 p(\psi)}{B_0^2} + \frac{2\tilde{B}(\psi)}{B_0}\right] \tag{6.95}$$

where, as before, B_0 is the vacuum toroidal field at the geometric center of the plasma $R = R_0$. Equation (6.95) implies that the deviation from a θ-pinch pressure balance relation is of order $\tilde{B}/B_\phi \sim \varepsilon^2$, which is one order smaller than the pressure itself.

Substituting the expansion into the Grad–Shafranov equation gives rise to a leading-order contribution which is of the form of a 2-D partial differential equation. This equation describes the behavior of high β tokamak equilibria and is given by

$$\nabla^2 \psi_0 = -R_0^2 B_0^2 \left[\frac{1}{B_0}\frac{d\tilde{B}}{d\psi_0} + \frac{2\mu_0}{B_0^2}\frac{dp}{d\psi_0}\left(\frac{r}{R_0}\right)\cos\ \theta\right] \tag{6.96}$$

Note that the second term on the right-hand side is often referred to as the large aspect ratio limit of the Pfirsch–Schluter (1962) current,

$$J_{PS} = 2\frac{dp}{d\psi_0} r\ \cos\ \theta \tag{6.97}$$

The quantity J_{PS} represents the return current flowing parallel to the magnetic field that is necessary to short out the vertical charge accumulation caused by the ∇B and curvature drifts.

Equation (6.96) is the desired equation that is used to investigate circular and elliptical high β tokamaks.

6.5.2 The circular high β tokamak

Mathematical solution

Since Eq. (6.96) is a non-linear partial differential equation it must in general be solved numerically. However, for special choices of $p(\psi_0)$ and $\delta B(\psi_0)$ it can be solved analytically, and it is such solutions that provide a great deal of

insight into the behavior of high β tokamak equilibria. A well-known example was first proposed by Solov'ev (1967) and later investigated by Haas (1972) as well as many other authors (see for instance Cerfon and Freidberg, 2010). Solov'ev suggested that $p(\psi_0)$ and $\tilde{B}(\psi_0)$ be chosen as linear functions of ψ_0 so that

$$\begin{aligned} R_0^2 B_0 \frac{d\tilde{B}}{d\psi_0} &= -A = \text{constant} \\ 2\mu_0 R_0 \frac{dp}{d\psi_0} &= -C = \text{constant} \end{aligned} \tag{6.98}$$

With this assumption Eq. (6.96) reduces to

$$\nabla^2 \psi_0 = A + C\, r\, \cos\, \theta \tag{6.99}$$

Observe that the linear dependence of the free functions on ψ_0 implies that the toroidal current density (proportional to the right-hand side) is nearly constant in the plasma and must abruptly jump to zero across the plasma surface into the surrounding vacuum region. This jump in the edge current density is probably the biggest drawback of the Solov'ev model in terms of realistic application to experiment. Still, all other important physical properties are well described by the model, which is why it has been so extensively used by the fusion community.

Consider next the boundary conditions on ψ_0. For simplicity, the first geometry investigated corresponds to a plasma with a circular surface located at $r = a$. Outside the plasma surface is a vacuum region. The free additive constant associated with the flux function is chosen to make $\psi_0 = 0$ on the surface. Also, the flux function must be regular in the plasma interior. These conditions are represented mathematically as follows:

$$\begin{aligned} &\psi_0(a, \theta) = 0 \\ &\psi_0(r, \theta) = \text{regular for } r \leq a \end{aligned} \tag{6.100}$$

The solutions for ψ_0, B_θ, and p are easily found and can be written as

$$\begin{aligned} \psi_0(r,\theta) &= \frac{A}{4}(r^2 - a^2) + \frac{C}{8}(r^2 - a^2) r\, \cos\theta \\ B_\theta(r,\theta) &= \frac{1}{R_0}\frac{\partial \psi_0}{\partial r} = \frac{1}{2R_0}\left[Ar + \frac{C}{4}(3r^2 - a^2)\cos\theta\right] \\ p(r,\theta) &= -\frac{C}{2\mu_0 R_0}\psi_0 = -\frac{C}{2\mu_0 R_0}\left[\frac{A}{4}(r^2 - a^2) + \frac{C}{8}(r^2 - a^2) r\, \cos\theta\right] \end{aligned} \tag{6.101}$$

The solutions, while formally correct, are not very intuitive since the two constants A and C do not have simple physical interpretations. It is shown below that one constant is related to the toroidal current and the other to the pressure. It is therefore convenient to replace them with the more physical parameters q_* and β_t. This is a straightforward task and the results are

$$\begin{aligned}\frac{1}{q_*} &= \frac{\mu_0 R_0 I}{2\pi a^2 B_0} = \frac{R_0}{2\pi a^2 B_0}\int_0^{2\pi} B_\theta(a,\theta) a d\theta = \frac{A}{2B_0} \\ \beta_t &= \frac{2\mu_0\langle p\rangle}{B_0^2} = \frac{2\mu_0}{\pi a^2 B_0^2}\int_0^{2\pi}\int_0^a p\ r\ dr d\theta = \frac{a^2 A\ C}{8R_0 B_0^2}\end{aligned} \tag{6.102}$$

Substituting these expressions leads to the following equilibrium solutions for the circular high β tokamak:

$$\begin{aligned}\frac{\psi_0}{a^2 B_0} &= \frac{1}{2q_*}[\rho^2 - 1 + \nu(\rho^3 - \rho)\cos\ \theta] \\ \frac{B_\theta}{\varepsilon B_0} &= \frac{1}{q_*}\left[\rho + \frac{\nu}{2}(3\rho^2 - 1)\cos\ \theta\right] \\ \frac{B_r}{\varepsilon B_0} &= -\frac{\nu}{2q_*}(\rho^2 - 1)\sin\ \theta \\ \frac{2\mu_0 p}{B_0^2} &= 2\beta_t(1-\rho^2)(1 + \nu\rho\ \cos\ \theta) \\ \frac{\mu_0 R_0 J_\phi}{B_0} &= -\frac{2}{q_*}(1 + 2\nu\rho\ \cos\ \theta) \\ \frac{B_\phi}{B_0} &= 1 - \varepsilon\rho\ \cos\ \theta - \beta_t(1-\rho^2)(1 + \nu\rho\ \cos\ \theta)\end{aligned} \tag{6.103}$$

Here, $\varepsilon = a/R_0$, $\rho = r/a$, and ν is the crucial high β tokamak parameter defined by

$$\nu = \frac{\beta_t q_*^2}{\varepsilon} \tag{6.104}$$

Having determined the analytic solutions one can now investigate the basic equilibrium properties of the high β tokamak.

Plasma parameters and figures of merit

Intuition into the nature of radial pressure balance and toroidal force balance can be developed by plotting the curves of B_ϕ, p, and B_θ along the midplane $Z = 0$. These curves are illustrated in Fig. 6.11. First, observe that there is a small diamagnetic depression of order ε superimposed on the $1/R$ decay of the vacuum toroidal field.

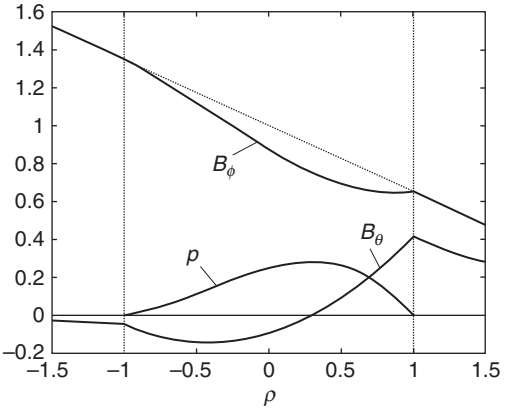

Figure 6.11 Profiles of B_ϕ, B_θ, and p along the $Z = 0$ axis for the slightly exaggerated case corresponding to $\varepsilon = 0.35$, $v = 0.8$, $q_* = 1.5$, and $\beta_t = 0.12$. Here, $\rho = (R - R_0)/a$.

It is in this depression that the plasma pressure $p \sim \varepsilon B_0^2/\mu_0$ is held in radial pressure balance. Since $B_\theta/B_\phi \sim \varepsilon$ when $q \sim 1$, the poloidal field can at most confine a pressure of the order $B_\theta^2/\mu_0 \sim \varepsilon^2 B_\phi^2/\mu_0$. As previously stated, this is one order smaller in ε than the actual plasma pressure, implying that the poloidal field has only a very small effect on radial pressure balance.

Next, note that the general equilibrium relation between β_t, β_p, and q_* is the same as for a circular ohmic tokamak

$$\beta_t = \varepsilon^2 \beta_p / q_*^2 \tag{6.105}$$

except that β_t and β_p are both one order larger in ε: $\beta_t \sim \varepsilon$, $\beta_p \sim 1/\varepsilon$, and $q_* \sim 1$. Furthermore, it follows from the definition of v given by Eq. (6.104) that

$$v = \frac{\beta_t q_*^2}{\varepsilon} = \varepsilon \beta_p \sim 1 \tag{6.106}$$

An examination of Eq. (6.103) suggests that it is useful to view v as the critical parameter that distinguishes different regimes of tokamak operation with $v \ll 1$ corresponding to the ohmic tokamak and $v \sim 1$, the high β tokamak.

Attention is now focused on how toroidal high β effects modify some of the basic equilibrium properties of the tokamak. To begin observe that the pressure profile is parabolic for small v but develops a finite shift and a modified shape for $v \sim 1$. This is demonstrated in Fig. 6.12, which illustrates the $Z = 0$ midplane curves of the pressure p. Also shown is the midplane curve of J_ϕ, which for small v is nearly constant across the plasma and jumps to zero at the plasma surface. For $v \sim 1$ the current accumulates on the outside in order to provide a stronger toroidal restoring force to balance the increased tire tube and

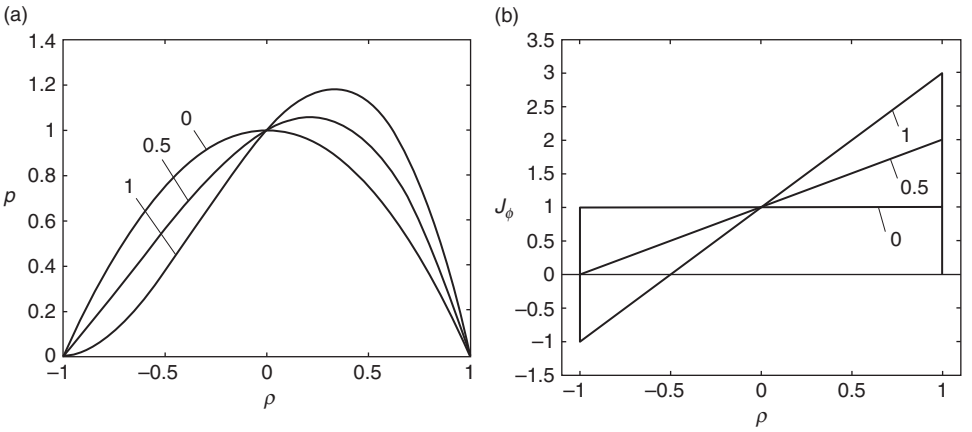

Figure 6.12 Midplane profiles of (a) p and (b) J_ϕ for $v = 0, 0.5, 1$. Here, $\rho = (R - R_0)/a$.

$1/R$ expansion forces. In fact for $v > 1/2$ the current reverses direction on the inside of the plasma surface $r = a$, $\theta = \pi$. A current reversal may be difficult to maintain in a plasma with finite resistivity but this issue lies beyond the scope of ideal MHD.

Another interesting feature in the $v \sim 1$ regime is that the flux surfaces $\psi_0 =$ constant, while round, are no longer pure circles except for the surface $r = a$. Equally importantly, the shift of the magnetic axis is now finite and not small as in the ohmic tokamak. These points can be quantified by examining the flux function in the vicinity of the magnetic axis, the point defined by $\partial\psi_0/\partial\theta = \partial\psi_0/\partial\rho = 0$. For the model under consideration the first condition $\partial\psi_0/\partial\theta = 0$ occurs at $\theta = 0$. The second condition $\partial\psi_0/\partial\rho = 0$ occurs at the point $\rho = \Delta_0/a$ whose value is determined by setting $\rho\cos\theta = x + \Delta_0/a$, $\rho\sin\theta = y$ (see Fig. 6.13), substituting into the expression for the flux function, and assuming that near the magnetic axis $\Delta_0/a \gg x, y \to 0$. A short calculation yields

$$\frac{2q_*}{a^2B_0}\psi_0 = [1 - (x + \delta_0)^2 - y^2][1 + v(x + \delta_0)]$$
$$\approx (1 - \delta_0^2)(1 + v\delta_0) - (3v\delta_0^2 + 2\delta_0 - v)x - (1 + 3v\delta_0)x^2 - (1 + v\delta_0)y^2 \quad (6.107)$$

where $\delta_0 = \Delta_0/a$ and in the approximate formula terms of the order x^3, xy^2 have been neglected. The magnetic axis condition in x, y coordinates is equivalent to setting $\partial\psi_0/\partial y = \partial\psi_0/\partial x = 0$ at $x = 0$, $y = 0$ and requires that the coefficient of the term linear in x vanishes. Carrying out this task yields the desired expression for the magnetic axis shift with respect to the plasma surface

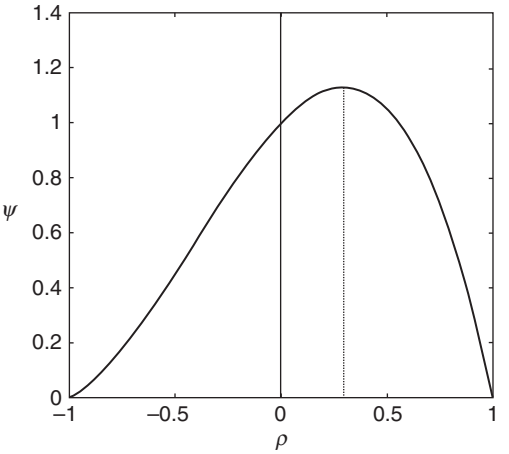

Figure 6.13 Midplane profile of ψ showing the location of the magnetic axis. Here, $\rho = (R - R_0)/a$.

$$\frac{\Delta_0}{a} = \frac{v}{1 + (1 + 3v^2)^{1/2}} \tag{6.108}$$

Clearly, for $v \sim 1$ the shift is finite and not small as in the ohmic tokamak.

With respect to the shape of the flux surfaces, the approximate form of the flux function given in Eq. (6.107) indicates that these surfaces are ellipses centered on the magnetic axis:

$$x^2 + \frac{y^2}{\kappa_0^2} = \text{constant} \tag{6.109}$$

Here, κ_0 is the on-axis elongation of the ellipses and is given by

$$\kappa_0^2 = \frac{1 + 3v\delta_0}{1 + v\delta_0} = 1 + \frac{2v^2}{1 + v^2 + (1 + 3v^2)^{1/2}} \tag{6.110}$$

For $v \ll 1$, then $\kappa_0^2 \approx 1$: the surfaces approach circles in the ohmic limit. However, in the limit $v \sim 1$ Eq. (6.110) shows that the surfaces have a finite ellipticity.

In essence, for a high β tokamak the increased tire tube and $1/R$ forces push the central plasma outward along R towards the outside of the torus. This results in a finite shift and a squashing of the interior flux surfaces causing them to become elliptical.

The final quantity of interest involves the evaluation of the MHD safety factor. This is in general a complicated calculation when the flux surfaces do not have simple shapes. For the circular high β tokamak numerical calculations show that the q profile is an increasing function of flux. Consequently, for present purposes it

is sufficient to calculate q at the two extremes, the magnetic axis and the plasma surface, to obtain an idea of the variation. Both of these values can be calculated analytically.

For the magnetic axis safety factor recall that an exact expression has been derived in Section 6.3.6 and is repeated here for convenience:

$$q_0 = \frac{B_\phi}{(\psi_{RR}\psi_{ZZ})^{1/2}} \tag{6.111}$$

All quantities are evaluated on the magnetic axis. This expression simplifies by substituting the high β tokamak expansion and transforming to the x, y coordinates defined above. The result is

$$q_0 = \frac{a^2 B_0}{(\psi_{0xx}\psi_{0yy})^{1/2}} \tag{6.112}$$

Eliminating the ψ_0 derivatives by means of Eq. (6.107) yields the desired result

$$q_0 = \frac{q_*}{(1+3\nu\delta_0)^{1/2}(1+\nu\delta_0)^{1/2}} = q_*\left[\frac{3}{\eta(2+\eta)}\right]^{1/2} \tag{6.113}$$

where $\eta = (1+3\nu^2)^{1/2}$. Since η is always greater than unity then $q_0 < q_*$. In the low β limit, $\nu \ll 1$ and $q_0 \to q_*$. As ν is increased the ratio q_0/q_* becomes progressively smaller.

Next consider the safety factor on the plasma surface. In the high β ordering the variation of the poloidal field B_θ around the cross section is of order unity. The value of B_θ is larger on the outside of the torus in order to support the higher pressure in toroidal force balance. This variation averages to zero when calculating the total plasma current, implying that $q_* \propto 1/I$ as required by the definition of q_*. However, when calculating q_a as defined by Eq. (6.35), the poloidal field appears in the denominator of the integrand, which is thus more heavily weighted on the inside of the torus where $B_\theta(a, \theta)$ is smaller. This leads to the result that $q_a > q_*$. Specifically, on the plasma surface $r = a$, q_a can be easily evaluated from Eq. (6.35) by using the high β expansion

$$\begin{aligned} q_a &= \frac{F(\psi)}{2\pi}\oint \frac{dl}{R^2 B_p} \\ &\approx \frac{aB_0}{2\pi R_0}\int_0^{2\pi}\frac{d\theta}{B_\theta(a,\theta)} \\ &= \frac{q_*}{(1-\nu^2)^{1/2}} \end{aligned} \tag{6.114}$$

In the low β limit, $q_a \rightarrow q_*$. In contrast in the high β regime it is important to distinguish between q_a and q_*, particularly since $1/q_a$ is no longer linearly proportional to I. The most striking feature of Eq. (6.114) is the breakdown of the solution when $v > 1$. The explanation is a very important aspect of high β tokamak behavior and is the next topic discussed.

The high β tokamak equilibrium limit

The breakdown of the analytic solution for $v > 1$ actually corresponds to an equilibrium β limit. Specifically, there is an upper limit on the value of β that can be confined assuming the plasma current is held fixed. This can be quantified by requiring that $v \leq 1$ in the basic plasma parameters and figures of merit assuming that $q_* \propto 1/I$ is held fixed as one attempts to raise β by external heating. The values of these quantities at the $v = 1$ limit are given by

$$\begin{aligned} \beta_t &= \varepsilon/q_*^2 \\ \beta_p &= 1/\varepsilon \\ \Delta_0/a &= 1/3 \\ \kappa_0 &= (3/2)^{1/2} \\ q_0 &= (3/8)^{1/2} q_* \\ q_a &\rightarrow \infty \end{aligned} \tag{6.115}$$

For a given inverse aspect ratio ε the actual maximum numerical value of β_t is obtained by setting q_* to its minimum allowable value (i.e., maximum I) as set by MHD stability limits.

The origin of the equilibrium limit can be understood by examining the magnetic field in the vacuum region. The solution $\hat{\psi}_0$ that matches onto ψ_0 at the plasma surface must satisfy the following equation and jump conditions:

$$\begin{aligned} \nabla^2 \hat{\psi}_0 &= 0 \\ \hat{\psi}_0(a,\theta) &= \psi_0(a,\theta) = 0 \\ \hat{B}_\theta(a,\theta) &= B_\theta(a,\theta) = (\varepsilon B_0/q_*)(1 + v\ \cos\ \theta) \end{aligned} \tag{6.116}$$

Note that the boundary conditions require matching the flux and its normal derivative across the boundary, which guarantees that no surface currents are allowed to flow. Equation (6.116) represents an ill-conditioned problem (i.e., Cauchy boundary conditions for an elliptic differential operator) but the difficulties can be overcome because the solutions are known analytically.

The solution for $\hat{\psi}_0$ satisfying Eq. (6.116) is found to be

$$\frac{\hat{\psi}_0}{a^2 B_0} = \frac{1}{q_*}\left[\ln \rho + \frac{v}{2}\left(\rho - \frac{1}{\rho}\right)\cos\ \theta\right] \tag{6.117}$$

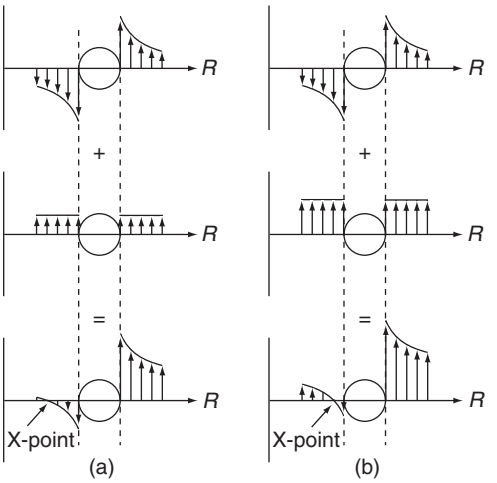

Figure 6.14 Schematic diagram illustrating the appearance of a separatrix in a high β tokamak: (a) low β case and (b) high β case. Note the increased vertical field in the high β case to provide toroidal force balance.

The first term represents the equivalent "cylindrical" contribution from the toroidal current. The last two terms represent the applied vertical field and corresponding plasma diamagnetic response, respectively. A critical feature of the solution is that the vacuum field has a particular flux surface known as the separatrix which is defined by the X-point condition $\hat{B}_r(r_s, \theta_s) = \hat{B}_\theta(r_s, \theta_s) = 0$. The separatrix is shown graphically in the bottom frame of Fig. 6.14.

A simple calculation shows that the separatrix is located at

$$\theta_s = \pi$$
$$\rho_s = \frac{r_s}{a} = \frac{1 + (1 - \nu^2)^{1/2}}{\nu} \tag{6.118}$$

For low β, $\nu \ll 1$ and the separatrix is located at $\rho_s \approx 2/\nu$, far from the plasma surface. As β increases at fixed current, the vertical field must increase to provide toroidal force balance. An increasing vertical field moves the separatrix closer to the plasma surface as shown in Fig. 6.14, which shows qualitatively how toroidal force balance is achieved by summing the contributions of the vertical field and the $1/r$ field due to the toroidal current.

Now, as $\nu \to 1$ then $\rho_s \to 1$. The X-point moves onto the plasma surface. It can move no further as long as the plasma surface is required to remain circular. It is this behavior that corresponds to the equilibrium β limit.

From the discussion above one can reasonably conclude that all high β tokamaks, regardless of profiles, have an equilibrium β limit with a similar scaling in ε.

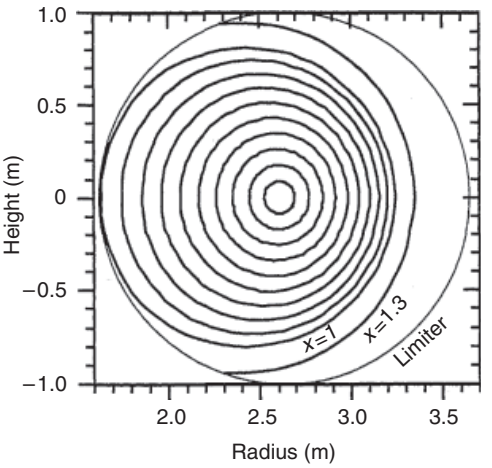

Figure 6.15 Numerically computed equilibrium for the TFTR tokamak at PPPL. Shown is a flux surface plot corresponding to auxiliary heated high β tokamak operation. From Budny, 1994. Reproduced with permission.

This is a correct conclusion but only under the condition that increasing values of β are maintained in toroidal force balance by *increasing the vertical field, while keeping the toroidal current fixed.* Experimentally, avoiding the equilibrium β limit turns out to not be a serious concern. The reasons for this are discussed in Section 6.5.3.

Numerical results for a high β tokamak

One of the large international experiments with circular cross section and substantial external heating was Tokamak Fusion Test Reactor TFTR at Princeton Plasma Physics Laboratory. This experiment had substantial neutral beam power (up to 40 MW) and used carbon limiters to protect the first wall. In other words, from the MHD point of view, the experiment closely satisfied the assumptions made in analyzing the high β tokamak. One disappointing result found on TFTR as well as all other tokamaks is that the energy confinement time degrades with increasing external heating power.

Many numerical simulations have been carried out to model the overall TFTR behavior. With respect to ideal MHD, the agreement between experiment and theory is quite good. One such numerical simulation is illustrated in Fig. 6.15. Observe the large shift of the peak plasma pressure on the outside of the torus.

All in all, in spite of its simplicity, the large aspect ratio Solov'ev equilibrium is a reasonably good model for realistic high β tokamaks.

Summary

A high β tokamak is a configuration in which radial pressure balance is provided almost entirely by a small diamagnetic depression in the large, nearly vacuum toroidal field. The B_ϕ field is also primarily responsible for MHD stability as in an ohmic tokamak. The toroidal current provides toroidal force balance but is limited in magnitude by the stability constraint $q > 1$ plus the maximum technologically allowable toroidal field. Qualitatively, by means of external heating, β_t is raised to the largest value consistent with the $q > 1$ constraint. This leads to the scaling $\beta_t \sim \varepsilon$, $\beta_p \sim 1/\varepsilon$, and $q \sim 1$. The value of β_t is one order larger in ε than in an ohmic tokamak.

An interesting feature of the high β tokamak is the existence of an apparent equilibrium β limit. This occurs by raising β by means of external heating while holding the toroidal current fixed. The increased outward tire tube and $1/R$ forces on the plasma are compensated by raising the vertical field, a strategy that causes the X-point of the vacuum separatrix to move onto the plasma surface, corresponding to the equilibrium limit.

At the limit the value of β_t is reasonably large. For example, for typical experimental values of $\varepsilon = 1/3$ and $q_* = 2$ one finds that $\beta_t = 8\%$, which is adequate, although without much safety margin, for reactor purposes.

6.5.3 *The flux conserving tokamak – avoiding the equilibrium* β *limit*

As has been stated, the existence of an equilibrium β limit for high β tokamaks is strongly coupled to the constraint that requires $I \propto 1/q_*$ be held fixed as β_t increases. This constraint does not necessarily represent the evolution of a typical tokamak discharge. An alternate constraint that in fact eliminates the equilibrium β limit was proposed by Clarke and Sigmar (1977) and leads to the flux conserving tokamak concept.

The basic idea behind flux conservation

The basic idea of the flux conserving tokamak is to model the actual evolution of a given plasma discharge by a sequence of plausibly chosen free functions $p(\psi, t)$ and $F(\psi, t)$. The rationale for prescribing this set of functions is as follows. Consider a plasma that is operating initially as an ohmically heated tokamak: $\beta_t \sim \varepsilon^2$, $\beta_p \sim 1$. The plasma is then heated by a high-power external source, for instance neutral beams or RF waves. It is a good approximation to assume that the time scale for heating τ_H is long compared to a typical MHD time τ_M:

$$\tau_H \gg \tau_M \tag{6.119}$$

Here, $\tau_M = a/V_{Ti}$ is the MHD time and $\tau_H = T/(\partial T/\partial t)$ is the time for the temperature to change by a finite amount. Under this assumption the MHD inertial effects are negligible (i.e., the $\rho\, d\mathbf{v}/dt$ term in the MHD momentum equation can be neglected). The plasma evolution can thus be viewed as a series of quasistatic equilibria, each one satisfying the Grad–Shafranov equation with slowly varying free functions $p(\psi, t)$ and $F(\psi, t)$.

In contrast, the time scale for heating is assumed to be short compared to the magnetic diffusion time τ_D,

$$\tau_H \ll \tau_D \tag{6.120}$$

where $\tau_D = \mu_0 a^2/\eta$ and η is the resistivity which can be classical or anomalous. This too is a well-satisfied approximation experimentally. The long diffusion time implies that the plasma behaves like a perfect conductor on the heating time scale.

Choosing p(ψ, t) *and* F(ψ, t)

These two assumptions lead to the following prescription for determining the time evolution of the free functions $p(\psi, t)$ and $F(\psi, t)$ corresponding to the flux conserving tokamak. The function $p(\psi, t)$ is treated as a known function. Initially $p(\psi, 0) = p_\Omega(\psi)$ where $p_\Omega(\psi)$ is the ohmic profile. As time progresses $p(\psi, t)$ increases due to the external heating. Since the theory and computation of heat deposition in a plasma is reasonably well understood, it is not difficult to generate a plausible model for the time evolution of the pressure. A simple model that is adequate for present purposes is to assume that

$$p(\psi, t) = K(t) p_\Omega(\psi) \tag{6.121}$$

with $K(0) = 1$. The function $K(t)$ is assumed to be known and increases with time. This model directly specifies the evolution of $p(\psi, t)$ in the Grad–Shafranov equation and eliminates the need for solving a separate set of particle and energy transport equations. Keep in mind that the time t enters calculation only as a parameter – there are no time derivatives. This is what is meant by the "quasistatic" assumption.

The interesting new feature of the flux conserving tokamak is the specification of $F(\psi, t)$. Since the plasma acts like a perfect conductor on the heating time scale, the function $F(\psi, t)$ must be chosen such that both the toroidal and poloidal fluxes are conserved. How exactly does one mathematically specify flux conservation? As the plasma is heated the shape of the poloidal flux function $\psi(\mathbf{r}, t)$ slowly evolves in time as the increased plasma pressure shifts the magnetic axis outward. Flux conservation requires that the toroidal flux contained within any given poloidal flux surface must remain constant during this evolution if the plasma is

a perfect conductor. No toroidal flux is allowed to diffuse into or out of any poloidal flux surface.

The flux conserving constraint can be expressed mathematically by calculating the toroidal flux $\Phi(\psi, t)$ from the definition

$$\Phi(\psi,t) = \int B_\phi \, dS = \int_0^\psi d\psi F(\psi,t) \oint \frac{dl_p}{R^2 B_p} = 2\pi \int_0^\psi q(\psi,t) d\psi \tag{6.122}$$

Therefore, the condition to conserve the toroidal flux within any given poloidal flux surface requires that

$$\frac{\partial \Phi(\psi,t)}{\partial t} = 2\pi \int_0^\psi \frac{\partial q(\psi,t)}{\partial t} \, d\psi = 0 \tag{6.123}$$

In other words, $F(\psi, t)$ must be chosen such that the safety factor $q(\psi, t)$ is identical in each quasistatic state. Since this applies in particular to the initial state, the actual functional dependence of $q(\psi, t)$ must correspond to the initial ohmically heated plasma,

$$q(\psi,t) = q_\Omega(\psi) \tag{6.124}$$

The desired expression for flux conservation relating $F(\psi, t)$ to $q(\psi, t)$ has already been obtained in Eq. (6.43), and is repeated here for convenience

$$F(\psi,t) = q_\Omega(\psi) \left[\frac{1}{2\pi} \oint \frac{dl}{R^2 B_p} \right]^{-1} \tag{6.125}$$

Note that in this equation the term in the square bracket is a slowly varying function of time since $B_p = B_p(\psi, l, t)$.

Implementing the flux conserving constraint

The Grad–Shafranov equation that incorporates the flux conserving p and F (i.e., Eqs. (6.121) and (6.125)) is equivalent to the form derived in Eq. (6.44), also repeated here for convenience,

$$\Delta^* \psi = -\mu_0 R^2 K \frac{dp_\Omega}{d\psi} - \frac{1}{2} \frac{d}{d\psi} \left[q_\Omega^2(\psi) \left(\frac{1}{2\pi} \oint \frac{dl_p}{R^2 \, B_p} \right)^{-2} \right] \tag{6.126}$$

This complicated equation must in general be solved numerically at each instant of time during the heating evolution. One can avoid this difficulty and obtain some insight by means of a simple idea as follows. As a reasonable approximation to flux conservation assume that as the plasma evolves only q_0 and q_a are exactly conserved. Since the $q(\psi)$ profile for most tokamaks is a monotonically increasing function, it should be sufficient to ascertain the main features of the evolution by conserving only the end points, even if the interior profiles are slightly modified.

One can attempt to implement this idea using the simple circular high β Solov'ev equilibrium discussed in Section 6.5.2. There is, however, a problem. The Solov'ev equilibrium is characterized by only two free parameters, A and C. Qualitatively, one parameter can be used to model the plasma heating, proportional to β_t, while the other can be used to model some form of the safety factor. The problem is that there is not enough freedom to fix two values of the safety factor and still have a free parameter available to allow the plasma β to increase as the heating increases. This would require three free parameters in the Solov'ev solution. The problem is overcome by making the gross approximation that flux conservation requires that only q_a, and not q_0, be conserved. Even with this gross approximation it is shown below that the model no longer exhibits an equilibrium limit; that is, well-behaved solutions exist for arbitrarily large values of β_t.

The flux conserving Solov'ev equilibrium

The flux conserving constraint can be applied to the Solov'ev equilibrium as follows. The key step is to introduce a heating parameter defined by

$$H = \beta_t q_a^2/\varepsilon \tag{6.127}$$

This is a useful measure of heating for a flux conserving evolution in which ε, B_0, and by definition q_a are held fixed. Under these conditions the heating parameter $H \propto p$ indicating that increases in plasma energy due to external heating correspond to increases in the value of H. For the high β tokamak operating at fixed q_* rather than fixed q_a the equivalent heating parameter would be defined as

$$H = \beta_t q_*^2/\varepsilon \tag{6.128}$$

with equilibria existing only in the range $0 < H < 1$.

The next step in the analysis is to evaluate the important plasma parameters q_*, I, β_p, ρ_s, and B_V as a function of the flux conserving heating parameter H. These quantities can be easily calculated from the high β tokamak results already derived in Section 6.5.2. To begin a simple relation can be obtained relating q_* to q_a and H by using Eqs. (6.106) and (6.114):

$$\left(\frac{q_a}{q_*}\right)^4 - \left(\frac{q_a}{q_*}\right)^2 - H^2 = 0 \tag{6.129}$$

The solution is given by

$$q_* = q_a \left[\frac{2}{(1+4H^2)^{1/2}+1}\right]^{1/2} \tag{6.130}$$

It immediately follows that the relation between the plasma current I and the initial ohmic current I_Ω (corresponding to $H = 0$ and $q_* = q_a$) is given by

$$\frac{I}{I_\Omega} = \frac{q_a}{q_*} = \left[\frac{(1+4H^2)^{1/2}+1}{2}\right]^{1/2} \tag{6.131}$$

The expression for $\varepsilon\beta_p$ is now obtained from Eq. (6.106),

$$\varepsilon\beta_p = \frac{2H}{(1+4H^2)^{1/2}+1} \tag{6.132}$$

The separatrix X-point location ρ_s is calculated by direct substitution into Eq. (6.118),

$$\frac{r_s}{a} = \rho_s = \left[\frac{(1+4H^2)^{1/2}+1}{2H}\right]\left\{1+\left[\frac{2}{(1+4H^2)^{1/2}+1}\right]^{1/2}\right\} \tag{6.133}$$

The last quantity of interest is B_V which is obtained from Eq. (6.117) after noting that the flux function for a vacuum vertical field is given by $\hat{\psi}_V = aR_0B_V\rho\cos\theta$,

$$B_V = \frac{\varepsilon B_0}{2q_a}\left[\frac{2H^2}{(1+4H^2)^{1/2}+1}\right]^{1/2} \tag{6.134}$$

These results are illustrated in Fig. 6.16. Also illustrated are the results for the high β tokamak with fixed q_* and H defined by Eq. (6.128). There are several points to be made. Each of the plasma parameters is finite and well behaved for arbitrarily large β_t (i.e., H) when q_a is held fixed; there is no equilibrium β limit for the flux conserving tokamak. This is in contrast to the high β tokamak for which q_* is held fixed. In this case there is an equilibrium limit given by $H = \beta_t q_*^2/\varepsilon = 1$. The explanation is that in the flux conserving case the current I must increase as β_t increases in order to keep q_a constant. A larger I requires a smaller increase in B_V to hold a given β_t in toroidal force balance. Thus, the ratio of B_V/I is smaller in a flux conserving tokamak than in a high β tokamak with fixed q_*. As one can see intuitively from Fig. 6.16, this behavior slows the motion of the separatrix X-point toward the plasma surface.

Another important aspect of flux conserving operation involves q_*. Since I increases with H, then $q_* \propto 1/I$ decreases. Consequently, a plasma that satisfies the kink stability condition $q_* > q_{*\min}$ in the ohmic regime may violate the condition as β_t is increased. One must start with a sufficient safety margin initially to prevent this from happening as the plasma is heated.

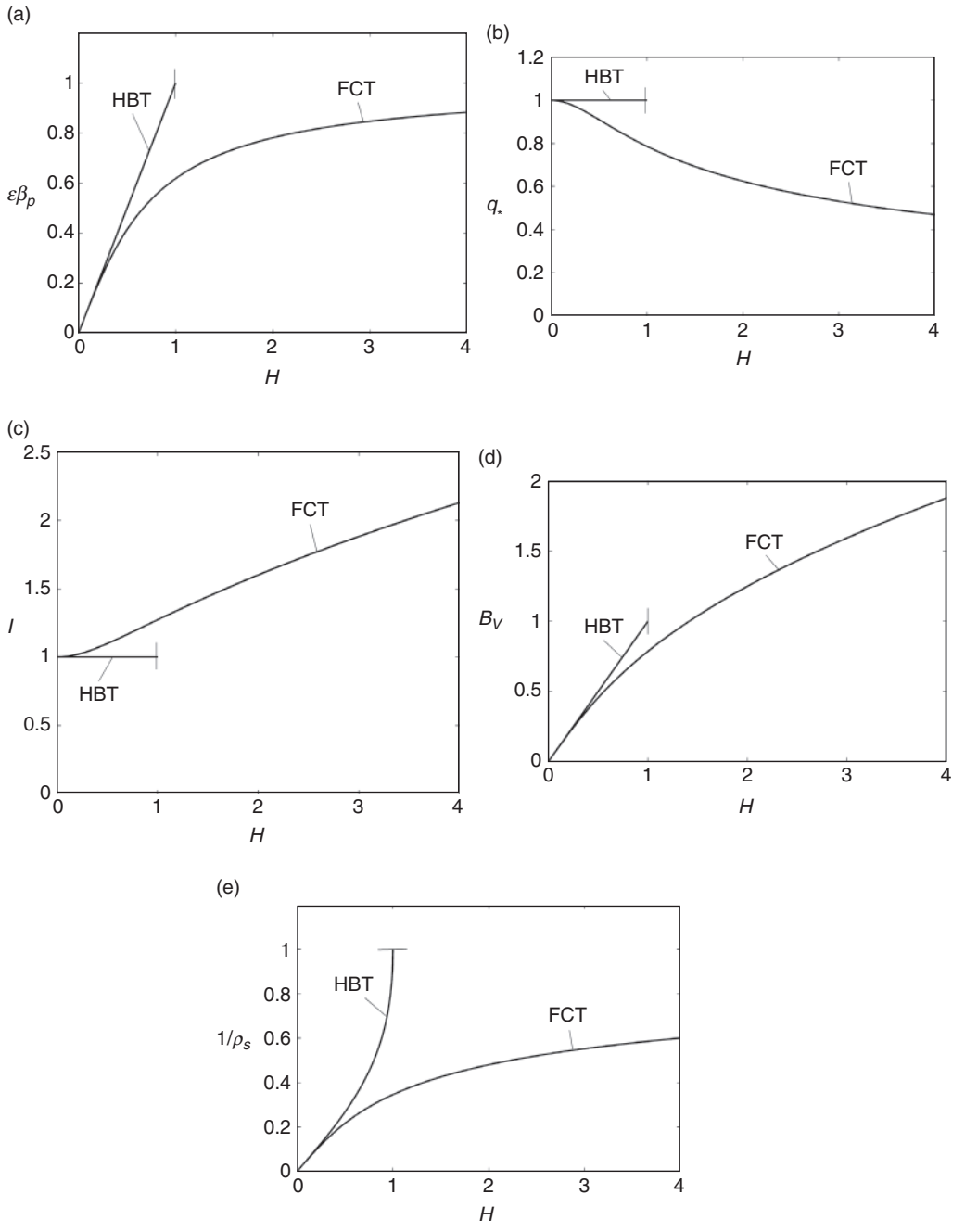

Figure 6.16 Curves of (a) $\varepsilon\beta_p$, (b) q_*/q_a, (c) I/I_Ω, (d) $(2q_a/\varepsilon B_0)\, B_V$, and (e) $1/\rho_s$ vs. the heating parameter H for a flux conserving equilibrium sequence. Also shown are the corresponding high β tokamak curves for I = constant. (HBT = high β tokamak, FCT = flux conserving tokamak.)

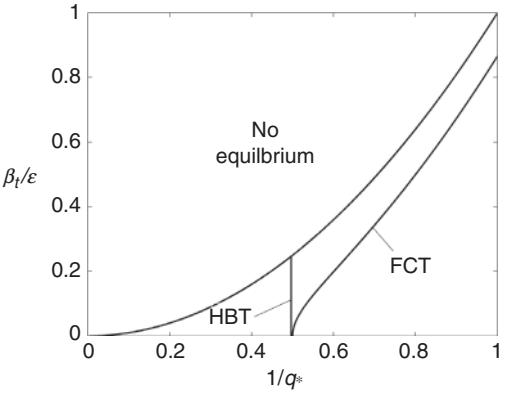

Figure 6.17 Flux conserving trajectory in β_t/ε vs. $1/q_*$ space. Also shown is the trajectory corresponding to the high β tokamak at fixed current.

These results can be conveniently summarized by plotting the trajectory of a flux conserving evolution in a β_t/ε vs. $1/q_*$ space as illustrated in Fig. 6.17 for the case $q_a = 2$. This relation is obtained by eliminating H between Eqs. (127) and (6.130),

$$\frac{\beta_t}{\varepsilon} = \left[\frac{1}{q_*^2}\left(\frac{1}{q_*^2} - \frac{1}{q_a^2}\right)\right]^{1/2} \tag{6.135}$$

Also plotted for comparison is the trajectory for the high β tokamak with fixed q_*: $\beta_t/\varepsilon = 1/q_*^2$. One sees that for a flux conserving equilibrium, as β_t increases the value of q_* decreases in such a way that the equilibrium limit is never crossed. However, for the high β tokamak the trajectory is a vertical line which will always intersect the equilibrium limit at a sufficiently large β_t/ε.

Summary and discussion

A flux conserving tokamak is an externally heated high β tokamak in which the heating rate is slow compared to the MHD time and fast compared to the magnetic diffusion time. In this regime the plasma behaves like a perfect conductor, evolving through a series of quasistatic equilibrium states as the heating increases. The requirements of flux conservation combined with a simple model of plasma heating serve to determine the free functions $p(\psi, t)$ and $F(\psi, t)$ for each quasistatic state. The most interesting feature of the flux conserving tokamak is that the high β tokamak equilibrium limit no longer exists. The reason is directly related to a reduction in the ratio B_V/I implied by the requirements of flux conservation which slows the motion of the separatrix X-point towards the plasma surface.

The relation between the high β tokamak and the flux conserving tokamak is very useful in developing physical intuition about the operation of externally heated tokamaks. In practice, however, flux conservation does not play a major role in the experimental operation of tokamaks. The reason is a negative one – well before the plasma can reach its potential equilibrium limit, its achievable β is limited by MHD instabilities. In fact, many tokamaks are programmed to operate at fixed current as heating occurs so as not to decrease q_*, which could excite current-driven instabilities. There is little concern about reaching the equilibrium limit because pressure-driven MHD instabilities will occur first.

6.5.4 The elliptic high β tokamak

Statement of the problem

While the achievable MHD stable values of β_t in an externally heated high β tokamak are much larger than for an ohmic tokamak, they are marginal for reactor applications if the plasma has a circular cross section. An important way to further increase the achievable β is by shaping the cross section, in particular, making it vertically elongated. This extra degree of optimization freedom is now investigated for the elliptically shaped high β tokamak, whose simple cross section allows for an analytic solution when used in conjunction with the Solov'ev profiles.

The strategy is as follows. As a simple measure of the potential gains in β, the equilibrium limit for an elliptical plasma is calculated as a function of elongation, and then compared with that of a circular plasma. Although recognizing that the actual β limit is set by stability and not equilibrium, one can still invoke the intuition (not yet proven) that a higher equilibrium β limit will lead to a higher stability β limit. It is also of interest to calculate and compare the total current I and average current density $\overline{J}_\phi$. The current is related to the energy confinement time and the current density to the ohmic heating capabilities.

In carrying out the cross sectional optimization and making the corresponding comparisons it is essential to identify the constraints that must be applied. In particular, which quantities should be held fixed as the plasma elongation is varied? Four constraints are applied in the analysis. First, the inverse aspect ratio ε is held fixed. Since $\beta_t \propto \varepsilon$, a fair comparison between different devices suggests that ε be held fixed as elongation is varied. Second, for the same reason the toroidal field B_0 is held fixed. Third, as an attempt to keep MHD stability constant, the value of q_* is fixed as the elongation changes. Numerical simulations of MHD stability indicate that the marginal stability value of q_* as defined by Eq. (6.29) is indeed almost independent of elongation. Fourth, when calculating I and $\overline{J}_\phi \equiv I/\text{area}$, which are un-normalized quantities, an additional constraint is required. The choice is to fix the device volume $V = 2\pi^2 R_0 a^2 \kappa$, which is a

rudimentary attempt to keep the cost constant. Here, κ (without a subscript) is the surface elongation.

To summarize, the goal of the analysis is to derive the condition corresponding to the equilibrium limit and then evaluate β_t, I, and $\overline{J}_\phi$ as functions of κ subject to the constraints of fixed ε, q_*, B_0, and V.

Mathematical solution

The task now is to solve the high β tokamak Grad–Shafranov equation with Solov'ev profiles for an elliptically shaped plasma. This is a straightforward task if one introduces rectangular coordinates $x = r\cos\theta$, $y = r\sin\theta$ into Eq. (6.99) leading to the following formulation of the equilibrium problem:

$$\begin{aligned} \frac{\partial^2\psi_0}{\partial x^2} + \frac{\partial^2\psi_0}{\partial y^2} &= A + Cx \\ \psi_0(S) &= 0 \\ \psi_0(x,y) &= \text{regular in the plasma} \end{aligned} \tag{6.136}$$

Here, the surface S corresponds to the ellipse

$$\frac{x^2}{a^2} + \frac{y^2}{\kappa^2 a^2} = 1 \tag{6.137}$$

Because of the simple Solov'ev profiles the solution can be easily found:

$$\begin{aligned} \psi_0 &= K_1\left(\frac{x^2}{a^2} + \frac{y^2}{\kappa^2 a^2} - 1\right)(1 + K_2 x) \\ K_1 &= \frac{a^2}{2}\left(\frac{\kappa^2}{1+\kappa^2}\right)A \\ K_2 &= \left(\frac{1+\kappa^2}{1+3\kappa^2}\right)\frac{C}{A} \end{aligned} \tag{6.138}$$

The next step is to rewrite the new constants K_1, K_2 in terms of more physical quantities and then evaluate the plasma parameters and figures of merit.

Plasma parameters and figures of merit

The constants K_1, K_2 can be readily evaluated by introducing yet another set of coordinates ρ, α defined by $x = \alpha\rho\cos\alpha$, $y = \kappa\alpha\rho\sin\alpha$. Note that the plasma surface corresponds to $\rho = 1$. In terms of these coordinates the flux function plus the surface values of the differential poloidal arc length and poloidal magnetic field are given by

$$\begin{aligned}\psi_0 &= -K_1(1-\rho^2)(1+K_2 a\rho\ \cos\ \alpha)\\ dl &= a(\kappa^2\ \cos^2\alpha+\ \sin^2\alpha)^{1/2}d\alpha\\ B_p &= (2K_1/R_0 a\kappa)(\kappa^2\ \cos^2\alpha+\ \sin^2\alpha)^{1/2}(1+K_2 a\ \cos\ \alpha)\end{aligned} \tag{6.139}$$

Using these relations one can show after a short calculation that K_1, K_2 are related to q_*, β_t (defined in Eqs. (6.29) and (6.24)) by the following relations:

$$\begin{aligned}K_1 &= \frac{B_0 a^2\kappa}{2q_*}\\ K_2 &= \frac{4\beta_t q_*^2}{\varepsilon a(1+3\kappa^2)}\end{aligned} \tag{6.140}$$

Sufficient information is now available to calculate the equilibrium β limit. The shortest path to this goal is to calculate the safety factor on the surface (i.e., q_a) and determine the condition under which $q_a \to \infty$. This is the condition for the separatrix to move onto the plasma surface. The value of q_a is found as follows:

$$\begin{aligned}q_a &= \frac{F(\psi)}{2\pi}\oint\frac{dl}{R^2B_p}\\ &\approx \frac{B_0}{2\pi R_0}\oint\frac{dl}{B_p}\\ &= \frac{q_*}{(1-\nu^2)^{1/2}}\end{aligned} \tag{6.141}$$

where

$$\nu = K_2 a = \frac{\beta_t q_*^2}{\varepsilon}\frac{4}{1+3\kappa^2} \tag{6.142}$$

Observe that the equilibrium β_t limit again occurs when $\nu \to 1$ and has the value

$$\beta_t = \left(\frac{\varepsilon}{q_*^2}\right)\frac{1+3\kappa^2}{4} \tag{6.143}$$

Here and below the quantity in the parenthesis corresponds to the circular value. Equation (6.143) implies that the β_t limit increases rapidly with elongation. For example, when $\kappa = 2$ the gain in β_t from a circle to an ellipse is about a factor of 3.3.

The other parameters and figures of merit can be calculated in a similar manner as for the circular case. At the equilibrium limit their values are

$$\begin{aligned}
\beta_p &= \left(\frac{1}{\varepsilon}\right)\frac{1+3\kappa^2}{2(1+\kappa^2)} \\
\frac{\Delta_0}{a} &= \left(\frac{1}{3}\right) \\
\kappa_0 &= \left(\frac{3}{2}\right)^{1/2}\kappa \\
q_0 &= \left(\frac{3}{8}q_*^2\right)^{1/2}
\end{aligned} \tag{6.144}$$

Equation (6.144) implies that as κ increases, β_p increases and then saturates, Δ_0/a and q_0 remain unchanged, and κ_0 scales linearly with κ.

Next, it is of interest to examine the behavior of I and $\overline{J}_\phi$ for arbitrary ν as κ increases subject to the constraints described above. Consider first the current, which is determined from

$$\mu_0 I = \oint B_p \, dl \tag{6.145}$$

A straightforward calculation yields

$$\begin{aligned}
\mu_0 I &= \left(2\pi\varepsilon\overline{a}\,\frac{B_0}{q_*}\right)\frac{1+\kappa^2}{2\kappa^{1/3}} \\
\overline{a} &= \left(\frac{\varepsilon V}{2\pi^2}\right)^{1/3}
\end{aligned} \tag{6.146}$$

where $\bar{a} = \bar{a}(\varepsilon, V)$ is the average plasma radius, which is held fixed as the elongation is varied. Note that $\bar{a} = a$ for a circular plasma. There is an important conclusion to be drawn from this relation based on experimental observations which show that the energy confinement τ_E is approximately linearly proportional to I. Equation (6.146) implies that when comparing different machines with the same aspect ratio and plasma volume, increasing the elongation increases the energy confinement time. Elongation is good for energy confinement as well as MHD.

The second quantity of interest is the average current density defined by

$$\overline{J}_\phi = \frac{I}{\pi a^2 \kappa} \tag{6.147}$$

The radius a is eliminated by means of the aspect ratio and volume constraints: $a = \bar{a}/\kappa^{1/3}$. The expression for the current density can thus be written as

$$\mu_0 \overline{J}_\phi = \left(\frac{2\varepsilon B_0}{\overline{a} q_*}\right) \frac{1+\kappa^2}{2\kappa^{2/3}} \tag{6.148}$$

The implication here is that the average current density also increases with elongation for a fixed aspect ratio and fixed volume plasma. A higher average current density is favorable for the ohmic heating phase of a tokamak. Once again elongation is good.

Numerical results

Since several important plasma properties – MHD, energy confinement, and ohmic heating – have been shown to improve with increasing κ, one might expect tokamak experiments to be designed with very elongated cross sections. This is true to a degree but there is a serious problem that arises which prevents this strategy from being implemented to the fullest desirable extent. Specifically, as a tokamak is elongated it becomes MHD unstable to axisymmetric instabilities which are only weakly affected by the value of q_*. These modes essentially correspond to a rigid vertical motion of the plasma causing it to strike the top or bottom of the vacuum chamber. When this occurs it is very bad for both the plasma and the chamber. To avoid these instabilities most tokamaks make use of an active feedback system. However, the technological constraints of the feedback circuits (e.g., amplitude and response time) become more severe as the plasma becomes more elongated. In practice, elongations are usually restricted to the range $\kappa \lesssim 2$ in order for the feedback to prevent these modes from occurring. Vertical instabilities are discussed in more detail in Chapter 12.

In terms of numerical studies, many investigations have shown that the overall stability of non-circular tokamaks can be further improved by adding an outward pointing triangularity to the elongated cross section. This is particularly useful in suppressing pressure gradient driven modes and is also discussed in Chapter 12. All modern tokamaks are designed to have this elongated, outward pointing "D" shaped cross section. One example is the DIII-D experiment located at General Atomics (GA) in San Diego. The GA group has produced long-lived plasmas with values of $\beta_t \sim 8\%$, indeed an impressive achievement. A numerically computed equilibrium of a high β_t DIII-D equilibrium is illustrated in Fig. 6.18. Observe that the plasma has an elongation of $\kappa = 1.8$ and that the magnetic axis has shifted out considerably, corresponding to $\Delta_0/a \approx 0.3$.

Summary

A non-circular cross section represents an additional degree of freedom in the design of tokamaks, allowing a further optimization in performance compared to the circular cross section. A comparison of tokamaks with fixed ε, B_0, q_*, and V shows that as κ increases the maximum attainable β_t, I, and $\overline{J}_\phi$ also increase. This

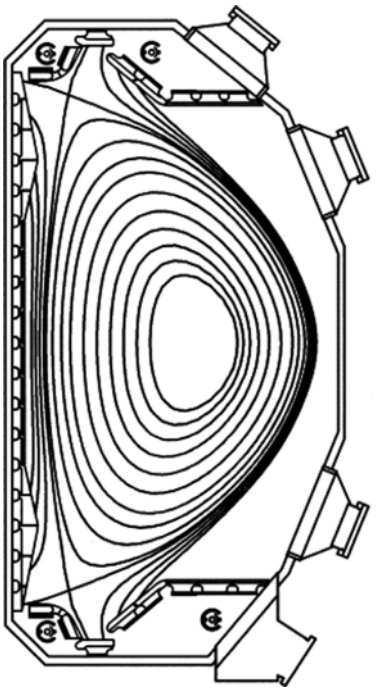

Figure 6.18 Numerically computed equilibrium for the DIII-D tokamak at General Atomics. Shown are flux surface plots corresponding to auxiliary heated high β tokamak operation. From DIII-D Team, 1998. Reproduced with permission from Elsevier.

conclusion has been accepted by the international fusion community and all modern tokamaks are designed to have elongated cross sections (with outward pointing triangularity). There is a practical limit on the maximum achievable elongation set by the onset of fast growing vertical MHD instabilities.

6.6 Exact solutions to the Grad–Shafranov equation (standard and spherical tokamaks)

The use of asymptotic expansions in ε has proven useful for developing intuition about radial pressure balance and toroidal force balance in tokamaks. However, since $\varepsilon \sim 1/3$ for a standard tokamak, this is not that small a value that one might expect the results to be quantitatively accurate for experimental applications. The situation is even more difficult for the ultra-tight aspect ratio spherical tokamak which has $\varepsilon \sim 3/4$. The implication is that for high-accuracy MHD applications to experiment, one needs "exact" solutions to the Grad–Shafranov equation.

In general exact solutions are obtained by numerically solving the Grad–Shafranov partial differential equation. Many such codes are in existence today.

Although the numerical solutions are essential for detailed experimental comparisons, they are not as convenient for developing simple scaling laws describing the effects of aspect ratio, elongation, and triangularity on tokamak equilibria. Stated differently, it would be desirable if in addition to the numerical codes there existed exact analytical solutions to the Grad–Shafranov equation.

Obtaining such exact analytic solutions is the main goal of this Section. It is shown how the exact problem for an up–down symmetric plasma with a smooth surface can be formulated and solved for the Solov'ev profiles. The results are first applied to a large circular tokamak (TFTR at Princeton Plasma Physics Laboratory, USA) and a large non-circular tokamak (JET in Abingdon, UK). A second application is the ultra-tight aspect ratio spherical tokamak (ST). A brief description of the ST, including its scientific motivation, is also presented. The analytic equilibrium solutions are then applied to an ST experiment (MAST at the Culham Laboratory, UK). A further related question addressed by means of the exact analytic solutions is the scaling of the equilibrium β limit with inverse aspect ratio.

An up–down symmetric configuration with a smooth plasma surface is the simplest case to analyze, although often not the most relevant experimentally because of the presence of a divertor. A brief discussion is presented describing the operation of a divertor which essentially consists of a set of coils and collector plates placed in close proximity to the plasma surface. It is the most common way that a plasma makes first contact with a material surface. The divertor has the dual goals of vacuum wall protection and impurity control. Modern tokamaks utilize divertors rather than limiters for these purposes. From the MHD point of view divertors are typically up–down asymmetric configurations with an X-point separatrix in either the upper or lower portion of the plasma. It is shown how the analytic solutions can be modified to treat the divertor geometry. The solutions are then applied to a large standard tokamak (the proposed ITER experiment being built in Cadarache, France) and a spherical tokamak (the NSTX experiment at Princeton Plasma Physics Laboratory, USA).

6.6.1 Mathematical formulation

Equations

The goal is to solve the exact Grad–Shafranov equation with the free functions again chosen as Solov'ev profiles: $F(dF/d\psi) = -A$ and $\mu_0(dp/d\psi) = -C$. With these choices the exact Grad–Shafranov equation becomes

$$R\frac{\partial}{\partial R}\left(\frac{1}{R}\frac{\partial \psi}{\partial R}\right) + \frac{\partial^2 \psi}{\partial Z^2} = A + CR^2 \tag{6.149}$$

At this point it is useful to normalize the flux function and the coordinates as follows: $R = R_0 X$, $Z = R_0 Y$, $\psi = \psi_0 U$ where $\psi_0 = R_0^2(A + CR_0^2)$. Also the signs are chosen so that $\psi_0 > 0$ and $U(X, Y) < 0$. The Grad–Shafranov equation reduces to

$$X\frac{\partial}{\partial X}\left(\frac{1}{X}\frac{\partial U}{\partial X}\right) + \frac{\partial^2 U}{\partial Y^2} = \alpha + (1-\alpha)X^2 \tag{6.150}$$

Here, $\alpha = A/(A + CR_0^2)$. Effectively α and ψ_0 have replaced A and C as the free parameters. The advantage of this normalization is that the differential equation itself is now a function of only a single parameter, α.

In terms of the formulation, there is a crucial difference in philosophy in the way that the exact equation is solved as compared to the previous asymptotic equations. For the asymptotic equations a standard approach is used. A surface is specified, for instance a circle or ellipse, and the equations are solved subject to the boundary conditions of regularity and $\psi = 0$ on the surface.

This approach does not readily work for the exact problem because simple analytic solutions cannot be found that exactly satisfy the boundary conditions on simple surfaces such as a circle or ellipse. Instead, the approach used is to find an exact analytic solution to Eq. (6.149) consisting of the superposition of a finite number of terms each with an undetermined amplitude. A series of boundary constraints is then applied, forcing the analytic solutions to a match a finite number of specified conditions on a known desired surface – one boundary constraint for each unknown amplitude. The resulting solution is now uniquely defined. One then simply plots the contours of $U =$ constant including the plasma surface $U = 0$. Obviously, matching properties at a finite number of points does not guarantee that the resulting $U = 0$ surface will be close to the desired matching surface at all points. One must just "take whatever the solution produces."

The mathematical challenges to make this approach work involve choosing (1) the right set of analytic basis functions, (2) the right number of terms in the finite sum, and (3) the right set of matching constraints, so that the resulting $U = 0$ surface closely matches the desired surface for a very wide range of plasma parameters. The procedure described in this Section does just that and follows the analysis presented in Cerfon and Freidberg (2010).

Mathematical solutions

The solution to Eq. (6.149) consists of particular and homogeneous contributions. A convenient way to write the particular solution is as follows:

$$U_P(X, Y) = \frac{\alpha}{2}X^2 \ln X + \frac{1-\alpha}{8}X^4 \tag{6.151}$$

The homogeneous solution satisfies

$$X\frac{\partial}{\partial X}\left(\frac{1}{X}\frac{\partial U_H}{\partial X}\right)+\frac{\partial^2 U_H}{\partial Y^2}=0 \tag{6.152}$$

Simple basis functions that exactly satisfy Eq. (6.149) consist of combinations of polynomials in X and Y. The exact form of each polynomial solution can be easily found by direct substitution.

The approach used here assumes that the overall solution can be written as a Taylor series in these polynomial solutions, starting from a constant and increasing up to and including sixth-order terms. Truncating the series at sixth-order polynomials is not an obvious choice and indeed was arrived at by trial and error. In any event, the exact analytic solution to the Grad–Shafranov equation used to model tokamaks is given by

$$\begin{aligned}
U(X,Y) &= \frac{\alpha}{2}X^2\ln X+\frac{1-\alpha}{8}X^4+\sum_0^6 c_j U_j\\
U_0 &= 1\\
U_1 &= X^2\\
U_2 &= Y^2-X^2\ln X\\
U_3 &= X^4-4X^2Y^2\\
U_4 &= 2Y^4-9Y^2X^2-(12Y^2X^2-3X^4)\ln X\\
U_5 &= X^6-12X^4Y^2+8X^2Y^4\\
U_6 &= 8Y^6-140Y^4X^2+75Y^2X^4-(120Y^4X^2-180Y^2X^4+15X^6)\ln X
\end{aligned} \tag{6.153}$$

Observe that all the polynomials are even in Y indicating that at this point attention is focused on up–down symmetric configurations.

Boundary constraints

The task now is to define seven boundary constraints that will serve to determine the seven unknown coefficients c_j. These constraints are chosen to match seven properties on a known desired plasma surface. A good choice for this reference surface, which is often used in the fusion community, is given parametrically in terms of τ as follows:

$$\begin{aligned}
X &= 1+\varepsilon\cos(\tau+\delta_0\sin\tau)\\
Y &= \varepsilon\kappa\sin\tau
\end{aligned} \tag{6.154}$$

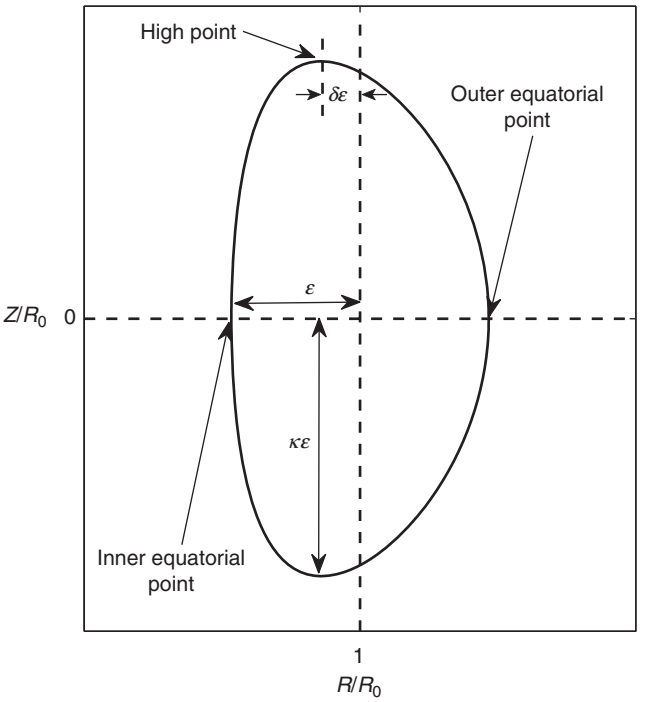

Figure 6.19 Geometry of the reference surface.

The surface and corresponding geometry, are illustrated in Fig. 6.19. Observe that there are three dimensionless parameters that define the geometry: the inverse aspect ratio $\varepsilon = a/R_0$, the elongation κ, and the triangularity $\delta = \sin \delta_0$.

The boundary constraints, again found by some trial and error, require matching the analytic flux function and its first and second derivatives at three separate points on the reference surface: the outer equatorial point, the inner equatorial point, and the high point maximum. This might appear to be nine constraints but two are automatically satisfied – the first derivative conditions at the outer and inner equatorial points by virtue of up–down symmetry. The seven boundary constraints can thus be written as

$$
\begin{aligned}
&1. \quad U(1+\varepsilon, 0) = 0 && \text{outer point flux} \\
&2. \quad U_{YY}(1+\varepsilon, 0) = -N_1 U_X(1+\varepsilon, 0) && \text{outer point curvature} \\
&3. \quad U(1-\varepsilon, 0) = 0 && \text{inner point flux} \\
&4. \quad U_{YY}(1-\varepsilon, 0) = -N_2 U_X(1-\varepsilon, 0) && \text{inner point curvature} \\
&5. \quad U(1-\delta\varepsilon, \kappa\varepsilon) = 0 && \text{high point flux} \\
&6. \quad U_X(1-\delta\varepsilon, \kappa\varepsilon) = 0 && \text{high point slope} \\
&7. \quad U_{XX}(1-\delta\varepsilon, \kappa\varepsilon) = -N_3 U_Y(1-\delta\varepsilon, \kappa\varepsilon) && \text{high point curvature}
\end{aligned}
\tag{6.155}
$$

Here, the curvature coefficients N_j can be easily calculated from the model surface

$$\begin{aligned} N_1 &= \left[\frac{d^2X}{dY^2}\right]_{\tau=0} = \frac{(1+\delta_0)^2}{\varepsilon\kappa^2} \\ N_2 &= \left[\frac{d^2X}{dY^2}\right]_{\tau=\pi} = -\frac{(1-\delta_0)^2}{\varepsilon\kappa^2} \\ N_3 &= \left[\frac{d^2Y}{dX^2}\right]_{\tau=\pi/2} = -\frac{\kappa}{\varepsilon\,\cos^2\delta_0} \end{aligned} \tag{6.156}$$

Once the free Solov'ev constants A and C, or equivalently α and ψ_0, are specified, the constraint conditions given by Eq. (6.155) translate into a set of seven linear inhomogeneous algebraic equations for the seven unknown coefficients c_j, a trivial numerical problem.

In analogy with the high β tokamak expansion, the last step in the formulation is to derive relationships between α and ψ_0 and the more physical parameters q_*, β_p, and β_t. From their definitions it can easily be shown that

$$\begin{aligned} \frac{1}{q_*} &= \frac{1}{2\pi}\left(\frac{2}{1+\kappa^2}\right)\left(\frac{\psi_0}{a^2B_0}\right)K_1 \\ \beta_p &= 8\pi^2\varepsilon^2(1-\alpha)\left(\frac{1+\kappa^2}{2}\right)\frac{K_2}{K_1^2K_3} \\ \beta_t &= \left[\frac{8\pi^2\varepsilon^4(1-\alpha)}{q_*^2}\right]\left(\frac{1+\kappa^2}{2}\right)^2\frac{K_2}{K_1^2K_3} \end{aligned} \tag{6.157}$$

where

$$\begin{aligned} K_1 &= \int dXdY\left[\frac{\alpha+(1-\alpha)X^2}{X}\right] \\ K_2 &= \int XdX\,dY(-U) \\ K_3 &= \int XdXdY \end{aligned} \tag{6.158}$$

and the integrals are carried out over the plasma cross section.

To summarize, exact Grad–Shafranov equilibria are found by specifying the geometric parameters ε, κ, and δ and the plasma parameters q_* and α. (Practically it is more convenient to specify α rather than β_t.) The equation for $U(X,Y)$ is now fully specified and the expansion coefficients c_j are easily found by applying the boundary constraints and solving the resulting set of linear algebraic equations.

Table 6.1 *MHD parameters for TFTR and JET.*

Parameters	Symbol	Units	TFTR	JET
Major radius	R_0	m	2.5	3
Minor radius	a	m	0.87	1
Aspect ratio	R_0/a	-	2.9	3
Elongation	κ	-	1	1.7
Triangularity	δ	-	0	0.25
Toroidal magnetic field	$B_0 = B(R_0)$	T	5.6	3.6
Plasma current	I	MA	2.7	4
Kink safety factor	q_*	-	3.1	2.7
Average temperature	$(\overline{T}_e + \overline{T}_i)/2 \equiv \overline{T}_k$	keV	23	10
Average density	$\overline{n}_{20}$	$10^{20}\,\mathrm{m}^{-3}$	1.0	0.5
Toroidal beta	β_t	-	2.9%	3%

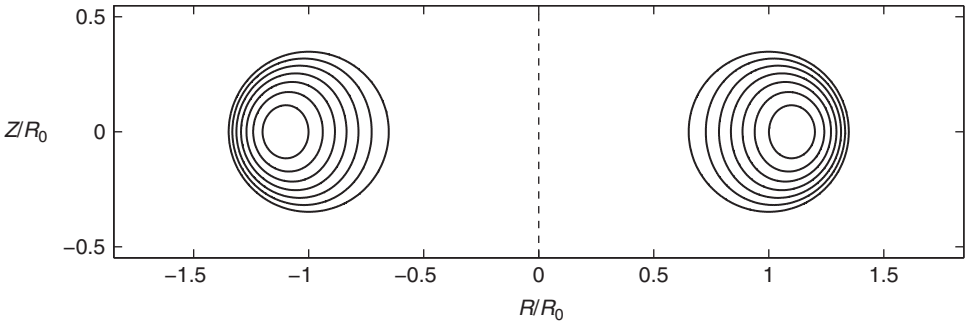

Figure 6.20 Exact Solov'ev equilibrium for TFTR.

Once $U(X, Y)$ is known then ψ_0/a^2B_0, β_p, and β_t are easily numerically evaluated from Eq. (6.157).

6.6.2 Examples: TFTR and JET

The simplest initial test of the analytic solution procedure is the previously discussed circular cross section TFTR experiment at Princeton Plasma Physics Laboratory, whose MHD parameters are given in Table 6.1.

The analytic solution procedure is applied and the resulting flux surfaces are illustrated in Fig. 6.20. One sees that the procedure reliably reproduces shifted circular flux surface equilibria.

Consider now MHD equilibria of the Joint European Torus (JET), a large tokamak built as a collaborative European project. It is located near Oxford, UK, adjacent to the Culham Laboratory site. JET has an elongated, outward pointing "D" cross section. It is a "standard" tokamak in the sense of having a typical aspect ratio of about $R_0/a \approx 3$. Compared to other tokamaks it is unique in that it has an

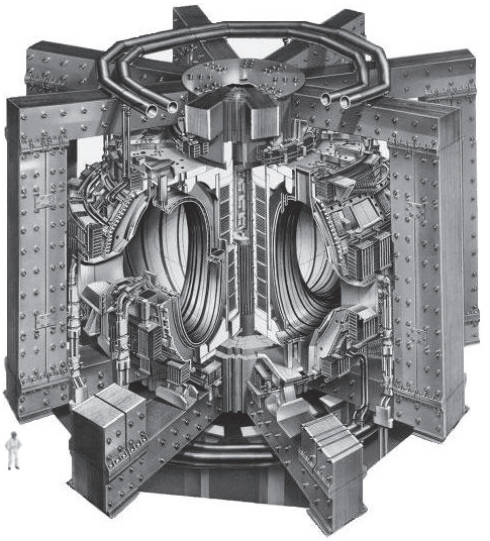

Figure 6.21 Schematic drawing of JET. Courtesy of EFDA-JET.

iron (rather than air) core transformer to produce the ohmic heating current. The iron core improves the efficiency of the primary of the ohmic transformer, but the experiment must live with the maximum field limitations imposed by saturation of the iron. JET, along with TFTR, are the only two tokamaks at this point in time that have operated with tritium. One of the most impressive experimental campaigns was carried out in the late 1990s. Here, 16 MW of fusion power was produced for a short period of time in a 50–50 D-T plasma. About 25 MW of external heating power was required to accomplish this goal.

A drawing of JET is shown in Fig. 6.21. It is indeed a large facility. The experimental MHD parameters characterizing high-performance D-T plasmas are also given in Table 6.1. Although JET normally operates with a divertor, the analytic procedure assumes that the surface has been smoothed out. JET, in fact, is a relatively easy test for the equilibrium procedure. Using the values given above, the equilibrium flux surfaces for the Solov'ev profiles have been calculated and are illustrated in Fig. 6.22. Observe the elongated "D" shaped plasma and the finite shift of the magnetic axis. The flux surfaces are smooth and nested showing that the analytic solutions provide a credible representation of high-performance JET equilibria.

6.6.3 Example: the spherical tokamak (ST)

Description of the spherical tokamak

A more challenging test for the analytic equilibrium procedure is the spherical tokamak (Peng *et al.*, 1985). As stated, a "spherical tokamak" is a tokamak with a

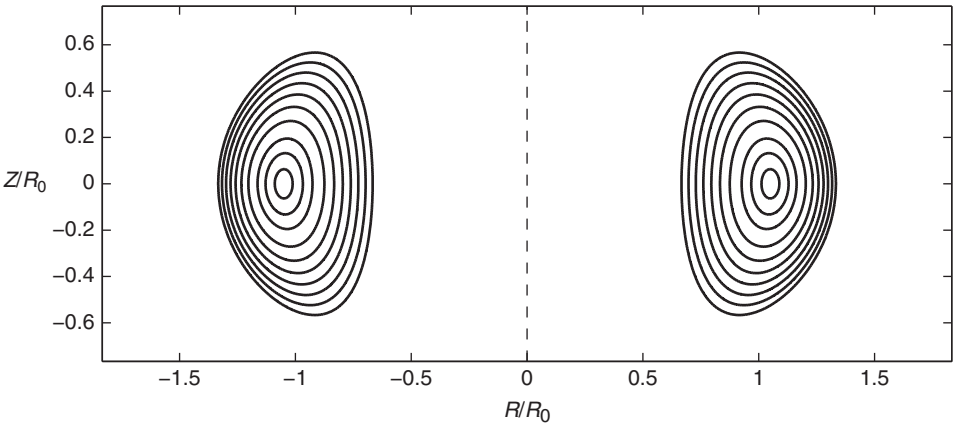

Figure 6.22 Exact Solov'ev equilibrium for JET.

very tight aspect ratio, typically $R_0/a \sim 1.2$–1.4. It is this tight aspect ratio that is challenging to model with the analytic solutions.

Before proceeding with the MHD equilibrium analysis it is useful to briefly review the basic physical properties of an ST, in particular, the motivation behind the concept. One of the primary motivations behind the ST is based on the fact that the maximum achievable β in a tokamak from both MHD equilibrium and stability limits scales as $\beta \sim \varepsilon$. Clearly as the aspect ratio becomes tighter, then the maximum β increases. Higher values of β could potentially add to the attractiveness of a fusion reactor either by allowing the use of lower magnetic fields or alternatively by resulting in a more compact design. Both options would lead to a lower cost.

However, the tight aspect ratio strategy has both pros and cons with respect to reactor desirability. In fact, the discussion below suggests that when engineering considerations are taken into account the ST is marginal at best in terms of leading to improved reactor designs as compared to a standard tokamak. Nevertheless, there is a different application for which the ST may be better suited – a volume neutron source for materials testing.

The basis for these statements is as follows. The gains in β and compactness must be balanced against several problems that are more serious than for the standard tokamak. First, achieving high power density in a fusion reactor requires high pressure which is related to but not the same as high β. Specifically, engineering constraints limit the maximum allowable magnetic field on the inner leg of the toroidal field magnet to a value $B_\phi(R_0 - a, 0) = B_{\max}$. Thus, tight aspect ratio leads to a much larger reduction in B_0 at the plasma center where β is defined, because of the strong $1/R$ dependence as $\varepsilon \to 1$: $B_0/B_{\max} = 1 - \varepsilon$. The implication

is that $\langle p \rangle \propto \beta_t B_{\max}^2 (1-\varepsilon)^2$. One sees that even if the maximum beta scales as $\beta_t \sim \varepsilon$ the gains in pressure ultimately diminish for a very tight aspect ratio.

Second, to achieve a very tight aspect ratio the blanket and almost all the shield must be removed from the inboard side of the plasma. With only a small shield it is no longer possible to use superconducting magnets for the toroidal field coils. They must be made of copper. One consequence is that a copper central leg dissipates a substantial amount of ohmic power. Detailed reactor studies show that favorable power balance in a reactor requires that $B_{\max}$ in an ST be less than about 7.5 T. This should be compared to $B_{\max} \approx 13$ T for superconducting magnets which are limited by stress and not ohmic losses. A lower $B_{\max}$ again leads to a lower plasma pressure.

The overall conclusion from this discussion, as well as from detailed systems studies, is that the ST does not lead to the large gains in reactor attractiveness over the standard tokamak that might have been originally anticipated. However, when viewed as a volume neutron source, the ST may be more desirable. A source of 14 MeV fusion neutrons is essential for developing and testing the advanced materials that are required in a reactor. No such source currently exists in the world fusion program. A key feature of such a source is that its main goal is the production of a high-intensity 14 MeV neutron flux in a relatively small volume compared to a power reactor. The goal is not economical fusion electricity. Therefore, even if the cost per ST neutron is somewhat higher than for a standard tokamak, the compact ST volume may lead to a lower absolute cost because the total number of neutrons produced is smaller, although still more than adequate for a volume neutron source. This would be highly desirable.

Example: the Mega Amp Spherical Tokamak (MAST)

Having motivated the ST concept, one can now focus on calculating a corresponding MHD equilibrium from the analytic solutions. Towards this goal note that several ST experiments are currently in operation in the world's fusion program with the two largest devices being the Mega Amp Spherical Tokamak (MAST) at the Culham Laboratory in the UK and the National Spherical Torus Experiment (NSTX) at the Princeton Plasma Physics Laboratory in the USA.

The MAST experiment serves as a good model to test the equilibrium procedure. A drawing of MAST is shown in Fig. 6.23. Observe the tight aspect ratio. MAST also has a large plasma–wall separation and poloidal field coils located inside the vacuum chamber. This latter feature allows more flexibility and easier experimental control of the plasma shape. On the other hand, with the large plasma–wall separation, smaller image currents flow as the plasma moves, thereby reducing the effects of external flux conservation on MHD equilibrium and stability.

Table 6.2 *MHD parameters for MAST.*

Parameters	Symbol	Units	MAST
Major radius	R_0	m	0.85
Minor radius	a	m	0.65
Aspect ratio	R_0/a	-	1.3
Elongation	κ	-	2.45
Triangularity	δ	-	0.5
Toroidal magnetic field	$B_0 = B(R_0)$	T	0.52
Plasma current	I	MA	1.35
Kink safety factor	q_*	-	3.35
Average temperature	$(\overline{T}_e + \overline{T}_i)/2 \equiv \overline{T}_k$	keV	0.94
Average electron density	$\overline{n}_{20}$	$10^{20}\,\mathrm{m}^{-3}$	0.5
Toroidal beta	β_t	-	0.14

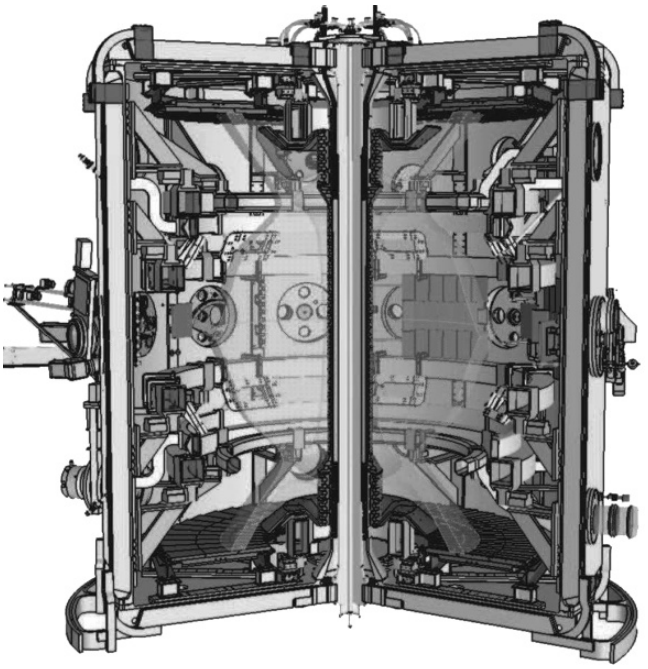

Figure 6.23 Schematic drawing of MAST. Courtesy of William Morris.

High-performance discharges on MAST are characterized by the MHD parameters listed in Table 6.2. The higher values of β_t anticipated for a spherical tokamak have indeed been achieved experimentally.

With all the input parameters specified it is now a straightforward matter to calculate an analytic MAST equilibrium. The resulting flux surface plots are

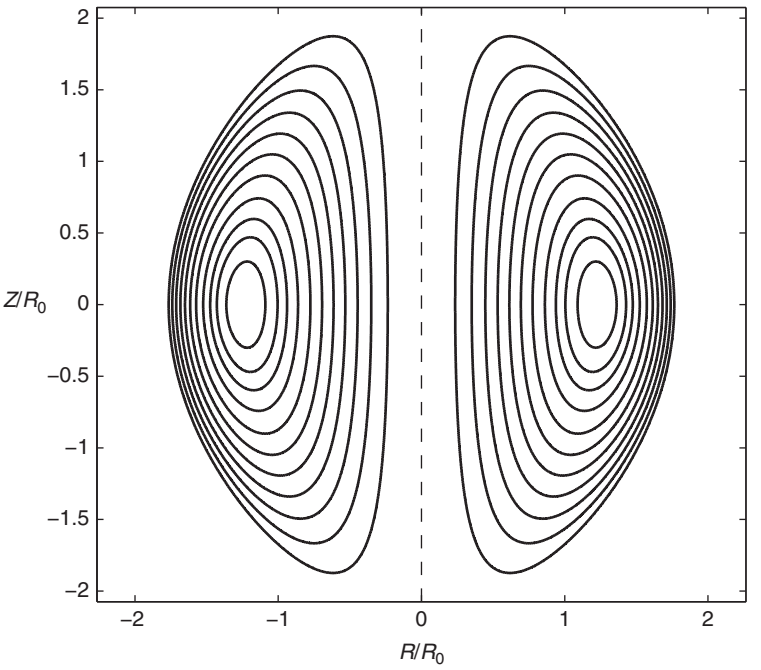

Figure 6.24 Exact Solov'ev equilibrium for MAST

illustrated in Fig. 6.24. Again, the procedure has no difficulty producing a set of realistic, nested flux surfaces, even with a very tight aspect ratio.

6.6.4 The equilibrium β limit

The JET and MAST examples demonstrate that it is possible to calculate exact analytic equilibria using realistic experimental parameters. It is also of theoretical interest to examine the equilibrium β limit using the exact solutions. The issue is to determine whether the basic scaling $\beta_t \propto \varepsilon$ extends into the regime of tight aspect ratio or is only valid for small ε where the asymptotic theories are accurate.

The question can be addressed in a straightforward manner as follows. Keep in mind that the free inputs to the exact solutions are the shape factors ε, κ, and δ and the plasma parameters q_* and α (with α simpler to specify than β_t). Now, the equilibrium β limit corresponds to the situation where the separatrix X-point moves onto the inside of the plasma surface. Mathematically, this is equivalent to setting $B_Z(R_0 - a, 0) = 0$, a condition that puts a constraint on the value of α; that is, α is no longer a free input parameter. In terms of the normalized equations the X-point constraint can be written as

$$U_X(1 - \varepsilon, 0) = 0 \tag{6.159}$$

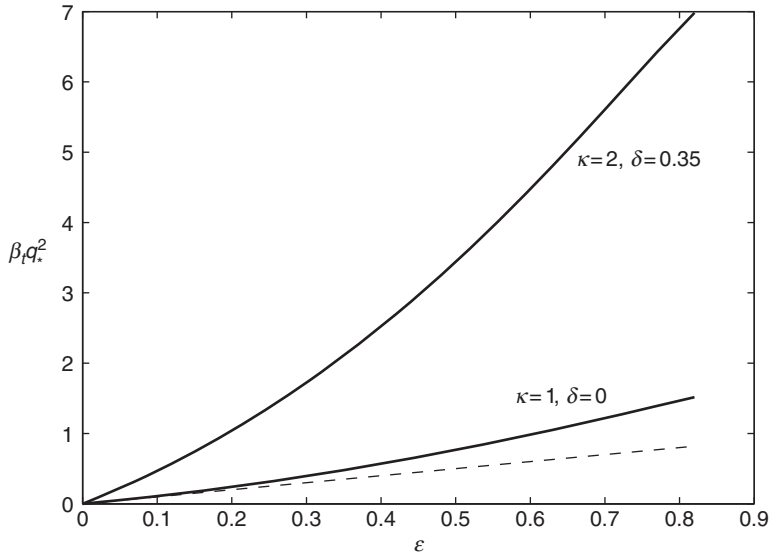

Figure 6.25 Exact equilibrium limit using the Solov'ev profiles.

With this extra condition the analytic problem has eight, not seven, unknown coefficients: the seven c_j plus α.

An examination of Eqs. (6.150) and (6.153) shows that the new constraint equation is also a linear algebraic equation with α being a new unknown. Thus instead of solving seven linear algebraic equations one now has to solve eight linear algebraic equations, a negligible issue computationally. This procedure has been carried out and the results are illustrated in Fig. 6.25. Plotted here are two curves of $\beta_t q_*^2$ vs. ε at the equilibrium limit. The first curve fixes $\kappa = 1$ and $\delta = 0$, approximately corresponding to circular surfaces. Also shown as a dashed line is the previously derived asymptotic result $\beta_t q_*^2 = \varepsilon$. The second curve fixes $\kappa = 2$ and $\delta = 0.35$, which is more typical of present day standard and spherical tokamaks.

There are two conclusions to note. First, a tokamak with an elongated cross section has a higher equilibrium β_t limit than a circular tokamak assuming the same aspect ratio and the same critical value of q_* for stability. This is in agreement with the simple analytic large aspect ratio limit for the Solov'ev profiles previously discussed.

Second, the actual scaling of critical β_t with ε is more optimistic than the simple linear relation predicted by the large aspect ratio analysis. In other words, tight aspect ratio may be even more desirable than originally thought in terms of increasing β_t. However, keep in mind that this conclusion is based on the simple definition of β_t, which is normalized to the central toroidal field. In a tight aspect

ratio tokamak one should realistically include the poloidal magnetic energy as well as the toroidal magnetic energy in the evaluation of β_t, which would reduce the improvements over the linear scaling of β_t with ε.

6.6.5 Up–down asymmetric solutions

The discussion related to exact analytic solutions has thus far been focused on up-down symmetric configurations with smooth plasma surfaces. However, as stated, most modern tokamaks operate with an up–down asymmetric geometry because of the presence of a single null divertor. This section shows how the analytical procedure can be extended to include the two new effects associated with a divertor: (1) up–down asymmetry and (2) the presence of an X-point separatrix.

The discussion begins with a brief description of the operation of a divertor. Next, it is shown how the analytic solutions must be modified to allow for up–down asymmetry. Lastly, it is shown how the boundary constraints must be modified to permit an X-point. The sections that follow demonstrate the analytic procedure by means of two examples. A standard tokamak (ITER) and a spherical tokamak (NSTX).

Operation of a divertor

In a qualitative sense a divertor and a limiter protect the vacuum chamber in the same way. Particles which diffuse across the edge of the plasma are lost by rapid parallel motion to a robust target plate before they can diffuse radially across the magnetic field and strike the vacuum wall. Recall though that a basic problem with the limiter is that neutral impurities from the target can diffuse back into the plasma and strongly degrade performance. This is difficult to prevent because the edge of the plasma is by construction in contact with the limiter.

The divertor has the attractive feature of substantially reducing impurity build-up while continuing to protect the vacuum wall. It does this by guiding a narrow layer of magnetic lines away from the edge of the plasma as shown in Fig. 6.26. Physically, the layer is produced by a set of poloidal coils in close proximity to the plasma surface. The currents in these coils are chosen to generate a magnetic field which opposes the poloidal field in the plasma. The result is the formation of a field null corresponding to an X-point on the separatrix flux surface. The magnetic lines in the region just outside the separatrix, known as the scrape-off layer, now must travel a substantial distance away from the plasma edge before they ultimately make contact with the target plate. This is the main benefit of the divertor. The first contact between the plasma and a material surface is a relatively large distance away from the plasma edge, and not the short distance as for a limiter.

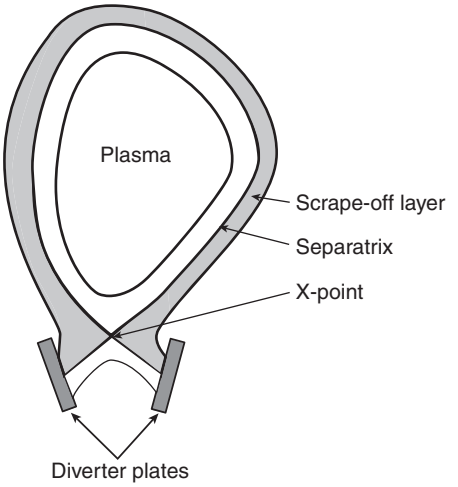

Figure 6.26 Schematic diagram of a divertor.

The divertor thus helps prevent impurity build-up as follows. Neutral impurities emitted from the target surface must now travel a substantial distance before crossing the plasma surface. There is a reasonably high probability that they will become ionized before doing so. Once ionized the charged particles flow parallel to the magnetic field where they are once again absorbed by the target plate – they do not cross the plasma surface.

Another advantage of the divertor over the limiter is that the target plates can be tilted at an angle with respect to the magnetic field as shown in Fig. 6.26. This allows the field lines to be spread over a larger surface area. These features cause a given plasma heat load to be deposited out over a larger area than is usually possible for a limiter. Lowering the heat load is a very important issue because typical values in a fusion plasma are very high – high enough in fact to cause melting if the field lines are concentrated and perpendicular to the target plate. Lower heat load has the added benefit of reducing the sputtering of neutral atoms from the target plate.

A final important advantage of the divertor occurs because the plasma edge is defined by the magnetic separatrix and not a solid surface such as a limiter. This allows the plasma to have a much higher edge temperature, on the order of several keV, which has a very favorable effect on overall plasma confinement and fusion power production.

Of course all of these advantages do not come without a price. One main disadvantage is that additional coils are necessary and extra volume is needed to make room for the divertor target plates. This disadvantage translates into higher costs. The general consensus at present is that the improved performance provided by a divertor is worth the extra cost.

Most modern tokamaks have a single null divertor. Clearly though it is possible to have an up–down symmetric double null divertor which could potentially halve the heat load on each target plate. This is often not the primary choice for two reasons. First, an additional divertor requires even more volume for coils and hence a further increase in cost. Second, the divertors must be very accurately balanced or else the entire heat load will be deposited on the closer X-point target plate, effectively "wasting" the second divertor.

Based on this discussion one sees that to model an MHD equilibrium containing a single null divertor the solutions must allow for an up–down asymmetric geometry with a separatrix containing an X-point.

Up–down asymmetric equilibria

The analytic solution to the Grad–Shafranov equation with Solov'ev profiles for up–down symmetric equilibria has been given by Eq. (6.153). It is straightforward to generalize the solution to include up–down asymmetric equilibria by adding polynomial solutions which are odd in Y. A short calculation shows that the generalized equilibrium can be written as

$$U(X,Y) = \frac{\alpha}{2}X^2 \ln X + \frac{1-\alpha}{8}X^4 + \sum_0^{11} c_j U_j \tag{6.160}$$

where five new terms have been added to the sum. The terms U_0–U_6 have already been defined in Eq. (6.153). The additional terms U_7–U_{11} are given by

$$\begin{aligned} U_7 &= Y \\ U_8 &= YX^2 \\ U_9 &= Y^3 - 3YX^2 \ln X \\ U_{10} &= 4Y^3X^2 - 3YX^4 \\ U_{11} &= 8Y^5 - 45YX^4 - (80Y^3X^2 - 60YX^4)\ln X \end{aligned} \tag{6.161}$$

Observe that polynomials up to fifth order have been maintained. This is the number, again found by trial and error, that makes the equilibrium procedure robust.

X-point boundary constraints

Consider now the boundary constraints that determine the 12 c_j coefficients. The original seven constraints specified in Eq. (6.155) are still assumed to be valid and apply to the upper half of the plasma surface. Five new terms have been added to the solution thereby requiring five new boundary constraints for closure. These are as follows. The slope conditions at the outer and inner equatorial points are no longer automatically satisfied since the solution contains polynomials that are odd

in Y. Satisfying the slope conditions corresponds to two new constraints. The remaining three constraints are used to define the single null X-point, which is assumed to be located at $X = X_{\text{sep}}$, $Y = Y_{\text{sep}}$ with $Y_{\text{sep}} < 0$. At the X-point the flux and both of its derivatives must vanish. The vanishing of the flux puts the X-point on the plasma surface while the vanishing of both derivatives corresponds to a null in the poloidal field, the definition of an X-point.

The new conditions can be written mathematically as follows:

$$\begin{array}{lll} 8. & U_Y(1+\varepsilon,0)=0 & \text{outer point slope} \\ 9. & U_Y(1-\varepsilon,0)=0 & \text{inner point slope} \\ 10. & U(X_{\text{sep}},Y_{\text{sep}})=0 & \text{X-point flux} \\ 11. & U_X(X_{\text{sep}},Y_{\text{sep}})=0 & \text{X-point } B_Y=0 \\ 12. & U_Y(X_{\text{sep}},Y_{\text{sep}})=0 & \text{X-point } B_X=0 \end{array} \tag{6.162}$$

The additional constraints also lead to linear algebraic equations. The total set of constraints now consists of 12 simultaneous linear algebraic equations, still a trivial numerical problem.

6.6.6 Example: the International Thermonuclear Experimental Reactor (ITER)

The overall goals of ITER are to (1) investigate burning plasma physics in a long pulse, high-temperature, D-T experiment and (2) address and solve a number of the fusion technology issues that will arise in a fusion reactor. ITER thus has the crucial role of being the flagship facility for the world's fusion program for the next two decades. The project is enormously important in that future progress towards a fusion reactor will be directly tied to the physics and technological performance of ITER. A brief technical description of ITER is presented below.

The primary physics mission of ITER is to produce a stable, well-confined, $Q = 10$ plasma lasting for a sufficiently long duration to reach quasi steady state operation. Here, Q = fusion power out/external heating power in. A second physics mission is to achieve steady state operation using non-inductive (i.e., no transformer) current drive at $Q \gtrsim 5$. With respect to technology, construction of ITER would demonstrate the viability of large superconducting magnets, various plasma facing materials, and large-scale remote handling. It would also test the effectiveness of the divertor design and begin to explore tritium breeding.

The ITER design is illustrated in Fig. 6.27. Note that ITER has a single null divertor and superconducting magnets constructed of niobium–tin. The magnetic field at the center of the plasma is $B_0 = 5.3\,\text{T}$. To keep the cost as low as possible, the size of the machine has been minimized subject to the constraint of achieving $Q = 10$ operation assuming high-performance energy confinement scaling (i.e., H-mode scaling) and MHD stability without a perfectly conducting wall. This

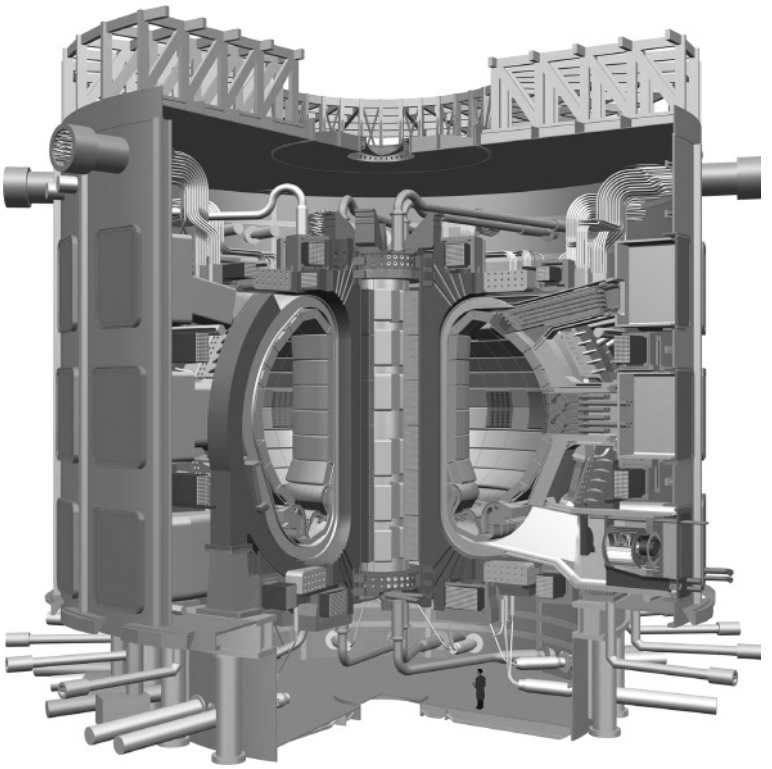

Figure 6.27 Schematic drawing of ITER. Courtesy of ITER.

leads to a machine design whose MHD related parameters are summarized in Table 6.3. Many parameters are quite comparable to those of a full power producing fusion reactor. The main difference is that ITER is still largely an experimental facility. Therefore it has not been designed to have the very high duty factor associated with a steady state power producing reactor. Also, the thermal power output is still about an order of magnitude lower than that required in a reactor.

For base operation, ITER will have about 70 MW of external heating power, divided among negative ion driven neutral beams, ion cyclotron heating, and electron cyclotron heating. ITER will operate for pulse durations of about $\tau_{\text{pulse}} \approx$ 400 sec, driven by the ohmic transformer. If successful, ITER should produce a $Q = 10$ plasma corresponding to a fusion performance factor of $\overline{p}\tau_E = 6.4$ atm-sec.

The parameters in the table have been used as inputs to the analytic solution procedure. The resulting flux surfaces have been calculated and are illustrated in Fig. 6.28. The flux surfaces are quite reasonable in appearance exhibiting smooth nested contours bounded by an up–down asymmetric single null separatrix. The analytic solution has thus just been shown to be capable of modeling a fusion relevant plasma with a sophisticated plasma shape.

Table 6.3 *MHD parameters for base operation of ITER.*

Parameters	Symbol	Units	ITER
Major radius	R_0	m	6.2
Minor radius	a	m	2.0
Aspect ratio	R_0/a	-	3.2
Elongation (95% flux surface)	κ	-	1.7
Triangularity (95% flux surface)	δ	-	0.23
Horizontal X-point location	$X_{sep} = R_{sep}/R_0$	-	0.93
Vertical X-point location	$Y_{sep} = Z_{sep}/R_0$	-	−0.65
Toroidal magnetic field	$B_0 = B\,(R_0)$	T	5.3
Plasma current	I	MA	15
Kink safety factor	q_*	-	1.9
Safety factor (95% flux surface)	q_{95}	-	3.0
Average temperature	$\overline{T}_e \approx \overline{T}_i \equiv \overline{T}_k$	keV	11.2
Average electron density	$\overline{n}_{20}$	$10^{20}\,\mathrm{m}^{-3}$	0.91
Toroidal beta	β_t	-	0.026

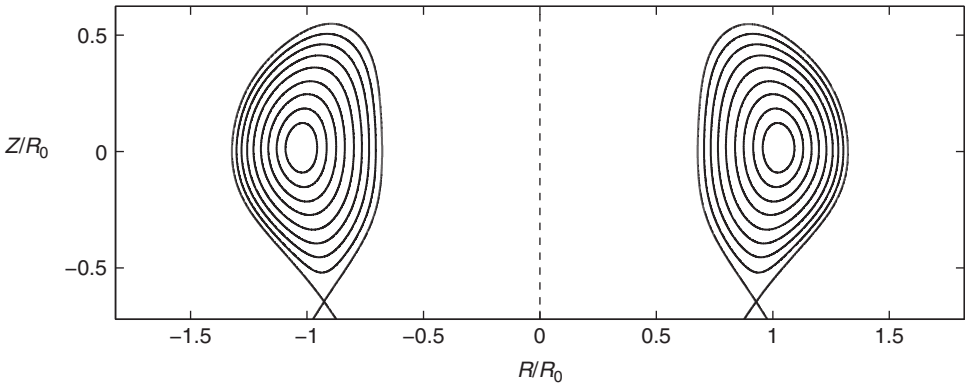

Figure 6.28 Exact Solov'ev equilibrium for ITER.

6.6.7 Example: the National Spherical Torus Experiment (NSTX)

The spherical tokamak (ST) is the most challenging test for the analytic solution procedure. The configuration is characterized by finite aspect ratio, up–down asymmetry, a single null divertor, and high β. The motivation and potential role for the ST in fusion research has been discussed in Section 6.6.3. The MHD parameters for a high-performance NSTX discharge are summarized in Table 6.4.

These parameters are supplied as input to the analytic solution procedure. The corresponding flux surfaces are illustrated in Fig. 6.29. The surfaces are smooth and bounded by a single X-point separatrix. Even for this relatively difficult test the analytic procedure produces a very reasonable solution.

Table 6.4 *MHD parameters for NSTX.*

Parameters	Symbol	Units	NSTX
Major radius	R_0	m	0.85
Minor radius	a	m	0.68
Aspect ratio	R_0/a	-	1.25
Elongation (95% flux surface)	κ	-	2
Triangularity (95% flux surface)	δ	-	0.4
Horizontal X-point location	$X_{\text{sep}} = R_{\text{sep}}/R_0$	-	0.59
Vertical X-point location	$Y_{\text{sep}} = Z_{\text{sep}}/R_0$	-	−1.76
Toroidal magnetic field	$B_0 = B\,(R_0)$	T	0.3
Plasma current	I	MA	1
Kink safety factor	q_*	-	2.0
Average temperature	$(\overline{T}_e + \overline{T}_i)/2 \equiv \overline{T}_k$	keV	1.1
Average electron density	$\overline{n}_{20}$	10^{20} m $^{-3}$	0.2
Toroidal beta	β_t	-	0.2

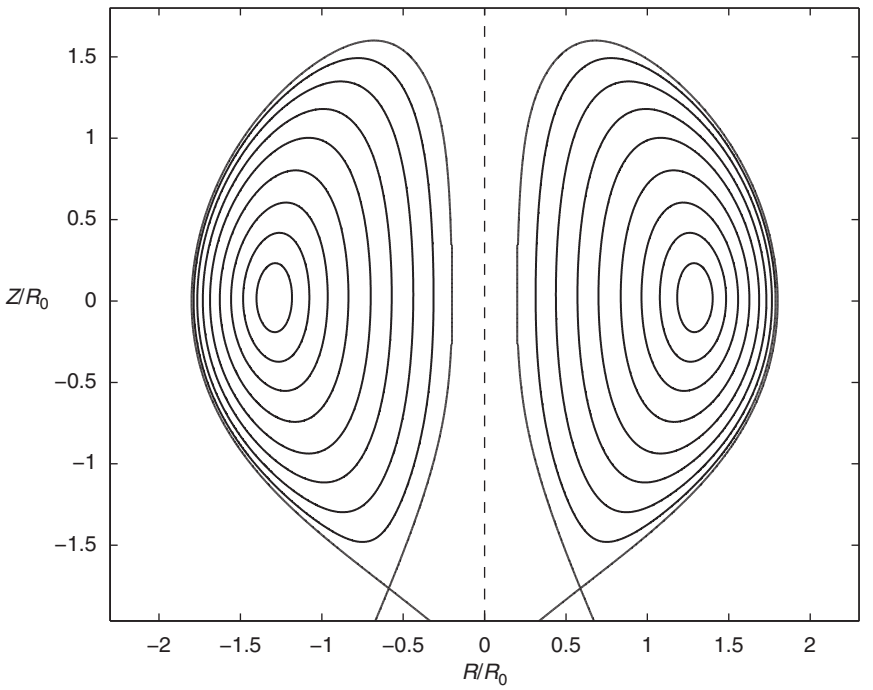

Figure 6.29 Exact single null divertor Solov'ev equilibrium for NSTX.

6.6.8 Summary

An exact analytic solution to the Grad–Shafranov equation using the Solov'ev profiles for $p(\psi)$ and $F(\psi)$ has been derived consisting of a finite number of polynomial solutions. A procedure involving the application of boundary

constraints is discussed which serves to determine the unknown amplitudes multiplying each polynomial. Solving for these coefficients requires the solution of a set of simultaneous linear algebraic equations, a trivial task numerically.

The procedure is robust and is capable of calculating a wide range of exact tokamak equilibria of interest to fusion research. The range of equilibria varies from the easiest case, an up–down symmetric circular plasma with an aspect ratio of $R_0/a = 3$, to the most challenging case, an up–down asymmetric non-circular plasma with a single null divertor and a tight aspect ratio, $R_0/a = 1.4$. The specific equilibria considered correspond to the following tokamaks: TFTR, JET, MAST, ITER, and NSTX.

Although "exact" fully numerical Grad–Shafranov solvers are readily available in the fusion community, the analytic solutions are useful for providing insight, deriving scaling laws, and benchmarking numerical codes.

6.7 The helical Grad–Shafranov equation (the straight stellarator)

6.7.1 Overview

The equilibrium analysis in Section 6.6 focused on 2-D systems with toroidal axisymmetry. It is a fact that the MHD equilibrium of systems with one degree of symmetry can always be described by a single partial differential equation – for example the Grad–Shafranov equation when $\partial/\partial\phi = 0$.

A second useful type of 2-D symmetry that also leads to a Grad–Shafranov-like equation is helical symmetry, a good model for a "straight stellarator." Stellarators are inherently 3-D helical–toroidal configurations but some insight to their behavior can be obtained by un-bending the torus into a straight helix. It is of particular interest to demonstrate one of the major attractive features of a stellarator, the ability to achieve good MHD equilibrium and stability without the need for a net toroidal current. A configuration with this property does not require an ohmic transformer or a means of external non-inductive current drive, both of which are key requirements for a tokamak. Also, a system with no net current is expected to be more stable against current-driven kinks (which often lead to major disruptions) than a tokamak.

Mathematically, helical symmetry can be understood by first recalling that toroidal axisymmetry assumes that all physical quantities have the following 2-D geometrical dependence: $\psi(R,\phi,Z) \rightarrow \psi(R,Z)$. Similarly, helical symmetry expressed in a standard r,θ,z straight cylindrical system implies that $\psi(r,\theta,z) \rightarrow \psi(r,l\theta + hz)$. All quantities are only a function of radius r and helical angle $\alpha = l\theta + hz$. The integer l refers to the poloidal periodicity number while $2\pi/h$ is the axial wavelength of the helix. A drawing of a straight helical system is shown in Fig. 6.30. If one wants to think in terms of an equivalent torus then r is the minor radius measured from the center of the vacuum chamber, $z = -R_0\phi$, where R_0 is the major radius, and $h = N / R_0$, where N is the number of helical periods around the torus.

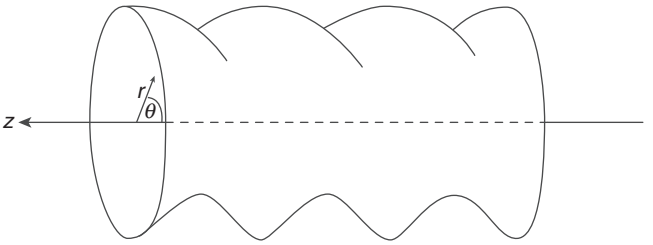

Figure 6.30 A straight helical model of a stellarator

There are three goals in this section. The first is to derive an analogous Grad–Shafranov equation for a system with helical symmetry. The second goal is to solve this equation in the limit of low β. A key question is to see whether or not it is possible to construct equilibria with zero net z current on every flux surface. The third goal is to calculate the rotational transform in order to address the following question. Can a system with no net current have a non-zero rotational transform? This is a non-trivial question since the magnetic lines in a helical system tend to oscillate back and forth on a flux surface. It is not obvious that in addition to oscillating, the lines also wrap around the plasma.

These "introduction to the stellarator" topics are now discussed in detail in the remainder of the section. A more detailed discussion of stellarators is presented in Chapter 7.

6.7.2 The helical Grad–Shafranov equation

The derivation of the helical Grad–Shafranov equation (Solov'ev, 1967) is similar to the toroidally symmetric version presented in Section 6.2. One modification though is the introduction of a new set of unit vectors which are convenient for carrying out the calculation. The new unit vectors and their inverse relations are defined as follows:

$$\begin{aligned} &\mathbf{e}_r && \mathbf{e}_r \\ &\mathbf{e}_\alpha = (l\,\mathbf{e}_\theta + hr\,\mathbf{e}_z)/l_0 && \mathbf{e}_\theta = (l\,\mathbf{e}_\alpha - hr\,\mathbf{e}_s)/l_0 \\ &\mathbf{e}_s = (l\,\mathbf{e}_z - hr\,\mathbf{e}_\theta)/l_0 && \mathbf{e}_z = (l\,\mathbf{e}_s + hr\,\mathbf{e}_\alpha)/l_0 \end{aligned} \tag{6.163}$$

where $l_0(r) = (l^2 + h^2r^2)^{1/2}$. Helical symmetry implies that $\mathbf{e}_s \cdot \nabla(\text{scalar}) = 0$. The basic steps in the derivation are now outlined below.

The first equation of interest is $\nabla \cdot \mathbf{B} = 0$. The 2-D symmetry again makes it possible to introduce a stream function ψ as follows:

$$\begin{aligned} B_r &= -\frac{1}{r}\frac{\partial \psi}{\partial \alpha} \\ B_\alpha &= \frac{1}{l_0}(lB_\theta + hrB_z) = \frac{1}{l_0}\frac{\partial \psi}{\partial r} \end{aligned} \tag{6.164}$$

The total magnetic field can thus be written in a compact form as

$$\mathbf{B} = \frac{1}{l_0}\mathbf{e}_s \times \nabla\psi + B_s\mathbf{e}_s \tag{6.165}$$

Here, $B_s = (1/l_0)(lB_z - hrB_\theta)$ is the third component of magnetic field and is unknown at this point.

The next step is to substitute into Ampere's law $\nabla \times \mathbf{B} = \mu_0\mathbf{J}$. A straightforward calculation yields an expression for $\mu_0\mathbf{J}$ which can be written as

$$\mu_0\mathbf{J} = -\frac{1}{l_0}\mathbf{e}_s \times \nabla(l_0 B_s) + \left(l_0\Delta^*\psi - \frac{2hl}{l_0^2}B_s\right)\mathbf{e}_s \tag{6.166}$$

where for the case of helical symmetry

$$\Delta^*\psi \equiv \frac{1}{r}\frac{\partial}{\partial r}\left(\frac{r}{l_0^2}\frac{\partial\psi}{\partial r}\right) + \frac{1}{r^2}\frac{\partial^2\psi}{\partial\alpha^2} \tag{6.167}$$

It is also of interest to single out the z component of $\mathbf{J}$ in view of the end goal of designing stellarators with no net current on every flux surface:

$$\mu_0 J_z = -\frac{hr}{l_0^2}\frac{\partial}{\partial r}(l_0\, B_s) + l\left(\Delta^*\psi - \frac{2hl}{l_0^3}B_s\right) \tag{6.168}$$

The calculation now proceeds with the momentum equation $\mathbf{J} \times \mathbf{B} - \nabla p = 0$. Forming the dot product of this equation with $\mathbf{B}$ yields

$$\mathbf{B}\cdot\nabla p = \left(\frac{1}{l_0}\mathbf{e}_s \times \nabla\psi + B_s\mathbf{e}_s\right)\cdot\nabla p = \frac{1}{l_0}\mathbf{e}_s \times \nabla\psi\cdot\nabla p = 0 \tag{6.169}$$

which implies that

$$p = p(\psi) \tag{6.170}$$

As expected, the pressure is a flux function.

A similar relation results from forming the dot product of the momentum equation with $\mathbf{J}$:

$$\mu_0\mathbf{J}\cdot\nabla p = -\frac{1}{l_0}\mathbf{e}_s \times \nabla(l_0 B_s)\cdot\nabla\psi\frac{dp}{d\psi} = 0 \tag{6.171}$$

In analogy with the toroidally axisymmetric case one finds

$$l_0 B_s = F(\psi) \tag{6.172}$$

Here $F(\psi)$ is a free function of flux. Note that an ideal stellarator, defined as one with zero net current on every flux surface, can only be realized by a special choice of $F(\psi)$. This is discussed further in the next subsection.

The final step in the derivation involves forming the dot product of the momentum equation with $\nabla\psi$. A short calculation leads to

$$\Delta^*\psi = -\mu_0 \frac{dp}{d\psi} - \frac{F}{l_0^2}\frac{dF}{d\psi} + \frac{2hl}{l_0^4}F \tag{6.173}$$

This is the desired helical Grad–Shafranov equation. As for the axisymmetric torus it is a non-linear partial differential equation with two free functions. Equation (6.173) reduces to the axisymmetric Grad–Shafranov equation for the special case of $l = 0$.

6.7.3 Low β analytic solution

The expansion

An analytic solution to the helical Grad–Shafranov equation can be obtained by means of an asymptotic expansion where the small parameter is the ratio of the helical magnetic field to the axial (i.e., toroidal) magnetic field. The analysis is qualitatively similar to the low β, large aspect ratio expansion for the tokamak presented in Section 6.4.

The basic idea is to expand about a vacuum magnetic field consisting of two components: a large axial field and a smaller helical field. As the expansion progresses, the free function $F(\psi)$ is chosen so that order by order the net current on every flux surface is zero. The end goal is to solve for ψ and see how a non-zero pressure modifies the vacuum flux surfaces.

To begin the analysis one must define the mathematical ordering scheme. The basic expansion parameter is denoted by δ, which measures the ratio of helical field B_h to the axial field B_0. The appropriate ordering scheme for present purposes is defined as follows:

$$\begin{array}{ll} B_h/B_0 \sim \delta & ha \sim 1 \\ \psi/aB_0 \sim 1 & \varepsilon = a/R_0 \sim \delta^2 \\ F/B_0 \sim 1 & \beta = 2\mu_0 p/B_0^2 \sim \delta^4 \end{array} \tag{6.174}$$

The ordering $ha \sim 1$ implies that the helical wavelength is comparable to the minor radius. The ordering $\varepsilon \sim \delta^2$ implies that there are many helical wavelengths around the torus. The ordering $\beta \sim \delta^4$ is equivalent to $\beta \sim \varepsilon^2$, which is the same as for the low β tokamak expansion. To determine the effect of β on the equilibrium therefore requires carrying out the analysis to include four orders in δ, not as daunting a task as one might expect since two orders correspond to simple vacuum solutions.

Now, the detailed expansion for the flux function consistent with this ordering can be written as

$$\psi(r,\alpha) = \psi_0(r) + \psi_1(r,\alpha) + \psi_2(r,\alpha) + \psi_3(r,\alpha) + \cdots \tag{6.175}$$

For simplicity the vacuum helical field $\psi_1(r,\alpha) = \overline{\psi}_1(r)\cos\ \alpha$ is assumed to have only a single harmonic.

The last point to consider is the boundary conditions. Clearly ψ must be regular in the plasma. With regard to the plasma surface there are two different ways in which to express the boundary condition: (1) specify a helical shape for the boundary and require that $\psi = 0$ on this surface or (2) specify the axial plus helical field on a simple surface, $r = a$. The second choice actually reduces the amount of analysis required and is the one used here. It can be conveniently expressed as

$$\left.\frac{1}{l_0}\frac{\partial\psi}{\partial r}\right|_{r=a} = B_\alpha(a,\alpha) = B_0\left(\frac{ha}{l_a} + \delta\ \cos\ \alpha\right) \tag{6.176}$$

where $l_a = (l^2 + h^2a^2)^{1/2}$, B_0 is the vacuum axial field, and δB_0 explicitly defines the amplitude of the helical field. Note that the constant term in the boundary condition (i.e., $B_0 ha/l_a$) has been chosen to make $B_\theta(a) = 0$, which is the requirement for no net z current in the plasma. In terms of the expansion, Eq. (6.176) translates into

$$\begin{aligned}
\left.\frac{\partial\psi_0}{\partial r}\right|_{r=a} &= haB_0 \\
\left.\frac{\partial\psi_1}{\partial r}\right|_{r=a} &= \delta l_a B_0\ \cos\ \alpha \\
\left.\frac{\partial\psi_2}{\partial r}\right|_{r=a} &= 0 \\
\left.\frac{\partial\psi_3}{\partial r}\right|_{r=a} &= 0
\end{aligned} \tag{6.177}$$

The problem has been properly formulated and the next task is to solve the helical Grad–Shafranov equation order by order to obtain the desired solution.

Zeroth-order solution

The zeroth-order equation and boundary condition determining $\psi_0(r)$ are given by

$$\begin{aligned}
\frac{1}{r}\frac{d}{dr}\left(\frac{r}{l_0^2}\frac{d\psi_0}{dr}\right) &= -\frac{F_0}{l_0^2}\frac{dF_0}{d\psi_0} + \frac{2hl}{l_0^4}F_0 \\
\left.\frac{d\psi_0}{dr}\right|_a &= haB_0
\end{aligned} \tag{6.178}$$

A short calculation shows that for no net current one must choose

$$F_0(\psi_0) = lB_0 = \text{constant} \tag{6.179}$$

which leads to the solution

$$\psi_0(r) = -\frac{1}{2}hB_0\left(a^2 - r^2\right) \tag{6.180}$$

The free constant associated with the flux function has been chosen to make $\psi_0 = 0$ on the surface. The resulting magnetic field and current density are easily evaluated

$$\begin{aligned} \mathbf{B}_0 &= B_0\mathbf{e}_z \\ \mathbf{J}_0 &= 0 \end{aligned} \tag{6.181}$$

which are the expected results.

First-order solution

The first-order equation and boundary condition determine $\psi_1(r, \alpha)$ and can be written as

$$\begin{aligned} \frac{1}{r}\frac{\partial}{\partial r}\left(\frac{r}{l_0^2}\frac{\partial\psi_1}{\partial r}\right) + \frac{1}{r^2}\frac{\partial\psi_1}{\partial\alpha^2} &= -\frac{F_0}{l_0^2}\frac{dF_1}{d\psi_0} + \frac{2hl}{l_0^4}F_1 \\ \left.\frac{\partial\psi_1}{\partial r}\right|_a &= \delta l_a B_0 \cos\alpha \end{aligned} \tag{6.182}$$

Observe that the helical terms on the left-hand side of the equation are all proportional to cos α while the terms on the right-hand side are only functions of r since $\psi_0 = \psi_0(r)$. The only way to resolve this incompatibility is to choose

$$F_1(\psi_0) = 0 \tag{6.183}$$

If one now writes $\psi_1(r, \alpha) = \overline{\psi}_1(r)\cos\alpha$ then $\overline{\psi}_1$ satisfies the following equation and boundary condition

$$\begin{aligned} \frac{1}{r}\frac{d}{dr}\left(\frac{r}{l_0^2}\frac{d\overline{\psi}_1}{dr}\right) - \frac{\overline{\psi}_1}{r^2} &= 0 \\ \left.\frac{d\overline{\psi}_1}{dr}\right|_a &= \delta l_a B_0 \end{aligned} \tag{6.184}$$

The solution for $\overline{\psi}_1$ is easily found and can be written as

$$\overline{\psi}_1(r) = \frac{\delta a B_0}{l_a I_a}\left[r\frac{d}{dr}I_l(hr)\right] \tag{6.185}$$

where $I_l(hr)$ is the modified Bessel function and $I_a = I_l(ha)$. The first-order fields and current density are easily evaluated:

$$\begin{aligned} B_{r1} &= \frac{\delta a B_0}{l_a I_a}\left[\frac{d}{dr} I_l(hr)\right] \sin\ \alpha \\ B_{\theta 1} &= \frac{l}{hr} B_{z1} = \frac{\delta a B_0}{l_a\, I_a}\left[\frac{l}{r} I_l(hr)\right] \cos\ \alpha \\ \mathbf{J}_1 &= 0 \end{aligned} \tag{6.186}$$

As expected, the solution corresponds to a vacuum helical field.

Second-order solution

The second-order equations are the first place where the effects of plasma pressure enter the equilibrium problem. The second-order equation and boundary condition are given by

$$\begin{gathered} \frac{1}{r}\frac{\partial}{\partial r}\left(\frac{r}{l_0^2}\frac{\partial \psi_2}{\partial r}\right) + \frac{1}{r^2}\frac{\partial \psi_2}{\partial \alpha^2} = -\mu_0 \frac{dp}{d\psi_0} - \frac{F_0}{l_0^2}\frac{dF_2}{d\psi_0} + \frac{2hl}{l_0^4} F_2 \\ \left.\frac{\partial \psi_2}{\partial r}\right|_a = 0 \end{gathered} \tag{6.187}$$

Since the right-hand side is only a function of r, this implies that $\psi_2\,(r, \alpha) \rightarrow \psi_2(r)$.

Consider next the choice for $F_2(\psi_0)$. In order for the net current on every flux surface to be zero one must set $B_{\theta 2}(r) = 0$. From the definitions of the B_α and B_s in terms of ψ and $F(\psi)$ this can be accomplished by setting

$$F_2[\psi_0(r)] = F_2(r) = lB_{z2}(r) = \frac{l}{hr}\frac{d\psi_2}{dr} \tag{6.188}$$

Equation (6.188) is substituted into Eq. (6.187). After a short calculation one finds

$$\frac{d}{dr}(B_0 B_{z2} + \mu_0 p) = 0 \tag{6.189}$$

which is just the equation for radial pressure balance in a θ-pinch. With zero average axial current it is only the diamagnetism in the axial magnetic field that can provide radial pressure balance.

A good way to think about Eq. (6.189) is to view $p[\psi_0(r)] = p(r)$ as a free function. The resulting second-order physical quantities can then be expressed in terms of $p(r)$ as follows:

$$\begin{aligned}\psi_2 &= \frac{\mu_0 h}{B_0}\int_r^a p\, r dr \\ \mathbf{B}_2 &= -\frac{\mu_0 p}{B_0}\mathbf{e}_z \\ \mathbf{J}_2 &= \frac{1}{B_0}\frac{dp}{dr}\mathbf{e}_\theta \\ F_2 &= -\frac{\mu_0 l\, p}{B_0}\end{aligned} \tag{6.190}$$

This completes the second-order solution.

Third-order solution

It is in third-order that the plasma pressure first has an impact on the structure of the helical fields. The third-order equation and boundary condition are given by

$$\begin{aligned}\frac{1}{r}\frac{\partial}{\partial r}\left(\frac{r}{l_0^2}\frac{\partial \psi_3}{\partial r}\right) + \frac{1}{r^2}\frac{\partial \psi_3}{\partial \alpha^2} &= -\left(\mu_0\frac{d^2p}{d\psi_0^2} + \frac{F_0}{l_0^2}\frac{d^2F_2}{d\psi_0^2}\right)\psi_1 - \frac{F_0}{l_0^2}\frac{dF_3}{d\psi_0} + \frac{2hl}{l_0^4}F_3 \\ \left.\frac{\partial \psi_3}{\partial r}\right|_a &= 0\end{aligned} \tag{6.191}$$

Note that the terms on the right proportional to $\psi_1(r, \alpha)$ all vary as cos α while those containing $F_3(\psi_0)$ are functions only of r. As shown below the correct choice for F_3 leading to no net current on every flux surface is

$$F_3(\psi_0) = 0 \tag{6.192}$$

Using this condition implies that $\psi_3(r, \alpha) = \overline{\psi}_3(r)\cos\ \alpha$ with $\overline{\psi}_3$ satisfying

$$\begin{aligned}\frac{1}{r}\frac{d}{dr}\left(\frac{r}{l_0^2}\frac{d\overline{\psi}_3}{dr}\right) - \frac{\overline{\psi}_3}{r^2} &= -\left(\mu_0\frac{d^2p}{d\psi_0^2} + \frac{F_0}{l_0^2}\frac{d^2F_2}{d\psi_0^2}\right)\overline{\psi}_1 \\ \left.\frac{d\overline{\psi}_3}{dr}\right|_a &= 0\end{aligned} \tag{6.193}$$

After a slightly lengthy calculation one can write down an exact but complicated solution to Eq. (6.193) as follows:

$$\begin{aligned}
\overline{\psi}_3 &= \overline{\psi}_1 U \\
U &= \frac{\mu_0}{B_0^2}\left[\int_r^a dx \frac{x l_0^2}{\overline{\psi}_1^2}\int_0^x \frac{\overline{\psi}_1^2}{y^2}\left(\frac{yp'}{l_0^2}\right)' dy + C\right] \\
C &= \frac{a l_a^2}{\overline{\psi}_1(a)\overline{\psi}_1'(a)}\int_0^a \frac{\overline{\psi}_1^2}{y^2}\left(\frac{yp'}{l_0^2}\right)' dy
\end{aligned} \tag{6.194}$$

In principle one can substitute profiles and carry out the integrals leading to an expression for $\overline{\psi}_3$ but this will require a numerical calculation. A simpler procedure, providing more intuition, is described below.

The loosely wound helix

The integrals in Eq. (6.194) can be evaluated analytically by introducing two assumptions. First one assumes a simple profile for the pressure:

$$p(r) = 2\langle p\rangle\left(1-\rho^2\right) \tag{6.195}$$

where $\rho = r/a$. The second assumption is that the helix is loosely, but not too loosely, wound: $\delta \ll ha \ll 1$. This leads to the simplifying approximations

$$\begin{aligned}
l_0^2(r) &\approx l^2 = \text{constant} \\
\overline{\psi}_1(r) &\approx \delta a B_0 \rho^l
\end{aligned} \tag{6.196}$$

Under these plausible assumptions the integrals can be easily evaluated:

$$U(r) = -\frac{\beta}{l^2}\left[2 + l - l\rho^2\right] \tag{6.197}$$

where $\beta = \beta_t = 2\mu_0\langle p\rangle/B_0^2$.

The contributions from the various orders can now be combined and simplified using the loose helix approximations. This results in the following expression for the total flux

$$\begin{aligned}
\psi(\rho,\alpha) &= \overline{\psi}(\rho) + \tilde{\psi}(\rho)\cos\ \alpha \\
\overline{\psi} &= -\frac{B_0 h a^2}{2}(1-\rho^2)\left[1 - \frac{\beta}{2}(1-\rho^2)\right] \\
\tilde{\psi} &= \delta a B_0 \rho^l\left[1 - \frac{\beta}{l^2}(2 + l - l\rho^2)\right]
\end{aligned} \tag{6.198}$$

where $\tilde{\psi}/\overline{\psi} \sim \delta/ha \ll 1$.

Two basic conclusions can be drawn from this expression. First, since $\tilde{\psi}/\overline{\psi} \ll 1$ the shape of the flux surfaces are readily obtained by letting $\rho(\rho_0, \alpha) = \rho_0 + \rho_1(\rho_0, \alpha)$ with ρ_0 serving as the flux surface label and $\rho_1 \ll \rho_0$. One finds $\rho_1 = -\left[\tilde{\psi}(\rho_0)/\overline{\psi'}(\rho_0)\right] \cos\ \alpha$. For the specific cases of $l = 1$, $l = 2$, and $l = 3$ the values of ρ_1 are given by

$$\begin{aligned} l &= 1 \qquad \rho_1 = -\frac{\delta}{ha}(1 - 2\beta)\cos(\theta + hz) \\ l &= 2 \qquad \rho_1 = -\frac{\delta}{ha}\left(1 - \frac{\beta\rho_0^2}{2}\right)\rho_0\ \cos(2\theta + hz) \\ l &= 3 \qquad \rho_1 = -\frac{\delta}{ha}\left[1 - \frac{\beta}{9}(6\rho_0^2 - 4)\right]\rho_0^2\ \cos(3\theta + hz) \end{aligned} \tag{6.199}$$

These flux surfaces are illustrated in Fig. 6.31. Observe that an $l = 1$ system corresponds to a rotating shifted circle similar to a corkscrew. An $l = 2$ system has the form of a rotating ellipse while $l = 3$ corresponds to a rotating triangular shape. Non-zero β effects make small modifications to the location of a given flux surface but do not alter its shape.

The second basic conclusion concerns a fundamental property of stellarators and should not get lost in the details of the analysis. Even as $\beta \to 0$ a stellarator magnetic field exhibits closed nested flux surfaces. There is a unique center to the field which automatically defines the location of the peak pressure. Contrast this with the tokamak. When no plasma is present and the poloidal field circuit is energized the resulting "flux surfaces" are a series of vertical lines, also shown in Fig. 6.31. Only when the plasma draws current and the vertical field is properly adjusted will a tokamak plasma be centered in the vacuum chamber. Stated differently, a stellarator provides a robust, immovable, magnetic cage to confine the plasma while a tokamak requires help from the plasma itself in the form of a toroidal current to provide equilibrium. This is indeed an advantage for stellarators, but as discussed in the next chapter other problems related to single-particle confinement arise.

The net z current

A final point to discuss in this subsection is the net z current flowing in a stellarator. In carrying out the analysis a choice for $F(\psi)$ has been made at each order in the expansion which is assumed to eliminate the net z current flowing on every flux surface. The task now is to verify this assumption. The required analysis is straightforward. Starting with the flux function given by Eq. (6.198) one can easily calculate B_r and B_θ. Taking the z component of $\nabla \times \mathbf{B}$ then leads to

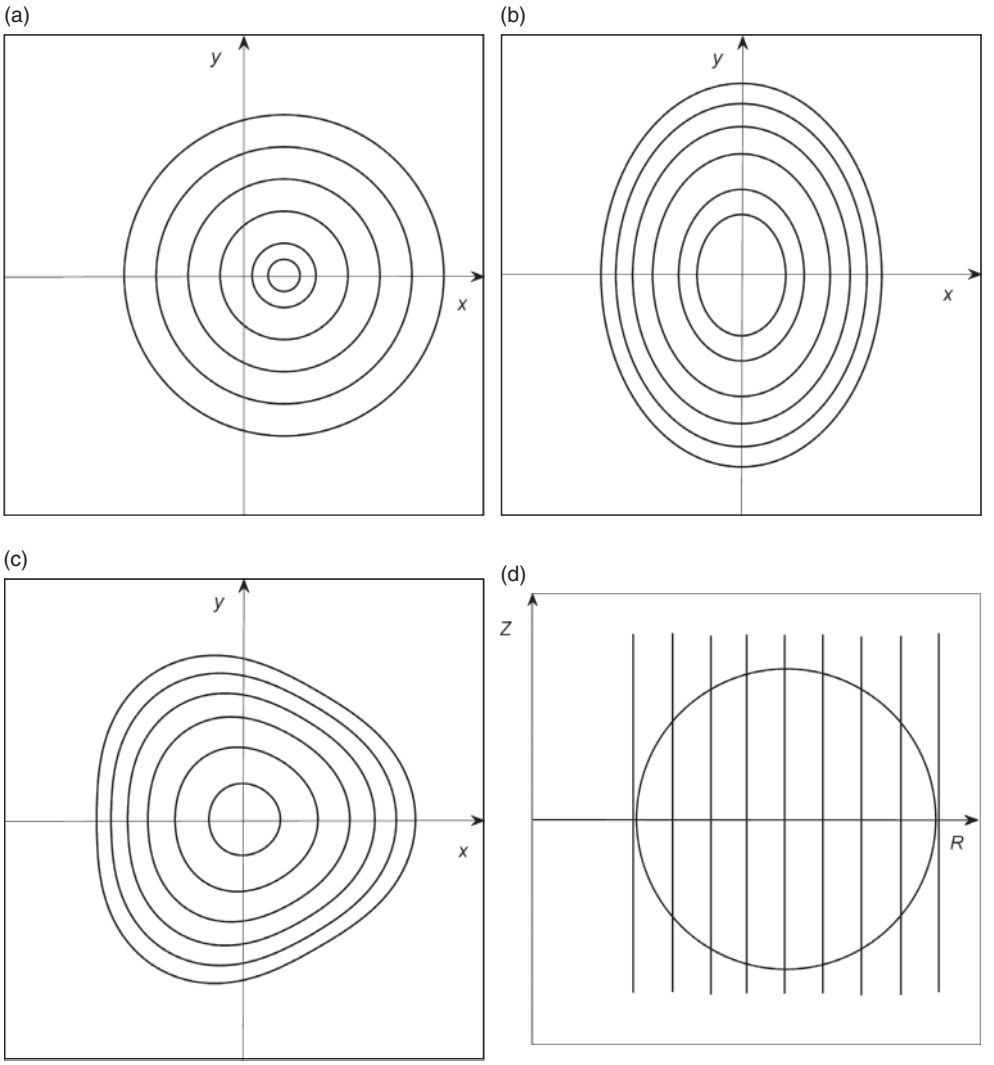

Figure 6.31 Vacuum flux surfaces for (a) $l = 1$, (b) $l = 2$, and (c) $l = 3$ stellarators. Also shown in (d) are the vacuum flux surfaces for a tokamak.

$$\mu_0 a J_z = \beta \delta B_0 \frac{(4 - 2l^2)}{l^2} \rho^l \cos\ \alpha \tag{6.200}$$

Note that this contribution corresponds to a third-order term in the expansion. All lower-order contributions have vanished identically because of the choices for $F(\psi)$. Since $J_z \sim \cos\ \alpha$ the integral over poloidal angle on any flux surface $\rho \approx \rho_0$ averages to zero. Stellarator equilibria are possible with no net current on any flux surface.

6.7.4 The rotational transform

The last topic of interest concerning the straight stellarator is the evaluation of the rotational transform. There is a key point to be made. Even without a plasma, a vacuum helical field produces a non-zero rotational transform. In the limit of small helical field amplitude the transform can be evaluated analytically. The existence of a vacuum rotational transform is not an obvious fact. The helical fields oscillate back and forth on a flux surface. One might think that the oscillating contribution to the transform would average to zero. It is shown that to leading order this is indeed true. The magnitude of the transform is a higher-order effect resulting from the fact that the flux surfaces have a small helical deformation.

Derivation of the rotational transform

The calculation starts with the general definition of transform given in Chapter 4 and then proceeds by exploiting the helical symmetry. The final result is then applied to several common stellarator fields corresponding to $l = 1$, 2, and 3. The details are as follows.

The general definition of rotational transform derived in Chapter 4, repeated here for convenience, is given by

$$\frac{\iota}{2\pi} = \frac{\lim\limits_{L\to\infty} \int_0^L \frac{B_\theta}{rB}\, dl}{\lim\limits_{L\to\infty} \int_0^L \frac{B_\phi}{RB}\, dl} \tag{6.201}$$

where now l and B represent the total (rather than poloidal) arc length and magnetic field, respectively. One now uses the geometric relations

$$\frac{dl}{B} = \frac{rd\theta}{B_\theta} = \frac{dz}{B_z} \tag{6.202}$$

and the definition of the helical angle $\alpha = l\theta + hz$ to obtain

$$\frac{dl}{B} = \frac{rd\alpha}{\partial\psi/\partial r} \tag{6.203}$$

Since the magnetic line geometry repeats itself every time α increases by 2π it is only necessary to integrate Eq. (6.201) over the range $0 \leq \alpha \leq 2\pi$ to evaluate the transform. Recall that a similar conclusion was derived for the tokamak where periodicity corresponds to one full poloidal transit $0 \leq \theta \leq 2\pi$. For the straight stellarator, helical periodicity thus implies that

$$\frac{\iota}{2\pi} = \frac{\displaystyle\int_0^{2\pi} B_\theta \frac{d\alpha}{\partial\psi/\partial r}}{\displaystyle\int_0^{2\pi} \frac{rB_\phi}{R}\frac{d\alpha}{\partial\psi/\partial r}} \tag{6.204}$$

The quantities appearing in the integrand need to be evaluated on the flux surface $r = r_0 + \overline{r}_1 \cos\,\alpha$ and must include leading- and first-order contributions. These quantities are obtained from the previous section in the vacuum limit $\beta \to 0$. A short calculation leads to

$$\begin{aligned}
\frac{\partial\psi}{\partial r} &= \frac{d\psi_0}{dr_0} + \left(\frac{d^2\psi_0}{dr_0^2}\,\overline{r}_1 + \frac{d\overline{\psi}_1}{dr_0}\right)\cos\,\alpha \\
B_\theta &= \frac{l}{l_0^2}\frac{d\overline{\psi}_1}{dr_0}\cos\,\alpha + \frac{d}{dr_0}\left(\frac{l}{l_0^2}\frac{d\overline{\psi}_1}{dr_0}\right)\overline{r}_1\cos^2\alpha \\
B_\phi &= -\frac{R}{R_0}B_z \approx -B_0 - \frac{hr}{l_0^2}\overline{\psi}_1\cos\,\alpha \approx -B_0
\end{aligned} \tag{6.205}$$

where $r_1(r_0,\alpha) = \overline{r}_1(r_0)\cos\,\alpha$, $\overline{r}_1 = -\overline{\psi}_1/\psi'_0$, and $\psi_0, \overline{\psi}_1$ are given by Eqs. (6.180) and (6.185) respectively. Note that only the leading-order contribution to B_ϕ enters the calculation.

One now substitutes this information into Eq. (6.204). The leading-order contribution averages to zero as expected. The first-order correction is obtained after a straightforward but slightly tedious calculation. The desired relation for the rotational transform is given by

$$\frac{\iota}{2\pi} = \frac{\delta^2 a^2 l R_0}{2hl_a^2 I_a^2}\left[\frac{1}{r}\frac{d}{dr}\left(\frac{I_l}{r}\frac{dI_l}{dr}\right)\right] \tag{6.206}$$

Here, for simplicity the subscript "0" has be suppressed from r_0.

The loose helix approximation

Equation (6.206), while exact in the context of the straight stellarator expansion, is still a relatively complicated expression. More intuition about the transform can be obtained by again introducing the loose helix approximation $\delta \ll ha \ll 1$ and using the small argument expansion of the Bessel functions

$$I_l(u) = \frac{1}{l!}\left(\frac{u}{2}\right)^l\left[1 + \frac{1}{l+1}\left(\frac{u}{2}\right)^2 + \cdots\right] \tag{6.207}$$

For $l \geq 3$ only the leading-order contribution to the Bessel functions is required. The expression for the transform reduces to

$$\frac{\iota(r)}{2\pi} \approx \frac{(l-1)\delta^2}{ha\varepsilon}\left(\frac{r}{a}\right)^{2l-4} \qquad l \geq 3 \tag{6.208}$$

Observe that when ha is reconsidered to be of order unity the transform is also of order unity: $\iota/2\pi \sim 1$. It is zero on axis and rises rapidly towards the edge, the rate of rise increasing as l increases. The profile has magnetic shear (i.e., $(r/\iota)(d\iota/dr) \neq 0$), which will be shown to be favorable for stability. Qualitatively, the profile shape is the opposite of that of a tokamak. For a stellarator $\iota/2\pi$ increases with r while for a tokamak $\iota/2\pi = 1/q$ decreases with r.

For an $l = 2$ system it is useful to include the first-order correction to the Bessel functions since, as shown in Eq. (6.208), the transform is constant to leading order. The first-order correction will show whether the profile increases or decreases with r although in either case the rate of change is small for $ha \ll 1$. A short calculation shows that for an $l = 2$ system the transform is given by

$$\begin{aligned} \frac{\iota(r)}{2\pi} &\approx \frac{i_H}{2\pi}\left(\frac{1+h^2r^2/2}{1+h^2a^2/2}\right) \qquad l=2 \\ \frac{i_H}{2\pi} &= \frac{\iota(a)}{2\pi} = \frac{\delta^2}{ha\varepsilon}\left(\frac{1+h^2a^2/2}{1+5h^2a^2/12}\right) \approx \frac{\delta^2}{ha\varepsilon} \end{aligned} \tag{6.209}$$

Observe that the transform increases with radius.

The last example of interest corresponds to $l = 1$. Equation (6.208) shows that to leading order in ha the rotational transform in an $l = 1$ system vanishes. To find the transform one must therefore keep the first-order correction to the Bessel functions. By definition the resulting transform is therefore smaller by a factor h^2a^2. Another short calculation shows that for an $l = 1$ system the transform can be written as

$$\frac{\iota(r)}{2\pi} \approx \frac{\delta^2 ha}{\varepsilon} \qquad l = 1 \tag{6.210}$$

The transform is constant in radius.

To summarize, a vacuum helical field produces a non-zero rotational transform. For $l \geq 3$ the transform is zero on axis but has shear across the entire profile. For $l = 2$ the transform is finite on axis and has weak shear across the profile. An $l = 1$ system has weak shear and a small transform.

6.7.5 Summary

The equilibrium of a plasma with helical symmetry (in a linear geometry) represents a simple model of a "straight stellarator." The system obeys a "Grad–Shafranov"-like partial differential equation with two free functions, one

being the pressure and the other related to the net toroidal current flowing on a flux surface. This latter function can be chosen so that the net current is zero on each flux surface. Even with zero plasma current, the vacuum helical field still possesses a non-zero rotational transform. As a consequence a helical system has a unique center determined by the external helical coil locations and forms a magnetic cage to confine the plasma.

While many features of a stellarator can be understood from the straight helical model the crucial problem of toroidal force balance has not yet been addressed. This is the topic of the next chapter where it is shown that even using a large aspect ratio expansion the analysis becomes considerably more complex.

6.8 Overall summary

Chapter 6 demonstrates how the ideal MHD model can be used to investigate the equilibrium properties of two-dimensional systems. Two types of systems are considered: a toroidally axisymmetric system and a linear helical system. For each system the equilibrium is described by a single non-linear partial differential equation.

For the toroidally axisymmetric case the equation, known as the Grad–Shafranov equation, provides a complete description of radial pressure balance and toroidal force balance. It can also be used to evaluate important plasma parameters and figures of merit related to equilibrium β limits and MHD stability. A number of concepts are discussed including the reversed field pinch, and various forms of tokamaks.

The helical Grad–Shafranov equation describes the equilibrium properties of a 2-D "straight stellarator" thereby providing a good introduction to the actual stellarator concept which is an inherently 3-D configuration. Certain important properties of stellarators are obtained from the 2-D model, although the critical problem of toroidal force balance is postponed until Chapter 7.

A summary of each of these systems is presented below.

The reversed field pinch (RFP)

The RFP is a large aspect ratio circular cross section configuration with $\beta_p \sim \beta_t \sim 1$ and $q_* \sim \varepsilon \ll 1$. Radial pressure balance is provided primarily by the toroidal current as in a Z-pinch. In fact the toroidal field is highly paramagnetic. Early RFPs were short pulsed devices in which toroidal force balance was provided by flux compression against a conducting wall. Modern RFPs have much longer pulses and are held in toroidal force balance by a vertical field. To achieve good MHD stability against modes driven by the pressure gradient the pressure profile must be very flat near the magnetic axis and the toroidal field must reverse sign near the edge of the plasma.

However, the low value of $q_* \sim \varepsilon$ is of concern with respect to current-driven kink modes and some form of feedback will likely be needed for good MHD stability. RFPs have been operated for many decades and experimental performance has been improving, getting close to, but still not as good as a tokamak.

The ohmically heated tokamak

Ohmically heated tokamaks are early fusion devices, usually having a circular cross section, and with characteristic parameters that scale as $\beta_t \sim \varepsilon^2$, $\beta_p \sim 1$, and $q_* \sim 1$. Radial pressure balance, toroidal force balance, and plasma heating are all provided by the toroidal plasma current. Even early ohmic tokamaks had long pulses requiring a vertical field rather than a conducting wall for toroidal equilibrium. The primary function of the large, costly, and slightly paramagnetic toroidal field is to provide MHD stability. The resulting high $q_* \sim 1$ provides stability against kink modes without a conducting wall or feedback. These early devices achieved quite good performance but were still limited in temperature and pressure since the only source of external power was the ohmic heating.

The high β tokamak

The high β tokamak is a large aspect ratio configuration whose goal is to achieve higher values of β than are possible in an ohmically heated tokamak. Initial high β tokamaks had circular cross sections. Higher values of β are accomplished by confining the plasma in a shallow diamagnetic well in the toroidal field produced by the application of a large amount of auxiliary power. Radial pressure balance is thus similar to that in a θ-pinch. The scaling relations in the high β regime are as follows: $\beta \sim \beta_t \sim \varepsilon$, $\beta_p \sim 1/\varepsilon$, and $q_* \sim 1$. This value of β is typically $1/\varepsilon$ times larger than in an ohmically heated tokamak. The scaling relations imply that the toroidal field is required for both radial pressure balance and MHD stability. The combination of poloidal field and vertical field provides toroidal force balance. The toroidal current also produces ohmic heating but this is usually a small effect compared to that due to the auxiliary power. Stability against current-driven kink modes is again provided by high q_*. Stability against pressure gradient driven modes is accomplished by profile shaping and keeping the value of β below a critical value. High β tokamaks have the interesting property of exhibiting an equilibrium β limit when the current is held constant and the pressure is increased, resulting from a separatrix moving onto the plasma surface. The equilibrium limit scales as $\beta_t \lesssim \varepsilon/q_*^2$.

Non-circular tokamaks

The experimentally achievable values of β_t in both ohmically heated and high β tokamaks can be substantially increased by allowing the plasma to have a non-circular cross section. The improvements are based on the observation that the

stability boundary against current-driven kink modes depends only on the value of q_*, essentially independent of elongation. Since elongated cross sections are characterized by higher values of I and J_ϕ for the same q_*, this leads to a higher equilibrium β_t limit, larger ohmic heating, and improved confinement. However, there is a limit to the allowable elongation of the cross section, typically $\kappa \lesssim 2$, set by axisymmetric vertical instabilities. Virtually all modern tokamaks have elongated cross sections with an outward pointing "D" shape.

The equilibrium β_t *limit*

In practice the equilibrium β_t limit is not a serious experimental problem. It can be avoided by relaxing the assumption that the plasma current be held fixed as the pressure is increased. If the plasma current instead increases in parallel with the pressure then less burden is placed on the vertical field to hold the plasma in toroidal force balance. A smaller increase in the vertical field slows the motion of the separatrix X-point onto the plasma surface thereby delaying and preventing the onset of the equilibrium limit. In actual experiments MHD instabilities occur at lower values of β_t than the equilibrium limit and are therefore more important in setting practical operational boundaries.

The spherical tokamak (ST)

The spherical tokamak attempts to achieve the highest possible values of β_t by exploiting the fact that both MHD equilibrium and stability limits scale as $\beta_t \sim \varepsilon$. Consequently, a compact tokamak with an ultra-tight aspect ratio, $R_0/a \sim 1.2$–1.6, should be able reach high values of β_t while maintaining $q_* \sim 1$. This has indeed been demonstrated experimentally. In practice, however, the pressure in an ST is similar to or even lower than in a standard tokamak in spite of the gains in β_t. The reason is that the toroidal field in the center of an ST is small because of the rapid $1/R$ fall-off of B_ϕ in a tight aspect ratio device. A possible attractive application of the ST is as a component test facility to test materials for a fusion reactor.

Limiters and divertors

An important practical problem in the operation of tokamak and stellarator experiments is the interface between the edge of the plasma and the first solid material with which it comes into contact. In high-performance experiments the plasma boundary is defined by either a mechanical limiter or magnetic divertor. The divertor offers a more flexible method of removing particles from the plasma, protecting the vacuum chamber, and preventing impurities from entering the plasma. However, divertors are more expensive and more costly. Both limiter and divertor tokamaks can be modeled by the Grad–Shafranov equation. Modern tokamaks almost always choose divertors as their first option.

The straight stellarator

A stellarator is a 3-D helical–toroidal fusion configuration. It receives much attention in the fusion community because of the possibility of operating with no net plasma current. This feature eliminates the need for external current drive (i.e., the plasma is inherently a steady state device) and reduces the possibility of major disruptions due to current-driven kink modes. As an introduction to stellarators a Grad–Shafranov equation for a straight cylindrical system with helical symmetry has been derived. Solutions are obtained using the low β, small helical amplitude expansion which demonstrate the following properties: (1) closed nested flux surfaces with a unique center exist even without plasma; (2) radial pressure balance similar to that in a θ-pinch; (3) zero net current on every flux surface; and (4) finite rotational transform. The important effects of toroidicity are addressed in the next chapter.

From the wide variety of realistic equilibria described by the two Grad–Shafranov equations one can see why the ideal MHD model is so widely used in the fusion program.

References

Budny, R.V. (1994). *Nucl. Fusion* **34**, 1247.
Cerfon, A.J. and Freidberg, J.P. (2010). *Phys. Plasmas* **17**, 032502.
Clarke, J.F. and Sigmar, D.J. (1977). *Phys. Rev. Lett.* **38**, 70.
DIII-D Team and Simonen, T.C. (1998). *Fusion Engineering and Design* **39**, 83.
Grad, H. and Rubin, H. (1958). In *Proceedings of the Second United Nations International Conference on the Peaceful Uses of Atomic Energy*. Geneva: United Nations, 31, p. 190.
Haas, F.A. (1972). *Phys. Fluids* **15**, 141.
Lust, R. and Schluter, A. (1957). *Z. Naturforsch* **12a**, 850.
Peng, M., Boroski, S.K., Dalton, B.R., *et al.* (1985). In *Proceedings of the Topical Conference on the Technology of Fusion Energy*, San Francisco, CA, p. 19.
Pfirsch, D. and Schluter, A. (1962). Max-Planck-Institut Report MPI/PA/7/62.
Shafranov, V.D. (1960). *Sov. Phys.-JETP* **26**, 682.
Shafranov, V.D. (1966). In *Reviews of Plasma Physics*, Vol. 2, ed. M.A. Leontovich. New York: Consultants Bureau.
Solev'ev, L.S. (1967). In *Reviews of Plasma Physics*, Vol. 3, ed. M.A. Leontovich. New York: Consultants Bureau.
Stratton, J.A. (1941). *Electromagnetic Theory*. New York: McGraw-Hill.

Further reading

Reversed field pinch

Bodin, H.A.B. and Newton, A.A. (1980). *Nucl. Fusion* **20**, 1255.
Butt, E.P., Curruthers, R., Mitchell, J.T.D. *et al.* (1958). In *Proceedings of the Second United Nations International Conference on the Peaceful Uses of Atomic Energy*. Geneva: United Nations, Vol. 32, p. 42.
Kikuchi, M., Lackner, K., and Tran, M.Q., eds. (2012). *Fusion Physics.* Vienna: International Atomic Energy Agency.
Martin, P., Adamek, J., Agostinetti, P. *et al.* (2011). *Nuclear Fusion* **51**, 1.
Robinson, D.C. (1971). *Plasma Phys.* **13**, 439.

Tokamaks (general)

Bateman, G. (1978). *MHD Instabilities*. Cambridge, MA: MIT Press.
Furth, H.P. (1975). *Nucl. Fusion* **15**, 487.
Kikuchi, M., Lackner, K., and Tran, M.Q., eds. (2012). *Fusion Physics.* Vienna: International Atomic Energy Agency.
Shafranov, V.D. (1966). In *Reviews of Plasma Physics*, Vol 2, ed. M.A. Leontovich. New York: Consultants Bureau.
Wesson, J.A. (1978). *Nucl. Fusion* **18**, 87.
Wesson, J. (2011). *Tokamaks*, 4th edn. Oxford: Oxford University Press.
White, R.B (2006). *Theory of Toroidally Confined Plasmas*, 2nd edn. London: Imperial College Press.

High β tokamak

Callan, J.D. and Dory, R.A. (1972). *Phys. Fluids* **15**, 1523.
Dory, R.A. and Peng, Y.-K.M. (1977). *Nucl. Fusion* **17**, 21.
Freidberg, J.P. and Haas, F.A. (1973). *Phys. Fluids* **16**, 1909.
Shafranov, V.D. (1971). *Plasma Phys*. **13**, 757.
Wesson, J. (2011). *Tokamaks*, 4th edn. Oxford: Oxford University Press.

Non-circular tokamaks

Laval, G. and Pellat, R. (1973). In *Controlled Fusion and Plasma Physics*, Proceedings of the Sixth European Conference, Moscow, Vol. II, p. 640.
Laval, G., Pellat, R. and Soule, J.L. (1972). In *Controlled Fusion and Plasma Physics*, Proceedings of the Fifth European Conference, Euratom CEA, Grenoble, Vol. I, p. 25.
Laval, G., Pellat, R. and Soule, J.L. (1974). *Phys. Fluids* **17**, 835.
Solov'ev, L.S., Shafranov, V.D., and Yurchenko, E.I. (1969). In *Plasma Physics and Controlled Nuclear Fusion Research* (1968), IAEA, Vienna, Vol. I, p. 173.
Wesson, J. (2011). *Tokamaks*, 4th edn. Oxford: Oxford University Press.

Flux-conserving tokamaks

Clarke, J.F. and Sigmar, D.J. (1977). *Phys. Rev. Lett.* **38**, 70.
Dory, R.A. and Peng, Y.-K.M. (1977). *Nucl. Fusion* **17**, 21.

Straight stellarator

Morozov, A.I. and Solev'ev, L.S. (1963). In *Reviews of Plasma Physics*, Vol. 2, ed. M.A. Leontovich. New York: Consultants Bureau.
Solev'ev, L.S. (1967). In *Reviews of Plasma Physics*, Vol. 3, ed. M.A. Leontovich. New York: Consultants Bureau.
Wakatani, M. (1998). *Stellarators and Heliotron Devices*. New York: Oxford University Press.

Numerical MHD equilibria

Goedbloed, J.P., Keppens, R., and Poedts, S. (2010). *Advanced Magnetohydrodynamics*. Cambridge: Cambridge University Press.
Jardin, S. (2010). *Computational Methods in Plasma Physics*. New York: CRC Press.

Problems

6.1 Consider the two-dimensional Grad–Shafranov equation for a straight stellarator (Eq. (6.173)). Show that in the limit where the helical field amplitude approaches zero (i.e., $\psi\,(r,\,\alpha) \rightarrow \psi(r)$), the general one-dimensional radial pressure balance relation for the screw pinch is obtained.

6.2 Using the ideal MHD model derive a Grad–Shafranov equation for stationary axisymmetric toroidal equilibrium in which there is a steady state velocity $V_\phi(R,\,Z)$ flowing in the toroidal direction. For simplicity assume $\rho = \rho(\psi)$. Hints: Show that

$$\mathbf{B} = B_\phi \mathbf{e}_\phi + \frac{1}{R}\nabla\psi \times \mathbf{e}_\Phi$$

$$\mu_0 \mathbf{J} = -\frac{1}{R}\Delta^*\psi \mathbf{e}_\phi + \frac{1}{R}\nabla\left(RB_\phi\right) \times \mathbf{e}_\phi$$

$$V_\phi/R = \Omega(\psi)$$

$$p - \frac{1}{2}\rho\Omega^2 R^2 = \Pi(\psi)$$

$$RB_\phi = F(\psi)$$

$$\Delta^*\psi = -FF' - \mu_0 R^2 \Pi' - \frac{\mu_0 R^4}{2}\left(\rho\Omega^2\right)'$$

6.3 Consider the transformation of coordinates (R,Z,ϕ') to (r,θ,ϕ) defined by

$$R = R_0 + r\,\cos\,\theta$$

$$Z = r\,\sin\,\theta$$

$$\phi' = -\phi$$

where (R,Z,ϕ') represents a standard cylindrical coordinate system. Show that the following relations hold in the (r,θ,ϕ) system:

$$\nabla\psi = \nabla_c\psi$$

$$\nabla \cdot \mathbf{B} = \nabla_c \cdot \mathbf{B} + \frac{\mathbf{e}_R \cdot \mathbf{B}}{R}$$

$$\nabla \times \mathbf{B} = \nabla_c \times \mathbf{B} - \frac{B_\phi}{R}\mathbf{e}_Z$$

$$\Delta^*\psi = \nabla_c^2\psi - \frac{\mathbf{e}_R \cdot \nabla\psi}{R}$$

Here

$$\nabla_c = \mathbf{e}_r \frac{\partial}{\partial r} + \frac{\mathbf{e}_\theta}{r}\frac{\partial}{\partial \theta} + \frac{\mathbf{e}_\phi}{R}\frac{\partial}{\partial \phi}$$

and

$$\mathbf{e}_R = \cos\ \theta \mathbf{e}_r - \sin\ \theta \mathbf{e}_\theta$$

$$\mathbf{e}_Z = \sin\ \theta \mathbf{e}_r + \cos\ \theta \mathbf{e}_\theta$$

$$\mathbf{e}_{\phi'} = -\mathbf{e}_\phi$$

6.4 Consider a static cylindrically symmetric reversed field pinch characterized by $p(r)$, $B_\theta(r)$, $B_Z(r)$. In realistic experimental situations Ohm's law should include an anisotropic resistivity: $\mathbf{E} = \eta_\parallel \mathbf{J}_\parallel + \eta_\perp \mathbf{J}_\perp$ with $\eta_\parallel$ and $\eta_\perp$ assumed constant for simplicity.

(a) In steady state show that $E_\theta = 0$ and $E_z = E_0 =$ constant.
(b) Show that B_z satisfies the differential equation

$$\frac{dB_z}{dr} = \frac{\eta_\parallel - \eta_\perp}{\eta_\parallel \eta_\perp}\frac{B_\theta B_z}{B_\theta^2 + B_z^2}\mu_0 E_0$$

(c) Show that under the assumptions made, *no* solutions exist with B_z reversed for any positive values of $\eta_\parallel$, $\eta_\perp$. What does this suggest to you about the steady state operation of an RFP?

6.5 Show that in an ohmically heated tokamak the normal curvature, correct to order ε^2, is given by

$$\kappa_n(r,\theta) = -\frac{B_{\theta 1}^2}{rB_0^2} - \left(1 - \frac{r\ \cos\ \theta}{R_0}\right)\frac{\cos\ \theta}{R_0} + \frac{\Delta\ \sin^2\theta}{rR_0}$$

Here, $\Delta(r) = -\psi_1(r)/\psi_0'(r)$ is the shift of the flux surfaces.
6.6 Show that Shafranov's formula for the vertical field required to hold a tokamak in toroidal force balance

$$B_V = \frac{\mu_0 I}{4\pi R_0}\left(\beta_p + \frac{l_i - 3}{2} + \ln\frac{8R_0}{a}\right)$$

can be written in the following more intuitive form:

$$2\pi R_0 I_0 B_V = \frac{I_0^2}{2}\frac{\partial}{\partial R_0}(L_e + L_i) + 4\pi^2 \int_0^a \left(p - \frac{B_0 B_{\phi 2}}{\mu_0}\right) r dr$$

where L_e and L_i are the external and internal inductances associated with the plasma current. Hint: Make use of the fact that L_i is linearly dependent on R_0.

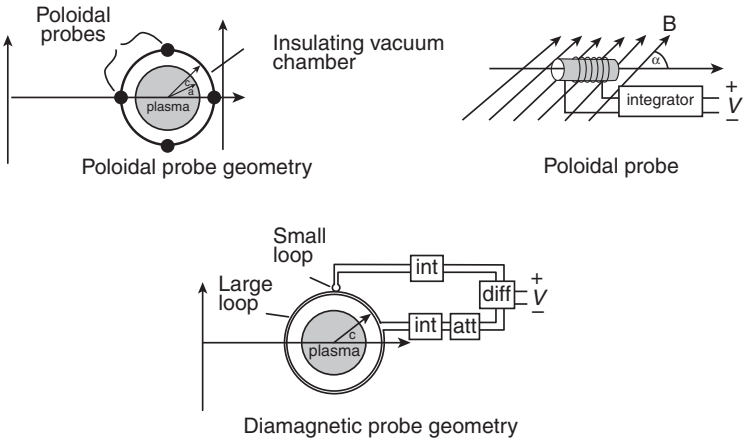

Figure 6.32 Diagram for Problem 6.7.

6.7 Consider an ohmically heated tokamak plasma held in equilibrium by a vertical field B_V. It is desired to measure β_p, l_i, and $\Delta(a)$ by placing various magnetic probes just outside the vacuum chamber, which for simplicity is assumed electrically insulating, and whose radius is c (see Fig. 6.32).

(a) Consider an individual probe as illustrated. Assume the probe has N turns and cross sectional area A. The **B** field makes an angle α with the axis of the probe. What signal appears on the output of the integrator?

(b) Show that the toroidal correction to the flux function $\psi_1(r, \theta)$, evaluated at a radius r in the vicinity of the vacuum chamber, is given by

$$\psi_1(r,\theta) = \frac{I_0}{2\pi}\left[\frac{r^2 - a^2}{2r}\left(\beta_p + \frac{l_i - 1}{2}\right) + \frac{r}{2}\ln\frac{r}{a} - \Delta(a)\frac{R_0}{r}\right]\cos\ \theta$$

(c) Calculate the difference in signals from two "B_θ" probes located at $r = c, \theta = 0$ and $r = c, \theta = \pi$

(d) Calculate the signal on a "B_r" probe located at $r = c$, $\theta = \pi/2$.

(e) Assuming $c = a(1 + \delta)$ with $\delta \ll 1$, show how the "B_r" and "B_θ" signals can be combined to give separate measurements of $\Delta(a)$ and $\beta_p + \ell_i/2$.

(f) Consider now a set of "diamagnetic" probes as shown in the diagram. This system consists of a small B_ϕ probe located at $r = c$, $\theta = \pi/2$ and a large single-turn loop of radius c, surrounding the vacuum chamber. By what factor must the large loop signal be attenuated in order to produce a null signal at the output of the "difference" circuit when no plasma is present? Calculate the difference signal V when plasma is present and show how it can be used to determine β_p.

(g) Which of these measurements do you think might be difficult in a high-field experiment like Alcator C? Explain.

6.8 Consider a low β ohmically heated tokamak. Probe measurements on the outside of the discharge indicate that

$$\beta_p + \frac{l_i}{2} = 0.75$$

Profile measurements indicate peaked densities such that

$$n(r) = CT^2(r), \quad C = \text{const}$$

In addition the plasma diamagnetism is non-zero and for simplicity is modeled as

$$\frac{B_{\phi 2}}{B_0} = \lambda \frac{\mu_0 p}{B_0^2}$$

with λ a constant, yet to be determined. The above data correspond to the "steady state" flat top portion of the current in an ohmic discharge. Assume Spitzer resistivity: $\eta = KT^{-3/2}$ with $T_e = T_i = T$ and $K = 3.0 \times 10^{-8}$, T in keV, η in Ωm.

(a) Calculate the profile $B_\theta(r)/B_\theta(a)$.
(b) If the discharge is operating just at the onset of sawtooth oscillations (i.e., $q_0 = 1$) calculate $q(a)$ assuming $J_\phi(a) = 0$.
(c) Calculate β_p and the diamagnetic constant λ. Is the discharge diamagnetic or paramagnetic?
(d) If $B_0 = 10$ T, $R_0 = 0.64$ m, and $a = 0.16$ m, calculate the electron temperature if the toroidal loop voltage is 1.6 V. See Table 6.5 for helpful relations involving Bessel functions $J_0(x)$ and $J_1(x)$.

Table 6.5 *Helpful relations for Bessel functions $J_0(x)$, $J_1(x)$.*

$xJ_0'' + J_0' + xJ_0 = 0$
$x^2J_1'' + xJ_1' - (1 - x^2)J_1 = 0$
$J_1 = -J_0'$
$J_0 \approx 1$ as $x \to 0$
$J_1 \approx x/2$ as $x \to 0$
$\int xJ_0^2 dx = x^2\left(J_0^2 + J_1^2\right)/2$
$\int xJ_1^2 dx = x^2\left(J_0^2 + J_1^2\right)/2 - xJ_0J_1$
$\int \frac{J_0}{J_1} dx = \ln(xJ_1)$
$\int \frac{xJ_0^2}{J_1^2} dx = -\frac{xJ_0}{J_1} + 2\ln(xJ_1) - x^2/2$
$J_0(x_0) = 0 \to x_0 = 2.4$ (first zero)
$J_1(x_0) = 0.52$

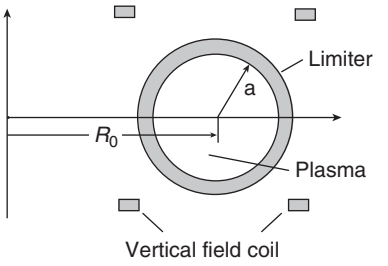

Figure 6.33 Diagram for Problem 6.9.

6.9 This problem demonstrates a practical application of MHD theory to the diagnosing of tokamak experiments. As a particular example, consider the geometry in Fig. 6.33. Assume that $B_0 = 8$ T, $R_0 = 0.64$ m, and $a = 0.16$ m and that the discharge is operating just at the onset of sawtooth oscillations (i.e., $q_0 = 1$). As a simple model of transport assume $n(r) \sim T(r) \sim J_\phi(r)$ and that $J_p(r) = 0$. Using the ohmically heated tokamak expansion calculate:

(a) $B_\theta\,(r)$
(b) $J_\theta\,(r)$
(c) $p\,(r)$
(d) I
(e) $q_a \approx q_*$
(f) β_t
(g) $B_t\,(0)$
(h) β_p
(i) l_i
(j) B_V (for zero shift of the outer surface)
(k) Δ_0 (shift of the magnetic axis relative to the outer surface).

See Table 6.5 for helpful relations involving Bessel functions $J_0\,(x)$ and $J_1\,(x)$.

6.10 The MHD equations describing the equilibrium of a plasma with an external force derivable from a potential are given by

$$\mathbf{J} \times \mathbf{B} - \nabla p - \rho \nabla \phi = 0$$
$$\nabla \times \mathbf{B} = \mu_0 \mathbf{J}$$
$$\nabla \cdot \mathbf{B} = 0$$

Assume (1) two-dimensional slab symmetry (all quantities are functions only of x and y), (2) $p = (T/m_i)\rho$ with T a constant, (3) all three components of $\mathbf{B}$ are nonzero, and (4) $\phi\,(x, y)$ is a known prescribed function.

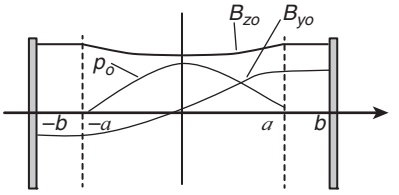

Figure 6.34 Diagram for Problem 6.10.

(a) Derive a two-dimensional Grad–Shafranov equation for this configuration. Hints: (1) Use A (the z component of vector potential) as the flux function; (2) show that $p \exp(m\phi/T) = \Pi(A)$, where $\Pi(A)$ is arbitrary; (3) show that $B_z = F(A)$, where $F(A)$ is arbitrary; and (4) the final equation is given by

$$\nabla^2 A = -FF' - \Pi' \exp(m_i \phi / T)$$

(b) Show that in the one-dimensional gravitational case ($\phi = -gx$ with $g = \text{const}$), the Grad–Shafranov equation reduces to the appropriate one-dimensional limit.

(c) Consider now a two-dimensional case

$$m_i \phi / T = \varepsilon f(x) y / L$$

with $\varepsilon \ll 1, y \geq 0, -b \leq x \leq b$. Assume the currents and pressure are confined to the region $-a < x < a$ and that p and B_z are even about $x = 0$ while B_y is odd (see Fig. 6.34). The region between a and b is a vacuum region and at $x = \pm b$ there is a perfectly conducting boundary. Expand $A\ (x, y) = A_0\ (x) + A_1\ (x, y)$. Find a solution for A_1 expressed in terms of integrals of the zeroth-order quantities.

(d) Derive an expression for the shift of the last flux surface carrying current for the case $f(x) = -x/a$. Sketch the contour describing this surface, including the correction, and give a physical description of the surface distortion resulting from $f(x)$.

6.11 It has been known since the time of Newton that the Earth's gravitational field causes objects to "fall" towards the center of the Earth. Thus, if unsupported, a tokamak plasma in a 200-msec discharge would fall almost 0.2 m during its lifetime. The purpose of this problem is to calculate the equilibrium of an axisymmetric toroidal tokamak under the influence of a downward gravitational force and to determine how effective the magnetic forces are in supporting the mass of the plasma against gravity.

(a) Consider the axisymmetric geometry shown in Fig. 6.35. Assume there is an external potential $\phi\ (R, Z)$ and calculate the Grad–Shafranov equation for this system. For simplicity, assume $p = (T/m_i)\rho$ with $T = \text{const}$.

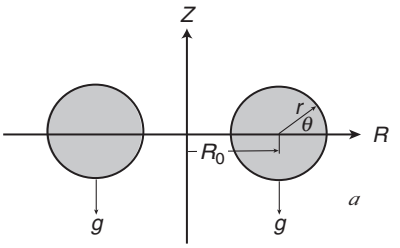

Figure 6.35 Diagram for Problem 6.11.

(b) What choice of ϕ (R, Z) corresponds to a downward gravitational force?
(c) Use this choice and treat ϕ as a small quantity; that is, assume gravitational effects enter in the same order as toroidal corrections. Expand the flux function as $\psi = \psi_0\,(r) + \psi_1\,(r, \theta)$ and find the contribution to $\psi_1\,(r, \theta)$ due to gravity. For simplicity, assume there is a conducting wall at $r = b$.
(d) Calculate the influence of gravity on the shape and position of the last flux surface that carries current. Estimate the size of these corrections for typical fusion plasmas. Is gravity an important effect?

6.12 Consider the simple model of the high β tokamak discussed in Section 6.5.

Assume that as the plasma evolves it is constrained by stability considerations to operate at $q_0 = 1$, rather than at fixed I or in a flux-conserving mode. Show that when $q_0 = 1$, the maximum achievable plasma β_t does not occur at the equilibrium limit $v = 1$, but at some lower value. Calculate the value of v and the corresponding value of $\beta_t q_0^2/\varepsilon$ at the optimum condition (see Fig. 6.36).

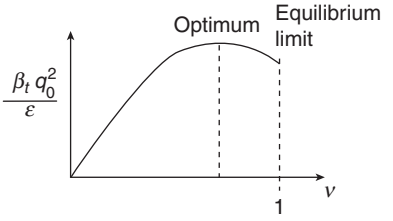

Figure 6.36 Diagram for Problem 6.12.

6.13 In Section 6.5 it was shown, using a simple elliptic model of a tokamak, that the highest equilibrium β_t occurs when $v = 1$ and $\kappa \to \infty$ assuming a fixed ε, q_*. Repeat the analyses assuming that the volume and major radius are held fixed rather than ε, q_*. Show that in the case there is an optimum elongation corresponding to the maximum β_t. Find the optimum κ and the corresponding values of β_t, J_ϕ, and I_0 and compare them to the circular case.

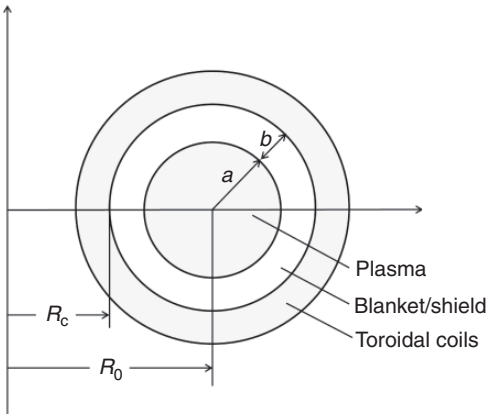

Figure 6.37 Diagram for Problem 6.14.

6.14 Consider a simple model of a superconducting tokamak fusion reactor as illustrated in Fig. 6.37.

(a) Derive an expression for the total thermal power P_T associated with the 14-MeV neutrons.

(b) Assume the wall loading $P_W \equiv P_T/S$ is fixed at the largest value consistent with the properties of the first wall material. Here, S is the plasma surface area. Also, assume the toroidal field coils operate at the maximum permissible value B_c which maintains superconductivity. Note that $B_\phi = B_c$ at $R = R_c$. Derive an expression for the required value of β_t/ε in terms of P_T, P_W, T_i, ε, ε_T, and B_c. Here, $\varepsilon = a/R_0$, $\varepsilon_T = (a + b)/R_0$, $T_i = T_e = T/2$, and β_t is defined as $\beta_t = 4\mu_0 n T_i/B_0^2$, with B_0 the field at the center of the plasma, $R = R_0$.

(c) Assume P_T, P_W, T_i, B_c, and b are fixed. Show that the required β_t/ε exhibits a minimum as a function of ε. Derive an expression for the optimum aspect ratio.

(d) At the optimum point calculate the values of ε, β_t/ε, β_t, a, and R_0 if $T_i = 15$ keV, $P_\mathrm{T} = 3500$ MW, $P_\mathrm{W} = 4$ MW/m^2, $b = 1$ m, and $B_\mathrm{c} = 11$ T. Note: At $T_\mathrm{i} = 15$ keV, $\langle \sigma v \rangle = 3 \times 10^{-22}\mathrm{m}^{-3}$/sec for D-T fusion reactions.